SEMMELWEIS EGYETEM

DOKTORI ISKOLA

Ph.D. értekezések

2977.

NAGY-PÁL PERTA

Funkcionális Idegtudományok
című program

Programvezető: Dr. Sperlágh Beáta, egyetemi tanár

Témavezető: Dr. Hájos Norbert, tudományos tanácsadó

Comparison of morphological and input-output characteristics of basket and chandelier cells in the mouse medial prefrontal cortex

PhD thesis

Petra Nagy-Pál

Semmelweis University Doctoral School

János Szentágothai Neurosciences Division

Supervisor: Norbert Hájos, Ph.D, D.Sc

Official reviewers: Hajnalka Ábrahám, MD, Ph.D, Habil

István Adorján, Ph.D

Head of the Complex Examination Committee:

Alán Alpár, Ph.D, Habil, D.Sc

Members of the Complex Examination Committee:

Lucia Wittner, Ph.D, D.Sc

Gergely Zachar, Ph.D

Budapest

2024

Table of contents

List of abbreviations

AAC – axo-axonic cell

ACC – anterior cingulate cortex

ACSF – artificial cerebrospinal fluid

ADHD – attention deficit hyperactivity disorder

AIS – axon initial segment

AnkG – ankyrin G

BA – basal amygdala

BAC – bacterial artificial chromosome

BC – basket cell

BLA – basolateral amygdala

Calb – calbindin

CB1 – type 1 cannabinoid receptor

CCK – cholecystokinin

CCKBC – cholecystokinin-expressing basket cell

ChC – chandelier cell

cPFC – contralateral prefrontal cortex

CTB – choleratoxin B subunit

Ctip2 – COUP-TF interacting protein 2

DR – dorsal raphe

DS – dorsal striatum

FG – Fluorogold

Flpo – Mouse codon-optimized flippase recombinase

FoxP2 – Forkhead-box protein P2

GABA – gamma-amino butyric acid

GAD-67 – glutamate decarboxylase 67

IL – infralimbic cortex

IN – interneuron

IPSC – inhibitory postsynaptic current

Lamp5 – lysosomal-associated transmembrane protein 5

LEnt – lateral entorhinal cortex

M2 – secondary motor cortex

MD thalamus – mediodorsal nucleus of the thalamus

MO – medial orbital cortex

mPFC – medial part of the prefrontal cortex

NDS – normal donkey serum

NGS – normal goat serum

nNOS – neuronal nitric oxide synthase

NPY – neuropeptide Y

PAG – periaqueductal gray

PB – phosphate buffer

PC – pyramidal cell

PFA – paraformaldehyde

PFC – prefrontal cortex

PrL – prelimbic cortex

PTI – perisomatic-region targeting inhibitory neurons

PV – parvalbumin

PVBC – parvalbumin-expressing basket cell

Sncg – synuclein gamma

SST – somatostatin

VGAT – vesicular gamma-amino butyric acid transporter

Vglut3 – type 3 vesicular glutamate transporter

VIP – vasoactive intestinal polypeptide

VTA – ventral tegmental area

WFS1 – wolfram syndrome 1 protein

WGA-HRP – wheat germ agglutinin conjugated with horseradish peroxidase

1. Introduction

1.1. Overview

Information processing in different cortical areas is based on the operation of well-organized, interconnected neuronal networks. Operation of these networks depends on the connections between excitatory pyramidal cells (PCs) and inhibitory interneurons (INs). Thus, these connections are essential for proper cortical function since abnormal changes in wiring features are often linked to different neurological or psychiatric disorders, including epileptic seizures or schizophrenia.

The most prevalent neurons in cortical structures are PCs releasing glutamate, while 15-20% of all cortical neurons are inhibitory INs using gamma amino butyric acid (GABA) as a neurotransmitter (DeFelipe & Farinas, 1992). These two main cell types form networks enabling specific circuit functions. Generally, PCs are responsible for information processing, storage and recall, whereas INs control and harmonize the activity of PCs (Buzsaki & Chrobak, 1995). Past research uncovered that INs form diverse groups that can be defined based on their targets, i.e. where their output synapses establish contacts. Based on this, GABAergic INs can be divided into the following groups: (I) the perisomatic region-targeting inhibitory neurons (PTIs) which innervate the soma, proximal dendrites and axon initial segment (AIS), the so-called perisomatic regions of PCs, (II) the dendritic inhibitory neurons, which form synapses on the dendrites of PCs. The third group of INs are (III) the interneuron-selective interneurons, which prefer to target other inhibitory neurons, thus, activation of them leads to disinhibition of PCs within the cortical networks, while (IV) the projecting GABAergic cells compose the fourth group, inhibitory cells that may play a role in synchronising the PC activity among remote areas. The members of the first group, which form synapses close to the action potential generation site, can regulate most effectively the PC activity, i.e. their output (Miles et al., 1996; Pouille & Scanziani, 2004; Veres et al., 2017). Basket cells (BCs) innervate the somata and proximal dendrites, whereas axo-axonic or chandelier cells (AACs or ChCs) specifically target AISs of PCs. We know from previous studies that these INs express different neurochemical markers (Kawaguchi & Kubota, 1997), based on which PTIs are divided further to BCs that express parvalbumin (PV/PVBCs) or cholecystokinin and type 1 cannabinoid receptors (CCK/CB1 or CCKBCs) (Freund &

Katona, 2007), while ChCs may or may not contain PV (Taniguchi et al., 2013). Interestingly, the two basket cell types possess distinct single-cell features and are proposed to have a distinct role in cortical computation (Freund, 2003; Klausberger et al., 2005; Klausberger & Somogyi, 2008).

Despite numerous studies that examined and described the anatomical and electrophysiological features of PTI cell types in different cortical regions, our knowledge about these INs is still limited in the medial part of the prefrontal cortex (mPFC). This cortical region is responsible for the proper operation of higher order cognitive processes like learning and attention (Baddeley, 1992; Cohen et al., 1996; Fuster, 2006; Goldman-Rakic, 1995). In this thesis we thoroughly examined the morphological features and the input-output characteristics of PTIs in the mPFC. In the next sections I will summarize our knowledge of the mPFC and PTIs expressing PV and CCK/CB1 in different brain regions – like the amygdala and hippocampus – since we possess more information about PTIs located in these regions, and then I will present our results and compare the features of these INs within the PFC.

1.2. The prefrontal cortex

The PFC is located in the frontal lobe of the brain and it has been widely studied in the past decades. The word 'prefrontal' has been used for the first time by Ferrier and Yeo in their lesion studies published in 1884 (Ferrier, 1884). Later Brodmann defined the prefrontal cortex as the granular frontal region of the brain based on his findings (Brodmann, 1909). After that, the definition formed by Rose and Woosley (Rose & Woolsey, 1948) was used for 70 years. They defined the prefrontal cortex as the part of cerebral cortex which receives projections from the mediodorsal nucleus of the thalamus (MD thalamus). This definition shows differences across species: in primates -among other parts- the dorsolateral part also receives projections from MD thalamus, while in rodents this projection is limited only in medial and orbital cortices (Carlen, 2017). Nowadays, we distinguish three regions within the rodent prefrontal cortex: the medial part (mPFC), which is located along the medial wall of the hemisphere, the ventral part that is termed the orbital prefrontal cortex and the lateral part, which is identified as the

agranular insular area (Figure 1) (Carlen, 2017; Ongur & Price, 2000; Van De Werd & Uylings, 2014).

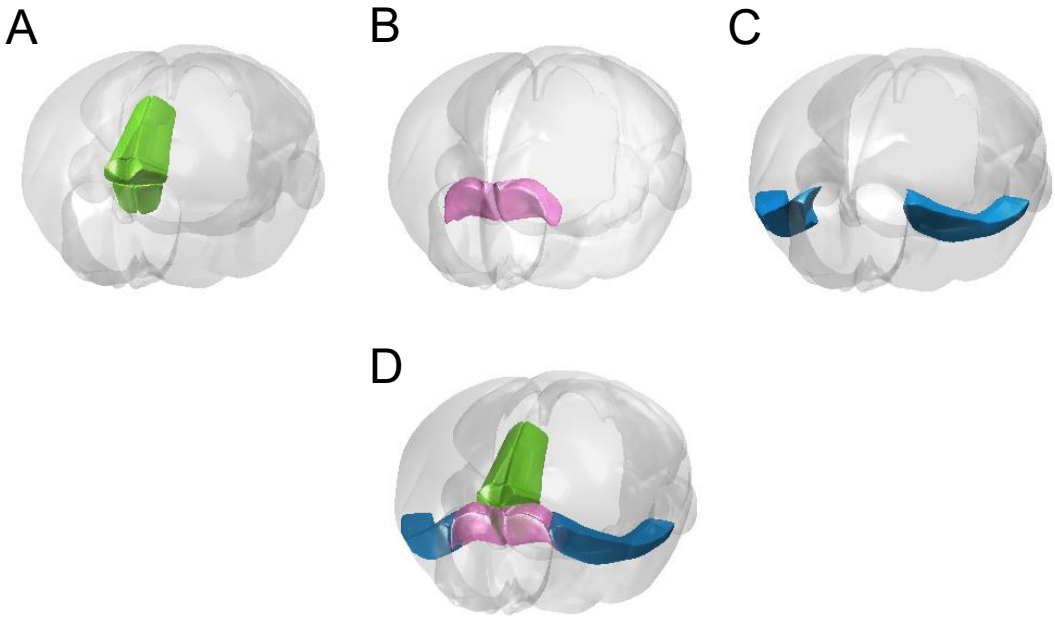

Figure 1: ***Distinct regions of the mouse prefrontal cortex*** *(A) Green colour presents the medial parts of the PFC. (B) In pink, the orbital area is presented. (C) Blue colour shows the agranular insular areas. (D) Three distinct regions of the PFC are presented together. The colours are the same as (A-C.) (Figure made by using (BrainMesh: A Matlab GUI for rendering 3D mouse brain structures, 2020)).*

In our studies we focused on the mPFC, therefore later I will detail its structure and connectivity system after describing the function of this brain region.

1.3. The role of the PFC

The PFC plays a critical role in controlling different higher order cognitive functions (Fuster, 2006; Goldman-Rakic, 1988; Mesulam, 1998; Miller, 2000), including the processing of task-relevant information over other information which is not tightly connected to the given task, thereby PFC takes part in task-relevant behaviour. Overall, the PFC has been shown to be involved in various cognitive and emotional functions, such as working memory, planning, decision making related to emotional and fear behaviours (Cohen et al., 1996). The first famous case supporting the role of PFC in

emotional functions and decision making was the accident of Phineas Gage, whose left frontal lobe was destroyed by a large iron rod. After the accident his personality and behaviour have been changed radically, indicating that injury or lesion of distinct part of the brain could affect the personality and behaviour. All these functions supported by the widespread connectivity system of the PFC. Additionally, distinct parts of the PFC, the medial, the ventral and the lateral parts might contribute to all these functions in a unique way dictated by their specific connections. The medial and ventral parts, which are highly connected with the amygdala and hypothalamus, are involved in goal-directed tasks and emotional behaviour, while the lateral region provides the cognitive support for the temporal organisation of the PFC-linked cognitive processes and plays a role in forming the association between the cue and reward (Euston et al., 2012; Gabbott et al., 2005; Heidbreder & Groenewegen, 2003).

Among the aforementioned functions, the working memory was the first which was examined by using electrophysiological methods. This is a complex cognitive activity that is able to manipulate or hold the information for a short time, thereby contributes for example to comprehension, learning and reasoning (Baddeley, 1992). Since we have known that these functions are compromised in different psychiatric disorders such as schizophrenia, many animal and human studies aimed to uncover the exact neuronal operation linked to the working memory (Gilmartin & McEchron, 2005; Gilmartin et al., 2013). In addition to the working memory, distinct memory types are implicated during decision making or goal directed behaviour, which are required to accomplish the aims. Furthermore, several studies have investigated the role of the mPFC in long-term memory formation (Bontempi et al., 1999; Quinn et al., 2008). It has been established that the activity of mPFC immediately after a given task is required for retrieval on the following days. Various imaging and mPFC inactivation studies suggested that the mPFC takes part even more actively in retrieval of remote memory compared to the recent memory retrieval (Blum et al., 2006; Frankland & Bontempi, 2005; Maviel et al., 2004). Moreover, the mPFC participates in consolidation of distinct memories. Activation of the mPFC immediately after learning is also necessary for the memory consolidation (Akirav & Maroun, 2006; Carballo-Marquez et al., 2007; Leon et al., 2010; Tronel & Sara, 2003). Additionally, another theory exists related to the consolidation which highlights the role of the hippocampus. According to this, the hippocampus reactivates the recently learned

tasks during the rest periods by a replay of the activity patterns within the hippocampus and in downstream cortical regions, including the mPFC, which leads to the strengthening of memory formation (McClelland et al., 1995). The link between the hippocampus and mPFC is indicated by the coupling of local field potential changes: the hippocampal sharp waves and cortical low-voltages spindles follow each other in a temporarily precise manner within a hundred of milliseconds (Battaglia et al., 2004; Molle et al., 2006; Siapas & Wilson, 1998; Sirota et al., 2003).

In close relationship with memory functions, several studies investigated the role of the PFC in goal directed behaviours. This requires predictions about events, appropriate internal states, reflecting the inner and motivational states, and actions that are necessary to achieve a goal. For the predictions, association should be formed between the internal representations of a given task. The neurons within the PFC seem to do this: their activity reflects the learned association between cues, voluntary actions and rewards (Miller, 2000). Thus, during, for example, a given auditory discrimination task, the PFC coordinates the attention for task-relevant sensory cues (light flashes and different auditory stimulus), the control of motor actions (go or no-go), and monitoring of the outcome of each action (reward or punish).

Besides the working memory, goal directed behaviour and decision making, the PFC mediates cognitive and emotional processes supporting adaptive behaviours such as fear learning. This process has a prominent evolutionary aspect because this is essential for survival and allows animals and humans, to react, escape and learn from dangerous situations. As this is also a learning process, for the appropriate fear learning the exact operation and consolidation of different memories is also required. Besides the consolidation, other two main memory processes related to the fear learning have been described: the expression and extinction of conditioned fear memory, cognitive processes which are highly related to the mPFC and its connections with other brain regions, like the basolateral amygdala (BLA) (Marek et al., 2018; Peters et al., 2009). All together, we can see from this overview of PFC functions that its proper operation is necessary in different cognitive functions which are essential in normal brain functioning.

1.4. The structure of the mPFC

The mPFC could be divided into several subregions based on cytoarchitectonic features and connectivity (Figure 2). Importantly, the parcellation and nomenclature of distinct mPFC subregions varies substantially between authors (Le Merre et al., 2021; Van De Werd & Uylings, 2014). Here, we used the following parcellation: the anterior cingulate (ACC), the prelimbic (PrL), the infralimbic (IL) and the medial orbital (MO) cortices from the dorsal to ventral direction at different anterior-posterior levels (Allen Reference Atlas - Mouse Brain, atlas.brain-map.org).

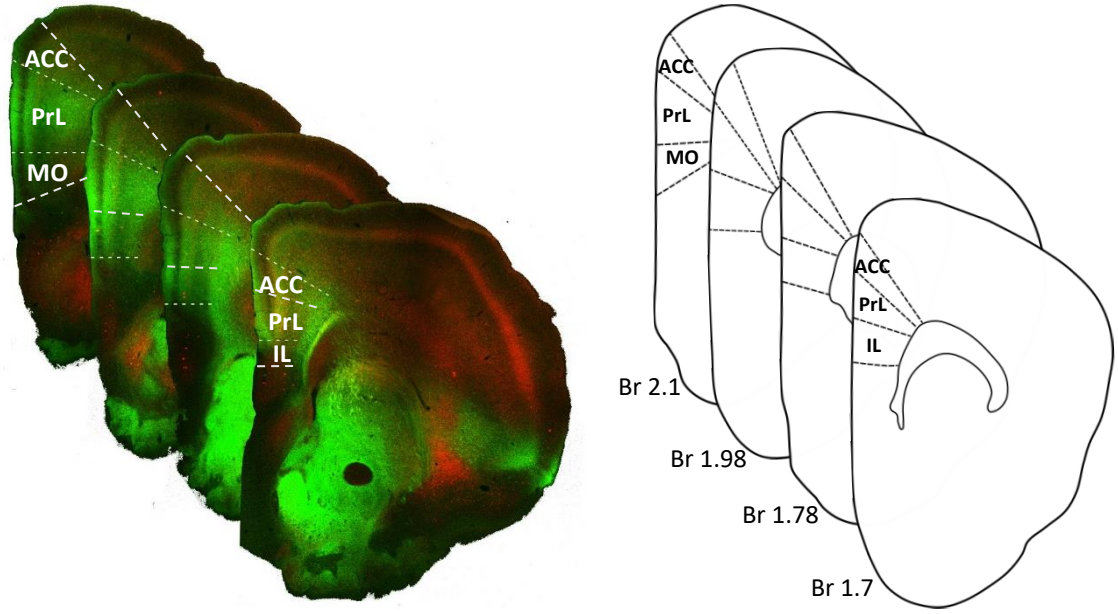

Figure 2: ***The structure of the mPFC.*** *Left panel: Axonal projection (green) from the MD thalamus defining the PFC. The density of axonal distribution outlines the borders of the mPFC. Red labels neurons expressing CCK. Right panel: consecutive coronal sections modified and taken from the online Allen Mouse Brain Atlas (Allen Reference Atlas - Mouse Brain,* atlas.brain-map.org*) showing the subregions of the mPFC. ACC: anterior cingulate cortex, PrL: prelimbic cortex, IL: infralimbic cortex, MO: medial orbital cortex.*

The dorsal border of ACC – between ACC and secondary motor cortex (M2) – can be defined by the change of the appearance of layer 2: in M2 this layer is generally homogeneous and in ACC it becomes darker and denser (Van De Werd et al., 2010). The main difference between ACC and PrL is noticeable in the arrangement of layer 5 cells:

in ACC, the layer 5 cells show columnar arrangement, whereas in PrL these cells appear in disorderly arrangement (Van De Werd et al., 2010). The PrL and IL can be differentiated by the homogeneity and inhomogeneity of the cells in different layer: in the PrL the layers are clearly distinguishable, while in IL these layers are homogeneous (Van De Werd et al., 2010). The border between PrL and MO, found only in the anterior part of frontal lobe, are hard to define. Similar to the IL, in the MO the cells show more homogeneous distribution in layer 2 and 3. Additionally, several studies use the nomenclature dividing the mPFC only to two regions based on functional criteria and the connectivity system of the subregions: the ventral part is composed of the IL and ventral PL, whereas its dorsal part consists of the dorsal PrL and ACC (Heidbreder & Groenewegen, 2003; Van De Werd et al., 2010). In contrast of the defined cytoarchitectonic differences between the distinct parts of the mPFC – based on previously rodent studies (Uylings et al., 2003; Van De Werd & Uylings, 2008) – like labelling the dopaminergic fibers, which shows differential distribution across the cortical subregions (Uylings et al., 2003), or PV and calbindin (Calb) staining, which have been used to define some cortical boundaries (Matyas et al., 2014), the borders in the mPFC could not be distinguished well (Van De Werd et al., 2010).

Moreover, it is important to notice that the laminar structure of the mPFC is different from the six layered cortical structures, because the granular layer 4 cannot be defined here, similarly to the other association cortices (Lein et al., 2007; Tasic et al., 2018; Uylings et al., 2003; Wang et al., 2018). The missing layer 4 is developed particularly in sensory cortices, which suggests that the processing of primary sensory information does not take place within the PFC. Different layers within the mPFC can be distinguished based on morphological/cytoarchitectonic changes of neurons. In layer 1, like in other cortices, only a few GABAergic neurons are located, while in layer 2/3 both PCs and GABAergic INs appear and show dense distributions. In layer 5, PCs possess larger cell bodies, than in layer 2/3 and 6. Moreover, due to the position of layers, we can distinguish superficial layers which consist of layer 1 and 2/3, and deep layers including layer 5 and 6 (Markham et al., 2007). In addition to all these well-described morphological/cytoarchitectonic properties of the cortical PCs, their neurochemical content can be a good marker to differentiate the distinct layers. In spite of the fact that Calb is not able to determine the border between the distinct parts of mPFC, it seems to

be a good marker for visualisation of the border between superficial and deep layers (Cruikshank et al., 2001; Van De Werd et al., 2010). Additionally, numerous layer 5 protein markers exist, like COUP-TF interacting protein (Ctip2) or calretinin which are capable to divide the PCs into target- or region-specific subtypes (Molnar & Cheung, 2006). Taken together, variegation of this layered structure suggests that it might have an important role not only in signal processing within the PFC, but in forwarding the information and communicate with other brain regions too.

1.5. Inputs and outputs of the mPFC

In contrast to the granular cortex, where the long-range excitatory inputs from the thalamus arrive into the layer 4 and the outputs arise from deep layers, in the mPFC this 'canonical circuit motif' cannot be applied due to the lacking layer 4. Instead, PCs located both in deep and superficial layers receive long-range excitation from distinct brain areas and send their long-range outputs to variety of their target areas (Figure 3) (Anastasiades & Carter, 2021). These projections of the mPFC have been mapped by retrograde and anterograde tracing methods. One of the most comprehensive studies, using the retrograde tracer wheat germ agglutinin conjugated with horseradish peroxidase (WGA-HRP), described several brain regions targeted by the mPFC in the rat (Gabbott et al., 2005). Moreover, in this study the high-resolution flat-map laminar density distribution of the retrogradely labelled mPFC cells showed that the PCs located in distinct layers and subdivision of the mPFC are differentially involved in the projections targeting the main subcortical areas (Gabbott et al., 2005). For example, PCs projecting to the dorsal striatum (DS) are located all over the layers across the mPFC with almost similar densities, while PCs labelled by tracer injection into the BLA or MD thalamus are restricted to distinct layers. BLA projecting cells are located in layer 2 and 5 and they are absent from the intermediate layer and layer 6, while MD thalamus projecting cells are restricted mostly to the deep layers, from the border of layers 5 and 6 and to layer 6 (Anastasiades & Carter, 2021; Gabbott et al., 2005). Overall, these observations indicated the widespread contribution of layer 5 PCs projecting to the subcortical regions, similarly to those found in other cortical structures: PCs located in layer 5 provide the major output of the mPFC towards subcortical areas with exception of the thalamus (DeFelipe & Farinas, 1992). All

these outputs can be associated with distinct functions which are present along the dorsal-ventral gradient in the mPFC. E.g., the ventral division of the mPFC, which consists of the IL and ventral PrL, takes part mostly in autonomic and emotional control (Gabbott et al., 2005; Heidbreder & Groenewegen, 2003). Particularly, the mPFC connections with periaqueductal gray (PAG) plays a prominent role in aggression, defensive behaviour, and modulation of pain, as the PAG is involved in these functions (Nelson & Trainor, 2007; Sewards & Sewards, 2002). Further, its unidirectional connections with the striatum participate in different learning-related actions, like reinforcement learning and reward-related behaviours (Balleine et al., 2007). Additionally, its bidirectional connections with the BLA have important roles in fear related behaviour, for example in expression and extinction of learned fear (Little & Carter, 2013; Marek et al., 2018; Sierra-Mercado et al., 2011), while its reciprocal connections with the MD thalamus contribute to proper operation of cognitive control and working memory (Bolkan et al., 2017; DeNicola et al., 2020). The ventral mPFC communicates with anterior insular areas, a cortical region which is involved in pain perception and aversive emotional processes (Jasmin et al., 2004). Furthermore, its bidirectional connections with the neuromodulatory systems, including the dorsal raphe (DR) and ventral tegmental area (VTA), have a prominent role in adaptive responses, including both rewarding or stressful situations (Kranz et al., 2010; Maier & Watkins, 2005). However, the function of mPFC-claustrum connections is not well understood, it is likely to play a role in various cognitive processes, like cortical control of behaviour (Jackson et al., 2018). Although the connectivity system of the dorsal part of mPFC, which is composed of the ACC and dorsal PrL, is similar to the ventral part, it has a stronger connection to the premotor and motor areas, and weaker connections to the emotional and autonomic systems (Gabbott et al., 2005; Heidbreder & Groenewegen, 2003). Interestingly, PCs located in the dorsal part of the mPFC project directly to the thoracic spinal cord (Euston et al., 2012; Gabbott et al., 2005), where they may influence local circuit operation.

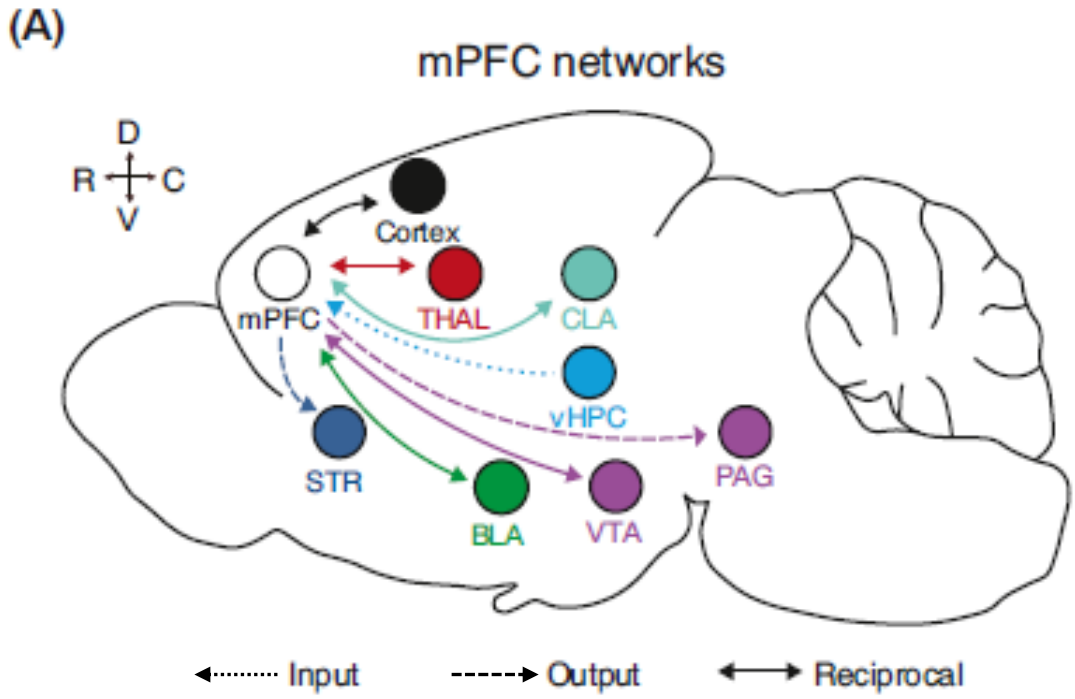

Figure 3: Key brain regions which are connected with mPFC. *Dotted line shows the afferent projection from the ventral hippocampus (vHPC), while dashed lines present the efferent projections to PAG and striatum (STR). Solid lines indicate the reciprocal connections of mPFC with the BLA, ventral tegmental area (VTA), claustrum (CLA), thalamus (THAL) and cortex. (Figure adapted from (Anastasiades & Carter, 2021)).*

The afferent projections of the PFC are at least as abundant as their efferent projections, indispensable for the proper function of this brain region. Several studies have examined the inputs of mPFC in rodents by using different methods. For instance, retrograde and rabies viral vector tracing studies were executed by injection of Fluorogold (FG) or rabies virus combined with adeno-associated virus into the different subregions of the rodent mPFC to reveal their afferents (Ahrlund-Richter et al., 2019; Hoover & Vertes, 2007). Each subdivision of mPFC received a specific set of afferents including projections from adjacent regions of mPFC, the insular and entorhinal cortices, CA1 region of the ventral hippocampus, BLA, midline and MD thalamic nuclei, VTA, DR, claustrum and contralateral cortices. Its unidirectional afferents from the hippocampus might have two possible roles: i) support the rapid associative learning and ii) provide the source of spatial

context (Jung et al., 1998; Spellman et al., 2015; Wise & Murray, 2000). Additionally, there is further evidence that these two regions are functionally coupled depicted by synchronous electrical activities. For instance, as I mentioned above, the hippocampal sharp wave ripple oscillations are followed by 10-14 Hz spindle oscillations in the mPFC and during spatial task the mPFC cell firing was phase locked to hippocampal theta oscillations (Adhikari et al., 2010; Benchenane et al., 2010; Colgin, 2011) . Interestingly, a shift has been observed dorsoventrally along the mPFC subregions regarding the thalamic afferents: sensorimotor/multisensory (non-limbic) cortical and thalamic inputs arrive to the dorsal part, where these afferents are integrated at, and involve this region in goal directed actions. In contrast, the ventral part receives primarily limbic cortical and thalamic inputs and participate in emotional and cognitive processes, suggesting that the distinct subdivisions of mPFC take part in different functions (Euston et al., 2012; Gabbott et al., 2005; Hoover & Vertes, 2007). Additionally, all the mPFC subregions strongly communicate with their adjacent regions, a connectivity motif, which may help the mPFC to exert its control over various functions (Hoover & Vertes, 2007). Overall, these studies demonstrated that mPFC establishes uni- and bidirectional connections with other brain regions and this complex afferent and efferent system of the PFC enables this region to fulfil an essential role related to the distinct higher order cognitive functions, goal-directed and emotional behaviour and its damage can cause impairments in these processes.

1.6. Excitatory principal neurons in cortical structures

Since spiny excitatory principal neurons compose the 80-85% of the whole cortical neuronal population and these cells provide the major output from the cortex to subcortical regions, in addition to the abundant cortico-cortical connectivity, to reveal their anatomical and electrophysiological features and operation is essential if one aims to understand the maladaptive operation in distinct psychiatric disorders. Principal neurons can be subdivided into two main groups in neocortical areas: the PCs and spiny stellate cells.

The name of PCs comes from their appearance: typically, they have a teardrop or rounded pyramid shaped soma, and their additional morphology is highly adapted to its functions

(Spruston, 2008). The single, thick apical dendrite emerges from the apex of the soma which rarely bifurcates to form two main apical dendrites. Usually, the apical dendrite spans through different layers and ramifies to oblique dendritic branches, which typically branch once or twice before terminating and composing the so-called dendritic tufts. These dendritic tufts often reach the pial surface. Additionally, numerous thinner basal dendrites emerge from the base of the pyramidal soma. Each basal dendrite branches up to several times before ending. This vertical asymmetries in the dendrites of PCs can add a further degree of specificity regarding to the inputs, as these often arrive in a layer specific manner (Megias et al., 2001). The apical and basal dendrites receive and integrate synaptic inputs arriving from different sources (DeFelipe & Farinas, 1992; Spruston, 2008). In neocortical structures, besides the typical pyramidal shape , the other well-known characteristic feature of PCs – similarly to spiny stellate cells – is that their dendrites are densely covered by spines (DeFelipe & Farinas, 1992). These structures provide the postsynaptic part of most excitatory glutamatergic inputs, while GABAergic inhibitory synapses target mostly the smooth dendritic shafts between the spines (Megias et al., 2001; Nimchinsky et al., 2002; Spruston, 2008; Yuste, 2011). Additionally, GABAergic inputs can arrive not only to the distal smooth dendritic parts, but they cover the soma, AIS and the proximal part of the dendrites (Megias et al., 2001), a membrane domain which compose together the perisomatic region of PCs (Freund & Buzsaki, 1996; Vereczki et al., 2016). The AIS is an essential part of the axon, where the summed up synaptic inputs coming from the dendrites and soma are translated to an output (Kole & Stuart, 2012; Somogyi, 1977). This part of the axon is targeted specifically by synapses of AACs (or ChCs), whereas the soma and proximal dendrites receive inputs from the BCs (Blackstad & Flood, 1963; Somogyi, 1977; Vereczki et al., 2016). Due to the proximity of these parts to the action potential generation site, the perisomatic region is a key part of PCs where their output can be controlled by PTIs most effectively (Cobb et al., 1995; Miles et al., 1996; Szabadics et al., 2006). Furthermore, GABAergic synapses arriving from dendritic INs innervate the distal dendritic parts of PCs where the excitatory and inhibitory inputs integrate during dendritic computation (Johnston et al., 1996; Lovett-Barron et al., 2012). This synaptic integration of the distinct inputs, which is an important function of PCs, can be influenced by the voltage-gated ion channels, present in the dendrites of PCs (Nusser, 2009, 2012). These channels make the dendrites excitable

and capable them to nonlinear integration (Johnston et al., 1996; Magee, 2000; Schulz et al., 2018). After PCs receive, compute, and forward information to the AIS, it transforms to an output signal driven by the collected information. Cortical PCs have only one axon emerging from the soma or proximal part of their dendrites and send collaterals locally as well as to cortical or subcortical regions. These cells use glutamate as a neurotransmitter and excite the other PCs and GABAergic INs via one or more synaptic contacts (Andrasi et al., 2017; Gulyas, Miles, Sik, et al., 1993; Miles et al., 1996). Their firing properties, correlating strongly with their inputs and intrinsic properties, show differences in the response of depolarizing current injection. Most PCs respond with a train of spikes that exhibits accommodation, while the others respond with a burst of action potentials. Previously, it was thought that PCs form a rather homogeneous population within a given cortical region, recent studies have revealed that several region- or even subregion-specific differences can be found within this cell population. For instance, as layer 5 PCs provide the major output of the cortex, several studies investigated their diversity uncovering many distinct subtypes in the past 15-20 years in different cortical regions based on their unique morphology, intrinsic physiological features, and synaptic properties (Hattox & Nelson, 2007; Le Be et al., 2007; Molnar & Cheung, 2006). The two major subtypes of layer 5 PCs were defined based on their distinct output target areas: the first group (type I or type A PCs) composed by so called pyramidal tract (PT) cells that innervate the ipsilateral pontine nuclei, target the thalamus, send axon to the spinal cord or ipsilateral striatum and cortices, while the second group often called intratelencephalic (IT) neurons (type II or type B PCs) similar to the first group innervate the ipsilateral cortex and striatum, but do not innervate the thalamus, moreover send their axons to the contralateral cortex and striatum, where the members of the type I PCs do not project (Anastasiades & Carter, 2021; Kawaguchi, 2017; A. T. Lee et al., 2014; Molnar & Cheung, 2006).

Spiny non-pyramidal stellate cells form the other cortical excitatory group. In contrast to the characteristic longitudinal shape of PCs, these cells show rather star-shape, vertically oriented morphology: they possess smaller and rounder cell bodies, more or less symmetric, vertically projecting, multipolar dendritic arborization and lack of extended apical dendrite to the pial surface. Moreover, their axonal appearance is also different: the axon of stellate cells originates from the basal part of soma, goes toward, but does not

enter to the white matter (Harris & Woolsey, 1983; Staiger et al., 2004). They innervate primarily their neighbouring stellate cells as well as superficial PCs.

The heterogeneity of PCs suggests that they contribute to network computation in various ways which suggests that their proper function in cortical structures is essential for appropriate cognitive processing.

1.7. GABAergic inhibitory neurons in the cortex

In cortical regions the information processing depends on the precise control of PC firing. Although GABAergic inhibitory cells compose only 15-20% of the entire neuronal population in the cortex, they operate precisely together with the PCs and control their function in a well-defined manner. Due to their morphological and physiological characteristics, GABAergic inhibitory neurons can be easily distinguished from the PCs: they dispose a round or oval shape soma, their dendrites are usually aspiny, and their axon is emitted from the soma or proximal dendritic parts and it densely arborizes around or near the cell except the long-range projection GABAergic cells (Gulyas et al., 2003; Jinno et al., 2007; Kubota et al., 2016; Tremblay et al., 2016). Moreover, in contrast to the PCs, cortical GABAergic cells exert their inhibitory effects via ionotropic $GABA_A$ or metabotropic $GABA_B$ receptors (Connors et al., 1988; Mody et al., 1994; Tamas et al., 2003).

Despite their small number, GABAergic INs display a prominent heterogeneity regarding morphological, electrophysiological, and neurochemical or transcriptomic features. Due to this variety among the GABAergic cells, their classification posed difficulties for researchers (DeFelipe et al., 2013; Petilla Interneuron Nomenclature et al., 2008). The most important property of this classification should be the applicability across the different brain regions, including the neocortical structures, hippocampus and amygdala. In the Petilla terminology a list of the essential features that differentiate GABAergic IN types in the neocortex was assembled (Petilla Interneuron Nomenclature et al., 2008). Regarding to morphological features, the researchers highlighted four main properties to differentiate GABAergic INs: the shape, size and orientation of somata; the size and orientation of dendrites; the morphology of axons; the connections, so their postsynaptic

targets which link the function of INs and the spatial characteristics of their axons (Petilla Interneuron Nomenclature et al., 2008). Using mainly the axonal arborization of the INs, eight well-defined groups can be observed across different species (Mihaljevic et al., 2019). According to physiological properties of GABAergic INs, the passive and subthreshold properties or the waveform characteristic of action potentials, the firing pattern and postsynaptic responses can be a good parameter to characterise a given cell type. For example, based on the firing patterns of GABAergic cells, the Petilla terminology differentiates fast-spiking, non-adapting and non-fast spiking, adapting, irregular spiking, intrinsic burst firing and accelerating cell subgroups (Petilla Interneuron Nomenclature et al., 2008). Additionally, the continuously developing gene sequencing techniques allow us to group GABAergic neurons more detailed based on their gene expression profiles. With the help of this classification method, five main subpopulations of GABAergic neurons can be distinguished, including PV, SST, VIP, synuclein gamma (Sncg) and lysosomal-associated transmembrane protein 5 (Lamp5) (Gouwens et al., 2020).

In spite of these different classifications based on axonal arborization, firing properties or transcriptomic features, probably the most wide-spread classification of GABAergic neurons is based on their function dictated by their postsynaptic target preference. Regarding to this feature, INs can be divided into four categories (Figure 4) (Kepecs & Fishell, 2014; Klausberger & Somogyi, 2008). The first group is composed by the PTIs (Figure 4, blue circles), i.e., INs that target the proximal dendrites, AIS and soma of PCs. Thus, the inhibition arriving via $GABA_A$ receptors to these membrane domains can influence mostly the spiking activity of PCs due to the spatial closure of the action potential generation site. The two main subpopulations of this group are composed by the distinct BC types and the AACs or ChCs (Freund & Katona, 2007; Kepecs & Fishell, 2014; Somogyi et al., 1998). The dendrite targeting INs belong to the second group (Figure 4, red circle). They innervate the distal part of the dendrites of PCs, thereby regulate the information processing in the early phase. The inhibition arriving to these parts can selectively block the initiation of dendritic action potentials without reducing the ability of the cells to discharge axonal action potential (Larkum et al., 1999; Miles et al., 1996). Two well-studied members of this group, namely Martinotti cells and neurogliaform cells, were investigated thoroughly in the last decades. Martinotti cells

located predominantly in deep layers send axon collaterals to upper layers and provide ionotropic $GABA_A$ receptor-mediated inhibition over the apical dendrites of PCs. In contrast, neurogliaform cells are located often in layer 1, thus these cells inhibit only the distal part of apical dendrites of PCs via $GABA_A$ and G-protein coupled $GABA_B$ receptors (Murayama et al., 2009; Palmer et al., 2012; Tamas et al., 2003). In contrast to these two groups, members of the third group, the interneuron-selective interneuron (Figure 4, black circle), innervate exclusively other inhibitory neurons. This inhibition over the local INs might result in disinhibition of PC populations, which can provide an additional level of control neuronal activity (Acsady et al., 1996; Gulyas et al., 1996; Hajos et al., 1996; Pi et al., 2013). Additionally, there is evidence that another specialized subpopulation, the fourth group of GABAergic inhibitory cells send long-range axonal projection to subcortical and other cortical areas (Figure 4, green circle), thereby these cells may play a role in synchronizing the activity of distal brain regions during slow wave sleep in contrast of the other IN types (Gulyas et al., 2003; Higo et al., 2009; Tomioka et al., 2005; Toth & Freund, 1992).

In addition to the functional variety showed by GABAergic neurons, all defined subtypes can be further differentiated based on their molecular features. These molecules are used to distinguish the different type of cortical INs and be grouped regarding to their functions. Thus, INs can express neuropeptides, calcium binding proteins, transcription factors, distinct kinds of neurotransmitters and neurotransmitter receptors, structural proteins, ion channels, connexins, pannexins or membrane transporters (Petilla Interneuron Nomenclature et al., 2008). For instance, PTIs often express PV which is a calcium binding protein or CCK which is a neuropeptide. In terms of the dendrite targeting INs, the somatostatin- and neuropeptide Y-expressing (SST, NPY) cells compose the neuropeptide-expressing subgroups, while the Calb-containing INs belongs to the calcium binding protein-expressing subgroups. The interneuron-selective interneurons express mostly either vasoactive intestinal polypeptide (VIP) or calretinin, the latter which is a calcium binding protein. The projecting GABAergic neurons often contain SST and NPY similar to dendrite targeting neurons, but these cell can express neuronal nitric oxide synthase (Sik et al., 1994; Tomioka et al., 2005). Noticeably, the distinct neurochemical markers and molecules can be co-expressed in GABAergic neurons that makes the whole population more and more variegated. In summary, cortical

INs can be organized into several subclasses based on their morphological and neurochemical features.

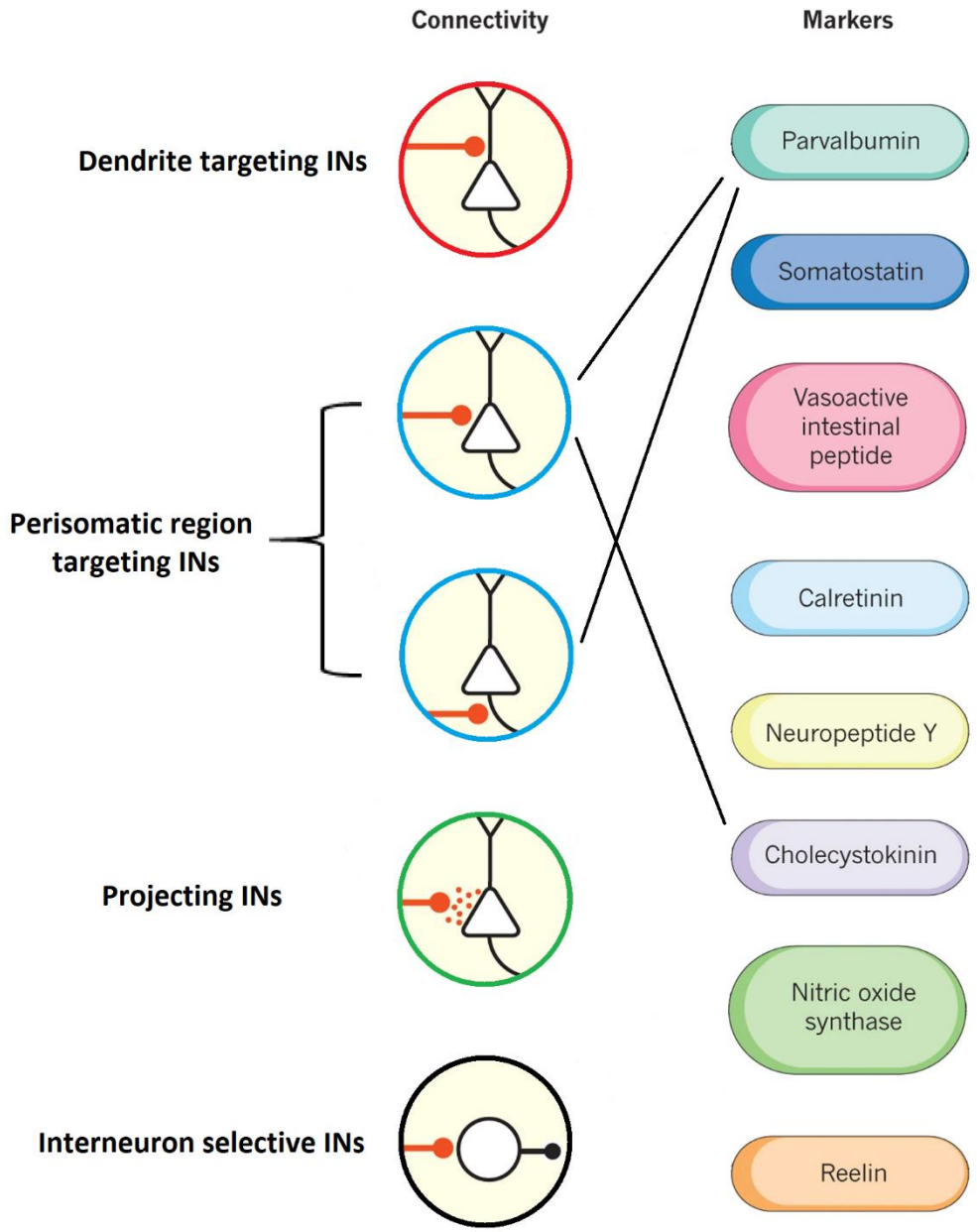

Figure 4: ***Classifying GABAergic neurons in the cortex.*** *Major GABAergic subclasses and cell types recognized by functional and molecular studies. In the middle panel the postsynaptic preferences are presented. Red circle shows the dendrite targeting INs, blue circles depict the perisomatic region targeting INs: soma and proximal dendrite targeting INs and AIS targeting INs are indicated. Projecting GABAergic cells are shown with green circle and interneuron selective INs with black circle, as the subscriptions indicate*

on the left side. On the right side the expressed neurochemical markers are listed. Black lines indicate the major neurochemical content of PTIs (Figure adapted and modified from (Kepecs & Fishell, 2014))

As it was previously mentioned, cortical GABAergic neurons receive numerous excitatory inputs from local axon collaterals of PCs and from distal PCs via long-range inputs, as well as from thalamic afferents (Delevich et al., 2015; McGarry & Carter, 2016; Yang et al., 2021), which alone or combined can drive their firing. The output of GABAergic cells provides an inhibitory brake over the network activity (Isaacson & Scanziani, 2011; Swanson & Maffei, 2019). The drop of this inhibitory brake makes possible to generate synchronized firing in PCs, if it occurs periodically, contributing to oscillatory patterns at different frequencies in the cortex (Isaacson & Scanziani, 2011). For example, in cortical regions, PV-expressing neurons generate gamma oscillations, while SST INs play a critical role in theta oscillations (Fanselow et al., 2008; Gulyas et al., 2010; Sohal et al., 2009). Synchronous neuronal activity between different brain regions is required for working memory, memory retrieval, cognitive integration and information processing (Swanson & Maffei, 2019). The morphological, physiological and neurochemical heterogeneity of GABAergic INs suggests their distinct functional role playing in normal brain functioning. To understand the proper mechanisms behind this, we should know the exact properties of different types of GABAergic cells.

1.8. PTIs in cortical structures

Since PTIs provide inhibitory synapses onto the perisomatic region of PCs, where the spike generation can be controlled the most effectively, they are in the centre of numerous research (Cobb et al., 1995; Freund & Katona, 2007; Kawaguchi & Kondo, 2002; Kepecs & Fishell, 2014; Miles et al., 1996; Somogyi et al., 1998). The perisomatic region of a PC consist of the soma, the proximal part of their dendrites – around the first 100 µm from the soma (Megias et al., 2001; Papp et al., 2001; Vereczki et al., 2016) – and the AIS, which extends to ~40-80 µm from the soma (Huang & Rasband, 2018; Leterrier, 2018). Additionally, the AIS disposes the lowest threshold for action potential generation between 20-40 µm from the soma (Kole et al., 2008; Kole & Stuart, 2012; Stuart & Sakmann, 1994) and this region of the AIS is innervated by the highest density of

GABAergic inputs (Veres et al., 2014). PTIs in cortical structures are composed by two BC types, expressing either PV or CCK/CB1, which target the soma and proximal dendrites of PCs, and AACs or ChCs, which innervate their AIS and avoid the other compartments (Figure 5) (Freund & Katona, 2007; Kepecs & Fishell, 2014; Somogyi et al., 1998).

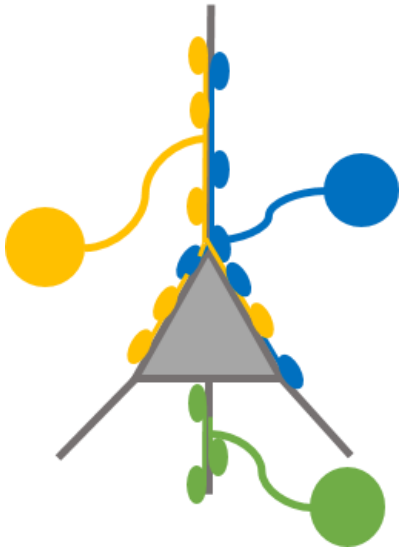

Figure 5: ***Schematic representation of the three PTIs innervating the different membrane domains of PCs.*** *In the middle of the figure a PC in grey is showed surrounding by the three different PTIs. A CCK/CB1 BC and a PVBC are shown in blue and orange, respectively. These two types of BCs innervate the soma and the proximal dendrites of PCs. In contrast, an AAC in green innervates exclusively the AIS of PCs.*

In addition to the difference between the targeted membrane domains of PCs, the BCs and AACs can be distinguished based on their morphological and electrophysiological features. BCs in frontal cortical regions are defined as at least 10% of their boutons should terminate on the soma of PCs (Karube et al., 2004). However, the ratio of this somatic and perisomatic contacts provided by the BCs show differences between distinct brain regions. In the neocortex, only 25-30 % of BC terminals innervate the perisomatic region of PCs evaluated by electron microscopy (Kisvarday et al., 1986) whereas in the amygdala around half of the boutons target the perisomatic regions, while in the hippocampus up to 80% of terminals contact these sites of PCs (Freund & Katona, 2007; Somogyi et al., 1998; Tamas et al., 1997; Vereczki et al., 2016). Individual BCs innervate single PCs with several boutons, and higher number of terminals can increase the efficacy

of inhibition (Gulyas, Miles, Hajos, et al., 1993; Kubota et al., 2015; Miles et al., 1996). Additionally, a single BC can target hundreds of PCs simultaneously, thereby they can synchronise their firing (Kubota et al., 2015; Vereczki et al., 2016; Veres et al., 2017). AACs target exclusively the AISs of postsynaptic PCs. Traditionally, different nomenclature is used for the same type of INs; the name chandelier cell (ChC) is traditionally used in the cortex, including the mPFC, while INs with the same morphology and target properties are called axo-axonic cells (AACs) in other brain regions, such as the hippocampus and amygdala. Examining their innervation profiles, a single AAC innervates hundreds of PCs with distinct number of boutons (Somogyi et al., 1982) and 3-6 AACs might participate in the innervation of single AISs of PCs in different cortical structures (Inan et al., 2013; Somogyi et al., 1982; Veres et al., 2014). Overall, the PTIs compose a large, heterogeneous, and important population of GABAergic inhibitory neurons and their function is essential for the precise inhibition and synchronization of PCs.

1.8.1. CCK/CB1-expressing basket cells

CCK is a gastrointestinal peptide which can be expressed in many neuron types within the central nervous system. Even CCK is one of the most abundant neuropeptides in the brain, its release mechanism under physiological condition is not well-known due to the degradation of peptide in tissue (Lee & Soltesz, 2011; Toledo-Rodriguez et al., 2005). Heterogeneity of CCK-expressing INs has been demonstrated by several studies in different brain regions (Bodor et al., 2005; Kubota & Kawaguchi, 1997; Nguyen et al., 2020; Rovira-Esteban et al., 2019). For example, the existence of two different CCK-expressing IN types have been shown in the neocortex in rodents: one is the small bipolar CCK-positive INs which often express calretinin, the other is the large multipolar INs which express CB1 and Calb (Bodor et al., 2005; Kubota & Kawaguchi, 1997). Moreover, in the PrL two molecularly different type of CCK-expressing INs were found in a recent study: one which showed fast spiking phenotype and expressed PV, while the other fired with regular spikes and lacked this calcium binding protein (Nguyen et al., 2020). Beside the neocortex, in the hippocampus several distinct populations of CCK-expressing INs was described and distinguished based on their axonal arborization and molecular

markers (Lasztoczi et al., 2011; Szabo et al., 2014). Furthermore, in the basal nucleus of the amygdala and the frontal cortex the majority of CCK-positive neurons express either the type 3 vesicular glutamate transporter (VGlut3), Calb or VIP (Kawaguchi & Kubota, 1997; Mascagni & McDonald, 2003; Rovira-Esteban et al., 2017). In addition, PCs can also express CCK which fact makes more difficult the selective examination of CCKBCs (Mascagni & McDonald, 2003; Taniguchi et al., 2011). In cortical structures none of these CCKBCs express PV, therefore the two BC types can be easily distinguished (Kawaguchi & Kubota, 1998). Generally, the CCKBCs have large soma and multiple smooth dendrites, their single axon emanates from the soma and arborizes densely (Freund & Buzsaki, 1996; Kawaguchi & Kondo, 2002; Vereczki et al., 2016). In the hippocampus the axonal boutons of CCKBCs contact their targets via several synapses and use N type voltage-gated calcium channels to mediate the Ca^{2+} influx during transmitter release (Hefft & Jonas, 2005; Takacs et al., 2012; Wilson et al., 2001). Additionally, in these brain regions, CCKBCs show regular spiking profile with accommodation. These cells possess slow membrane time constant which enable them to summarize the independent afferent excitatory and inhibitory events over a longer time window. CCKBCs receive weak and depressing excitation from local PCs which conduct to respond less likely to the repetitive activation of inputs but enable CCKBCs to integrate sequential activity of independent inputs (Andrasi et al., 2017; Glickfeld & Scanziani, 2006; Hefft & Jonas, 2005). In addition to the excitatory inputs, these cells are strongly innervated by calretinin-expressing INs and receive inhibitory inputs from other CCKBCs in the amygdala and hippocampus (Andrasi et al., 2017; Gulyas et al., 1996; Kohus et al., 2016). The output of CCKBCs is not only regulated by the firing but also via the effects of the retrograde messengers, the endocannabinoids that are endogenous lipophilic molecules (Katona & Freund, 2008). Endocannabinoids possess their affects via CB1 receptors which are G-protein coupled receptors and found in the axon terminals of CCKBCs. The endogenous ligands of CB1, like the anandamide and 2-arachidoniol-glycerol are released from the postsynaptic neurons and bind to CB1 receptors on the presynaptic cells, leading to the decrease in neurotransmitter release (Katona & Freund, 2008; Wilson & Nicoll, 2001). This process is called depolarization-induced suppression of inhibition (Pitler & Alger, 1992). In addition, a single CCKBC contacts the local PCs via several boutons. Neurotransmitter release via several boutons with numerous release sites generates long-

lasting, fluctuating and asynchronous inhibition on PCs and results in loose, not accurate response in the postsynaptic neurons in the hippocampus (Glickfeld & Scanziani, 2006; Hefft & Jonas, 2005). So far, our knowledge about CCKBCs is limited regarding *in vivo* studies. Only a few papers have investigated the firing properties and their contribution to rhythm generation of the CCKBCs in the hippocampus (Dudok, Klein, et al., 2021; Klausberger et al., 2005). These findings showed that CCKBCs discharged during the ascending phase of theta rhythm and none of them showed any correlation to the ripple episode (Klausberger et al., 2005). Besides this, a recent *in vivo* paper presented the role of CCK-expressing INs during the retrieval or use of working memory representations in the PFC (Nguyen et al., 2020). The function of these neurons was correlated in the appearance of schizophrenia also (Curley & Lewis, 2012; Eggan et al., 2008). Eggan et al. demonstrated that the CB1 level significantly decreased and highly correlated with the schizophrenia in the dorsolateral PFC of human patients. This reduced level of CB1 receptors may lead to the increased GABA release from CCK INs which could contribute to working memory impairments in schizophrenia (Eggan et al., 2008). Although, all these data suggest that CCKBCs might play a role in several important brain functions, the details of their morphological and electrophysiological properties are still largely elusive especially in the mouse mPFC.

1.8.2. PV-expressing basket cells

PV-expressing neurons are one of the most investigated IN types in cortical neuronal networks. PV is a calcium binding protein and has a role in buffering the Ca2+ ions by which impacts the cell function. PV is expressed in basket cells, AACs or ChCs and dendritic inhibitory neurons like bistratified and oriens-lacunosum moleculare cells in the hippocampus (He et al., 2016; Kawaguchi & Kubota, 1997; Klausberger et al., 2004; Taniguchi et al., 2013). Generally, PVBCs have round or oval shape soma, their dendrites are smooth, multipolar, radially oriented and densely branched (Freund & Buzsaki, 1996; Lagler et al., 2016; Tukker et al., 2013; Vereczki et al., 2016). Their single axons originate from the soma or one of the proximal dendrites and form basket-like structurers around the soma and proximal dendrites of their postsynaptic neurons (Kawaguchi & Kubota, 1997). In rat PrL, these axons are mostly restrained to the layer where the soma locates

and to the neighbouring layers (Lagler et al., 2016). In contrast to CCKBCs, PVBCs show a fast spiking firing pattern due to their unique Kv3 potassium channel expression (Rudy & McBain, 2001). On average, PVBCs receive two-, three times more excitatory inputs than CCKBCs (Andrasi et al., 2017; Freund & Katona, 2007; Gulyas et al., 1999; Matyas et al., 2004). Interestingly, the number of contacts originating from single PCs differs between the distinct brain regions. For instance, PVBCs in the hippocampus are often innervated via few synaptic connections from PCs, while in the cortex and in the amygdala they receive several boutons from individual PCs (Andrasi et al., 2017; Buhl et al., 1997; Gulyas, Miles, Sik, et al., 1993; Karlocai et al., 2021; Kuramoto et al., 2022; Sik et al., 1993). The larger number of excitatory inputs generate a higher excitation in PVBCs with higher amplitude than it was detected in CCKBCs in the hippocampus and amygdala (Andrasi et al., 2017; Glickfeld & Scanziani, 2006). Furthermore, excitatory synapses received by PVBCs contain special GluR4 calcium permeable AMPA receptors (Geiger et al., 1995), which can play a role in long term potentiation at excitatory synapses (Mahanty & Sah, 1998; Nissen et al., 2010). Besides the excitatory inputs, PVBCs receive inhibition from VIP-, SST- and other PV-expressing neurons, but not from calretinin-expressing INs (Gulyas et al., 1996; Hioki et al., 2013; Kohus et al., 2016; Pfeffer et al., 2013).

PVBCs provide strong, precise and fast inhibition on their postsynaptic partners. In the neocortex the strength and the effect of this inhibition is decreased with the distance from the soma of BCs which means that the number of synapses and the size of inhibitory postsynaptic currents (IPSCs) also decrease (Packer & Yuste, 2011). These observations suggest that PVBCs prefer to innervate PCs in a distance dependent manner (Packer & Yuste, 2011). In contrast to the irregular shape and often inseparable synapses observed on the axon terminals of CCKBCs, small, clearly separated and round or oval shape synapses were found on the boutons of PVBCs in the hippocampus (Takacs et al., 2015). In addition, the release of transmitter molecules occurs upon opening of P/Q type calcium channels on the axon terminals. The presence of this type of calcium channels ensures the synchronous transmitter release from PVBC axon endings over asynchronous release (Hefft & Jonas, 2005; Szabo et al., 2010). In contrast to CCKBCs, the fast and precisely timed inhibition provided by PVBCs over a large population of PCs make them capable to generate fast oscillations, like gamma oscillations and sharp-wave ripples (Gulyas et

al., 2010; Schlingloff et al., 2014; Sohal et al., 2009). The latter oscillation occur during slow-wave sleep and consummatory behaviour when PVBCs fired at high frequencies at the troughs of sharp-wave associated ripples (Dudok, Klein, et al., 2021). Gamma oscillations are required for the correct functioning of working memory and it seems to largely correspond to synchronous IPSCs in PCs originating from PVBCs (Atallah & Scanziani, 2009; Buzsaki & Wang, 2012; Klausberger et al., 2003; Sohal et al., 2009). In addition to fast oscillations, during the theta oscillations PVBCs discharge on its descending phase (Klausberger et al., 2003; Varga et al., 2014). Moreover, the firing of these cells was coupled to local spindle oscillation in the PFC and fired at the trough and early ascending phase of this oscillations (Hartwich et al., 2009). In summary, due to the fact that PVBCs can be unequivocally identified, several morphological and functional studies have already been investigated their features in the PFC (Delevich et al., 2015; Gabbott et al., 2006; Kim et al., 2016; Lagler et al., 2016). Their important function and contribution for generating different types of oscillations suggest that PVBCs have a critical role in the network operation and dysfunction of these cells can lead to development of various mental problems, including schizophrenic or epileptic disorders.

1.8.3. Axo-axonic or chandelier cells

The third group of PTIs is composed by AACs or ChCs that often express PV: these cells form synapses almost exclusively on the AIS of PCs which has the lowest threshold for action potential generation due to the high number and density of voltage-gated sodium channels (Lorincz & Nusser, 2010; Somogyi, 1977; Stuart & Sakmann, 1994). These cells have round and smaller somata which results in a higher input resistance and smaller capacitance in comparison to PVBCs. The dendritic length of ChCs is shorter and the end of the dendrites often arborize. In the PFC, these dendritic branches reach the surface of the pia where they bend (Kawaguchi, 1995; Massi et al., 2012; Taniguchi et al., 2013). Their axons show characteristic cartridges and form “candle stick” like structures around the AISs of PCs in the cortex, providing the reason for naming them as chandelier cells (Szentagothai & Arbib, 1974). The electrophysiological properties of ChCs are very similar to that of PVBCs: these cells can respond to current injection steps with a high frequency and show fast repolarisation (Barsy et al., 2017; Kawaguchi, 1995; Papp et al.,

2013). Their firing does not show an accommodation similarly to PVBCs. In contrast to PVBCs, however, these cells do not innervate each other, or other INs (Kisvarday et al., 1986; Kohus et al., 2016; Somogyi et al., 1982), but they can connect to each other via gap junctions at their dendrites (Andrasi et al., 2017). This gap junctions may help to synchronize the activity of ChCs, thereby contribute to the synchronization of the PC activity (Tamas et al., 2000). Alternatively, the gap junction coupling may help to de-synchronize their activity like it has been shown for cerebellar Golgi cells (Vervaeke et al., 2010). In addition to the differences in their morphological and electrophysiological features, ChCs and PVBCs can be distinguished based on their neurochemical content, which shows diversity between brain regions and species. For instance, in the mouse mPFC only a small fraction of ChCs express the calcium binding protein PV, while in the barrel cortex the co-localization reached 50% (Taniguchi et al., 2013). Moreover, ChCs do not express Calb, while PVBCs do in the rodent amygdala (Bienvenu et al., 2012; Vereczki et al., 2016), whereas in human temporal cortex some ChC showed immunoreactivity for Calb (del Rio & DeFelipe, 1997). In addition, calretinin can be also expressed in some of the ChCs in the hippocampus (Ishino et al., 2017).

In the mPFC ChCs receive excitatory inputs from PCs (Lu et al., 2017), while PV- and VIP-expressing INs can inhibit them (Lu et al., 2017). In contrast to PVBCs, SST-expressing GABAergic cells do not innervate these cells (Lu et al., 2017). Regarding the output features and connectivity pattern of ChCs, single ChCs innervate individual AISs with 4 boutons on average in the somatosensory cortex and around 3-4 ChCs converge on single AISs, which suggests that ChCs compose a densely overlapped population (Inan et al., 2013). Additionally, a recent study in mice PrL revealed that ChCs had few reciprocal connections from PCs and showed unidirectional, highly selective connectivity pattern, in contrast to PVBCs which possessed extensive and nonselective reciprocal connections with PCs (Lu et al., 2017). Based on these data, ChCs may ensure a highly directional microcircuit operation and mediate the dynamic segregation and hierarchical interaction of selected PCs (Lu et al., 2017). The other main difference between PV-expressing ChCs and PVBCs is their output features and their effect on the postsynaptic PCs. There is some evidence that in a few brain areas ChCs can excite or inhibit their postsynaptic partners depending on the state of the postsynaptic neurons, including the resting membrane properties, the reversal potential for the chloride ion in the AIS and the

increasing bicarbonate ion efflux from the AIS, thereby activating the KCNQ potassium channels which dampen the excitability and reduce the probability of action potential (Jones et al., 2014). For instance, in the cortex ChCs can excite or inhibit their postsynaptic partners *in vitro* (Szabadics et al., 2006*)*, while in the hippocampus they seem to have solely inhibitory actions both *in vitro* (Glickfeld et al., 2009) and *in vivo* (Dudok, Szoboszlay, et al., 2021). Beside this difference, several *in vivo* and *in vitro* studies proved that the activity of ChCs does not overlap with the activity of PVBCs during distinct brain oscillations (Joshi et al., 2017; Klausberger & Somogyi, 2008; Massi et al., 2012; Varga et al., 2014). During theta rhythm, AACs fired preferentially before the peak of the theta cycle, in the ascending phase, while the PVBCs increased their firing activity during the descending phase. In addition, firing of AACs during the sharp-wave ripples is suppressed, thus, these cells do not fire in contrast of PVBCs which fired with one or several spikes per ripple episode in the hippocampus (Hajos et al., 2013; Klausberger et al., 2003; Klausberger & Somogyi, 2008; Viney et al., 2013). Taken together, due to the recently developed specific labelling technique of ChCs, we have gained insights into their morphological and connectivity features in distinct cortical structures, including the PrL (Lu et al., 2017; Massi et al., 2012; Taniguchi et al., 2013). Moreover, these data and comparison suggest that AACs/ChCs and PVBCs are driven by different excitatory inputs and might have a distinct role in the function of cortical networks.

1.9. Organization of microcircuits within the mPFC

In cortical regions different functional microcolumnar systems are found where distinct information is represented in a supramodal manner (Duncan, 2001; Miller, 2000). This mechanism could generate, process and store different incoming information at higher levels with less details (Tettamanti & Weniger, 2006). One of the best examples for this information processing is the barrel cortex, where each column represents a given whisker (Petersen, 2007). Although, our knowledge is still limited about the exact operation of microcircuits in the mPFC, it presumably functions similarly to other cortical region with the exception of missing layer 4. PCs located in layer 2/3 of mPFC receive long-range inputs from a wide range of brain regions, such as from the hippocampus, amygdala,

VTA, MD thalamus, contralateral mPFC and DR (Hoover & Vertes, 2007). Next, these cells send the information within their columns and target PCs in layer 5 (Cheriyan & Sheets, 2018; Collins et al., 2018). Some evidence suggest that these connections are topographically organized interlaminar projections, so PCs located in the upper part of layer 2/3 target PCs in the upper part of layer 5, while PCs in the bottom part of layer 2/3 innervate PCs located in the bottom part of layer 5 (Otsuka & Kawaguchi, 2008). In addition to these interlaminar inputs from layer 2/3 PCs, layer 5 PCs receive long-range inputs from distinct brain areas, like thalamus, amygdala and limbic neuromodulatory regions (Bolkan et al., 2017; DeNicola et al., 2020). Moreover, callosal inputs can arrive on the layer 5 PCs, too (Anastasiades et al., 2018; A. T. Lee et al., 2014). Finally, the layer 5 PCs integrating this convergent information provide the major output of mPFC and send efferent projections to several ipsi- or contralateral downstream cortical and subcortical regions (Anastasiades & Carter, 2021; Kawaguchi, 2017; A. T. Lee et al., 2014; Molnar & Cheung, 2006). Additionally, there is some evidence that layer 5 PCs can project back and innervate layer 2/3 PCs (Hirai et al., 2012). In addition to the interlaminar projections, the intralaminar communication between PCs is also abundant (Brown & Hestrin, 2009; Harris & Shepherd, 2015; Printz et al., 2023).

To make the whole intra- and interlaminar information processing more colourful, the inhibitory INs located in different layers also receive local and long-range excitatory inputs from different brain regions and control the excitation-inhibition balance. As a result of these two types of excitation received by INs, inhibitory cells can provide feedback or feedforward inhibition on local PCs. The feedback inhibition is defined when cortical PCs target with their excitatory inputs the local INs that in turn innervate PCs with their inhibitory synapses. This type of inhibition limits the actual activity of a given set of PCs. Feedforward inhibition is generated when long-range excitatory inputs innervate both PCs and INs, thereby limiting the network excitation (Isaacson & Scanziani, 2011). Important to notice, that due to their electrophysiological properties, both BC types are able to generate feedforward and feedback inhibition in cortical circuit, as shown in the hippocampus (Basu et al., 2013; Glickfeld & Scanziani, 2006; Knowles & Schwartzkroin, 1981; Zemankovics et al., 2013). Through these types of inhibition of

neighbouring PCs, GABAergic INs provide an effective regulation in excitatory signalling by controlling the spike generation and timing.

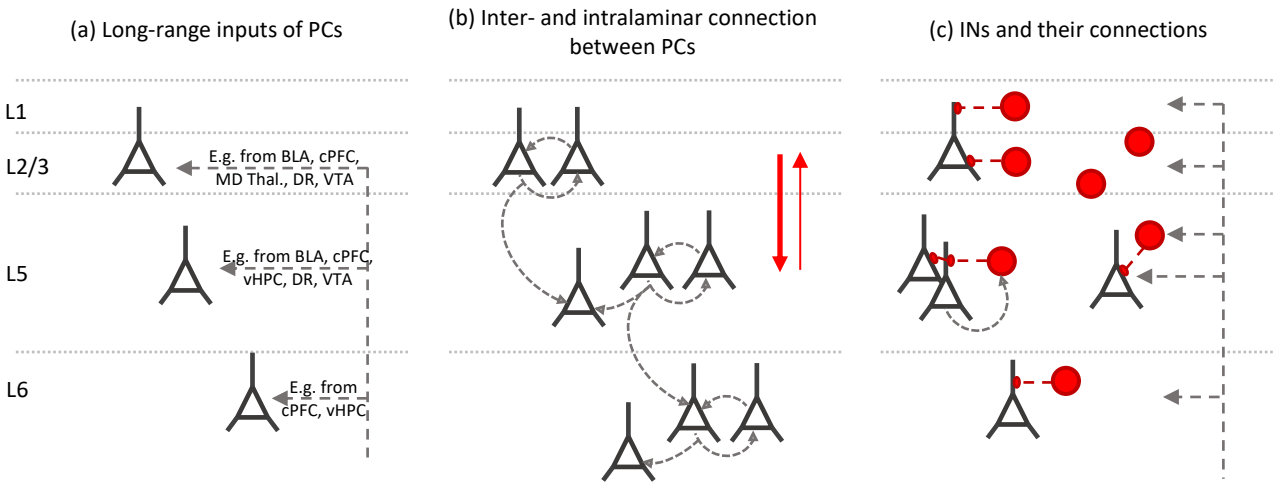

Figure 6: ***Schematic representation of microcircuit organization within the mPFC.*** *(a) Left panel represents the long-range inputs of pyramidal cells located in distinct layers. L1: layer 1, L2/3: layer 2/3, L5: layer 5, L6: layer 6, PC: pyramidal cell, BLA: basolateral amygdala, cPFC: contralateral PFC, MD. Thal.: mediodorsal nucleus of thalamus, vHC: ventral hippocampus, VTA: ventral tegmental area, DR: dorsal raphe. (b) Middle panel shows inter-and intralaminar connections of pyramidal cells. Red arrows (c) Right panel represents interneurons and their connections. In L5 the feedback- and feedforward inhibition are presented, too. Grey triangles represent PCs, while red circles show distinct INs. Dotted lines show the border between layers. Dashed lines indicate the connections and projections from different regions and between PCs and INs. The arrows at the end of dashed lines indicate excitatory connections, while small circles indicate inhibitory connections.*

Several studies determined the presence of feedforward inhibition in the mPFC by examining excitatory inputs from distinct brain regions (Anastasiades et al., 2018; Delevich et al., 2015; Dilgen et al., 2013; McGarry & Carter, 2016). For instance, although the BLA sends excitatory inputs, the stimulation of this region predominantly inhibits the cell firing in the PFC (Dilgen et al., 2013; McGarry & Carter, 2016). This discrepancy could be explained if the inhibitory INs were primarily activated by BLA inputs. Indeed, these excitatory inputs arriving to the PFC can evoke feedforward

inhibition by activating INs earlier than PCs, an inhibition which can then affect the postsynaptic responses in PCs (Dilgen et al., 2013; McGarry & Carter, 2016). In the upper layers, both PV INs and SST INs receive monosynaptic, glutamatergic excitatory inputs from the BLA (McGarry & Carter, 2016). These synapses exhibit a marked depression and facilitation onto PV and SST INs, respectively, a difference in their synaptic dynamics which suggest two types of feedforward inhibition: the rapid inhibition provided by PV INs is followed by sustained inhibition dictated by SST-expressing GABAergic neurons (McGarry & Carter, 2016). In contrast to these long-range excitatory inputs, excitatory afferents from contralateral cortex give rise to stronger inputs on deep layer PV-expressing INs than SST INs (Anastasiades et al., 2018). Thus, the contribution to feedforward inhibition evoked by recruiting SST-expressing neurons upon cortico-cortical afferent stimulation is less determinant, than those driven by PV-positive INs in layer 5 PCs (Anastasiades et al., 2018). Furthermore, there is evidence that afferents from MD thalamus provide this feedforward inhibitory effect via PV-containing INs solely, avoiding SST-positive INs, which seem to suppress MD-evoked feedforward inhibition (Delevich et al., 2015). Considering the diversity of long-range inputs and outputs, and the construction of microcircuits within the PFC, different loops can be identified, which might help understand the PFC function (Kawaguchi, 2017).

Consequently, these highlighted studies showed how cell type-specific excitation, inhibition, and intrinsic properties of neurons operate together to shape the microcircuit activity within the mPFC.

1.10. Role of mPFC GABAergic neurons in cognitive control

As it was mentioned in the first part of the introduction, the PFC plays a critical role in the control of different higher order cognitive functions. It is known that distinct microcircuits composed of excitatory PCs and inhibitory GABAergic neurons underlie the proper circuit operation. Due to the heterogeneity of GABAergic cell population and they potential role in cognitive control, much research focused on revealing their operation. For instance, Kim et al. examined the role of GABAergic INs during the delay period of working memory in a delayed non-match-to-place task (Kim et al., 2016). To investigate the role of PV- and SST-expressing INs, their discharge characteristics and

impact on neuronal function were monitored. Several differences were found between these two IN types, but probably the two most important ones are (I) the strong PV INs suppression after the reward delivery and (II) the difference in delay-period activity of SST, but not PV-containing INs between correct and error trials, results which suggest more important role of SST neurons in maintaining the content of working memory (Kim et al., 2016). During a goal directed go or no-go task PC populations and three IN types were examined (Pinto & Dan, 2015). Clear differences were found across the cell types, especially among INs, which were consistent with previous electrophysiological study (Insel & Barnes, 2015). The 'go' or target sensory stimulus evoked responses in many PCs, PV- and VIP-expressing INs, but not in SST INs, while the 'no-go' or non-target stimulus evoked responses only in PV-expressing neurons. Regarding the motor-related activity, all of these cells increased their firing, but SST-expressing INs showed the strongest activity compared to other cells. In contrast, SST INs showed the less outcome-related activity, while in case of PV- and VIP-expressing INs strong outcome-related activity was observed. Noticeably, not all PV-positive INs fired in action-related or outcome-related manner due to the strong activity of VIP-expressing neurons which inhibit PVBCs (Pinto & Dan, 2015). PCs also showed strong outcome-related activity, but with a high degree of variability, responses which may be related to their layer-specific synaptic connectivity (Lagler et al., 2016; Pinto & Dan, 2015). These two highlighted examples reflect the role and contribution of GABAergic INs throughout these processes to cognitive control.

1.11. Functioning and malfunctioning the PFC

The PFC is known to be a critical regulator of higher order cognitive functions and emotional guided behaviours (Cohen et al., 1996; Fuster, 2006; Mesulam, 1998; Miller, 2000; Peters et al., 2009). Yet, we know that the PFC operation is altered in many psychiatric disorders. In line with this, several studies have investigated the dysfunctions of this region to understand the background mechanisms underlying schizophrenia, depression, attention deficit hyperactivity disorder (ADHD) or drug addiction both in human and preclinical animal models. Patients suffering in schizophrenia show three major clusters of symptoms. Positive symptoms include hallucinations, negative

symptoms representing deficits in speech, social behaviour and diminished motivation, while the cognitive symptoms cause impairments in working- and episodic memory and deficits in conscious control of behaviour. All these impaired functions are coupled to PFC malfunctioning and its reduced connections with other brain regions (Arnsten et al., 2012; Meyer-Lindenberg, 2010; Ross et al., 2006). Several changes were observed in the local circuits, including a decrease in the PFC size which can be explained by a reduction in axon arbours and dendritic trees, in addition the extracellular space between the cells (Glantz & Lewis, 2000; Pierri et al., 2001; Rajkowska et al., 1998). Moreover, the number of GABAergic INs and the level of glutamate decarboxylase 67 (GAD-67), which is one of the GABA synthesizing enzymes are also decreased, which is linked to a consistent reduction in GABA transmission and GABAergic signalling (Lewis et al., 2005; Volk & Lewis, 2002). The reduction of GAD-67 level was observed predominantly in axon terminals of PVBCs, which may lead to weaker inhibition on PCs (Curley et al., 2011). Furthermore, there is evidence that both somatic and axonal expression of μ opioid receptor in PVBCs increase in schizophrenia, which might contribute to the reduced activity and GABA release from these INs (Capogna et al., 1993; Curley & Lewis, 2012; Glickfeld et al., 2008). In addition to the decreased GAD-67 level, the density of GABA membrane transporter 1, which is located in the axon terminals of ChCs and responsible for reuptake of GABA, is also decreased (Pierri et al., 1999). Moreover, as I mentioned above, the reduced CB1 receptor level was also observed in the PFC of human schizophrenic patients, which may lead to impairment inhibitory circuit function (Curley & Lewis, 2012; Eggan et al., 2008). This decreased inhibition and impairment in GABA release can lead to disturbance in the precisely modulated task-evoked gamma oscillations and overturning of excitation-inhibition balance (Ferguson & Gao, 2018a, 2018b; Gonzalez-Burgos et al., 2015). Additionally, recent human transcriptomic studies showed that in the dorsolateral PFC of patient suffering in schizophrenia, the expression of a large number of genes is significantly altered, indicating the involvement of several neuron types in this disorder, which suggests a general network impairment leading to changes in information processing (Batiuk et al., 2022; Reiner et al., 2021). For instance, they observed a general decrease in gene expression level in GABAergic INs, including those contianing PV, SST, VIP and calretinin and an increase in a fraction in distinct PC types (Batiuk et al., 2022). Interestingly, the reduction of PV and SST gene itself or their

messenger ribonucleic acid level did not affect the number and the density of these cells (Dienel et al., 2023).

In addition to schizophrenia, depression is the other common psychiatric disorder which affects primarily people living in countries with high economical incomes (Huang et al., 2020). Depression is often induced by stress, which causes structural, functional, and molecular changes in the PFC that are correlated with emotional disturbances both in human and rodents (Holmes & Wellman, 2009). In rats the depression-caused structural changes can be observed in dendritic remodelling, synaptic spine reduction as well as in the reduction in the number of glia cells (Holmes & Wellman, 2009; Sanacora et al., 2012). Previous studies have shown that in depression the glutamate level in the PFC is enhanced upon stress exposure (Musazzi et al., 2010; Sanacora et al., 2012). Additionally, human imaging studies showed that the activity level of ventromedial PFC was abnormally high, while the dorsolateral PFC activity was abnormally low in patient with depression. This imbalance between the two regions of the PFC might also contribute to the depression (Koenigs & Grafman, 2009).

Besides psychiatric disorders, the PFC might be involved in neurodegenerative diseases such as Alzheimer disease because of the connective and functional architecture of this cortical area. Due to the reciprocal connections between the PFC and temporal lobe or limbic regions which degenerate in early and preclinical stages of Alzheimer disease, the PFC could be more susceptible and vulnerable for this disease than other brain regions (Salat et al., 2001). Several human and animal studies investigated the molecular differences between the aging and Alzheimer disease on the PFC, and determined that changes occurred in molecular processes and genes related to neuronal plasticity, lipid metabolic processes, immune processes, and mitochondrial function (Folke et al., 2019; Stefanova et al., 2019). Conspicuously, the dysfunctions of the PFC can cause different pathological conditions. In order to better understand what types of mechanisms underlie these pathological conditions, and how we can treat them, first we should better understand the physiological operation of the PFC.

In summary, PTIs are essential for the regulation of normal mPFC function. Their fundamental role is further underlined by the fact that some psychiatric disorders such as schizophrenia specifically affect these INs. However, little is known about their detailed

morphological properties, input-output relationships, and local innervation patterns. Diversity in these parameters allows a more precise and potentially projection-specific control of mPFC activity. Thanks to the rapidly developing different genome modifying methods – like the transgenic technique, inserting bacterial artificial chromosomes (BAC) carrying the gene of a fluorescent protein, expression of which is controlled by the gene of interest or using the Cre-lox and Flpo-frt recombinase systems driven by specific gene promoters, the visualization of selected neuronal populations can be achieved. These approaches allow us studying the features of PTIs in a targeted manner.

2. Objectives

The main goal of my thesis was to uncover and examine the anatomical diversity of perisomatic inhibitory neurons in the PrL region of mPFC. We aimed to address the following questions organized in four topics.

I. To identify the sources and the ratio of different perisomatic inhibitory inputs on PCs:

- What types of GABAergic neurons provide perisomatic inhibition in the mPFC and what is the ratio of their innervation on single cells or at the population level?
- What are the morphological features of these INs?
- Is there any difference in the postsynaptic target distribution of BCs on randomly sampled cells or on PCs projecting to distinct brain areas?

II. To examine the innervation of AISs of PCs by distinct ChCs originating from different genetically modified mouse lines:

- What types of GABAregic boutons target the AISs of PCs and what is the ratio of their innervation?
- Are the two types of ChCs originating from BAC-PV-EGFP or Nkx2.1-CreERT2 X LSL-Flpo mouse lines morphologically similar or distinct?
- What is the innervation pattern of these ChCs along the AIS of PCs?

III. To reveal the interneuronal targets of extrinsic inputs in the mPFC:

- What types of INs are targeted by amygdalar inputs?
- What proportion of PV-expressing INs in distinct PrL layers are targeted by extrinsic inputs from the amygdala, thalamus and entorhinal cortex?

IV. To study the local inputs of INs, we should examine the specificity of CaMKIIα-promoter controlled genetic construct labelling in the mPFC:

- Is the usage of CaMKIIα promoter eligible for specific targeting the cortical PCs?

3. Material and methods

3.1. Experimental animals

Experiments were approved by the Committee of the Scientific Ethics of Animal Research (22.1/360/3/2011) and all procedures involving animals were performed according to methods approved by Hungarian legislation (1998 XXVIII. section 243/1998, renewed in 40/2013.) and institutional guidelines of ethical code. All procedures complied with the European convention for the protection of vertebrate animals used for experimental and other scientific purposes (Directive 86/609/CEE and modified according to the Directives 2010/63/EU). Every effort was taken to minimise animal suffering and the number of animals used. Adult mice (P50-140) were used from the following lines: C57BL/6J, FVB/Ant-Fx (wild types, Charles River), BAC-PV-eGFP (Meyer et al., 2002), BAC-CCK-DsRed (Mate et al., 2013), Ai6 reporter line (CAG-LSL-ZsGreen1, #007906, www.jax.org), Pvalb-IRES-Cre (PV-Cre, #017320, www.jax.org) and Nkx2.1-CreERT2:: LSL-Flpo (Nkx2.1-CreERT2, #014552; LSL-Flpo, #028584, www.jax.org) (He et al., 2016).

3.2. Chandelier cell labelling

ChC labelling was carried out similarly as described earlier in details (He et al., 2016), with only exception of the time of tamoxifen induction. Briefly, we generated Nkx2.1-CreERT2:: LSL-Flpo mice, in which tamoxifen induction at P0 result in persistent mouse codon-optimized flippase recombinase (Flpo) expression in postmitotic ChCs. After several weeks, anaesthesia was induced with a mixture of 125 mg/kg ketamine and 5 mg/kg xylazine and mice from both sexes (n=5 male and n=4 female) were secured in a stereotaxic frame and uni- or bilateral injection of 200 nl of Flpo-depentent eYFP virus construct to specifically label cells which express Flpo ((AAVdj eYFP-EF1a-fDIO; Lot# AV6219, UNC) or (AAV5-eYFP-EF1a-fDIO; Lot# AV6154C, UNC)) were aimed at the following coordinates for PrL injection from Bregma (in cm): anterior-posterior (AP) 0.178, medio-lateral (ML) next to the sinus, dorso-ventral (DV) 0.1. After 4 weeks of recovery, coronal slices were prepared and eYFP+ cells were recorded in whole-cell mode as described later. This strategy provided specific and intense labelling of ChCs.

3.3. Additional surgical procedures

3.3.1. Retrograde cell labelling

Anaesthesia was induced and maintained with a mixture of 125 mg/kg ketamine and 5 mg/kg xylazine. Wild type mice from both sexes (n=2-2 for basal amygdala (BA) and periaqueductal grey (PAG) injection and n=5-5 for contralateral PFC (cPFC) and dorsal striatum (DS) injection) were secured in a stereotaxic frame and unilateral or bilateral injections of Fluorogold or choleratoxin B subunit tracers dissolved in glycerol (FG 2% iontophoresis by 2 µA pulses with 2/2 s on/off duty cycle for 5 minutes and CTB 0.5% iontophoresis by 5 µA pulses with 2/2 s on/off duty cycle for 7-10 minutes) or retrograde pAAVrg-CAG-GFP (Addgene: 37825-AAVrg) or retrograde AAVrg-EF1a-mCherry-IRES-Flpo (Addgene: 55634-AAVrg) viruses (200 nl injected at a 3 nl/sec rate) were aimed at the following coordinates from Bregma (in cm): for BA injections (n=1 with FG, n=1 with CTB): AP -0.15, ML 0.31, DV 0.43; for DS injections (n=3 with FG, n=2 with pAAVrg-CAG-GFP): AP 0.06-0.07, ML 0.13, DV 0.23; for PAG injections (n=1 with FG, n=1 with CTB): AP -0.46-0.49, ML 0.05, DV 0.11-0.12; for cPFC injections (n=3 with CTB, n=2 with AAVrg-EF1a-mCherry-IRES-Flpo): AP 0.15-0.18, ML next to the sinus, DV 0.1-0.15. After 4-8 days of tracer injections and after 4 weeks of virus injections, mice were transcardially perfused with 4% paraformaldehyde (PFA) in 0.1M phosphate buffer (PB) for 30-40 min and PFC containing sections of 50-100 µm thickness were prepared using a Vibratome (Leica VT1000S) and stored in 0.1M PB with 0.05% Na-azide until further processing.

3.3.2. Retrograde cell labelling for *in vitro* experiments

Anaesthesia was induced with 125 mg/kg ketamine and 5 mg/kg xylazine. BAC-PV-eGFP animals (n=3) were secured in a stereotaxic frame and bilateral injections of FG (2% iontophoresis by 2 µA pulses with 2/2 s on/off duty cycle for 5 minutes) and CTB (0.5% iontophoresis by 5 µA pulses with 2/2 s on/off duty cycle for 7-10 minutes) were aimed respectively at the following coordinates from Bregma (in cm): for BA injections AP -0.15, ML 0.31, DV 0.425; for nucleus accumbens injections AP +0.11, ML 0.10, DV 0.44; for DS injections AP 0.06, ML 0.13, DV 0.23. After 4-8 days of recovery, coronal slices were prepared and eGFP+ cells were recorded in whole-cell mode as described later.

3.3.3. Anterograde trans-synaptic viral labelling

Anaesthesia was induced with 125 mg/kg ketamine and 5 mg/kg xylazine. Male PV-Cre (n=15) and both male and female Ai6 reporter mice (n=8) were secured in a stereotaxic frame and bilateral injections of 200-300 nl AAV1 virus vectors (AAV1-EF1a-DIO-ChETA-eYFP (Addgene: 26968) to PV-Cre mice and pENN-AAV1-hSyn-Cre-WPRE-hGH (Addgene: 105553) to Ai6 mice were aimed with a 3 nl/sec flow rate at the following coordinates from Bregma (in cm): for BA injections (n=8 PV-Cre and n=2 Ai6 mice) AP -0.15, ML 0.32-0.35, DV 0.44-0.50; for midline thalamus injections (n=3 PV-Cre and n=4 Ai6 mice) AP -0.12-0.13, ML next to the sinus, DV 0.30-0.33; for lateral entorhinal cortex (LEnt) (n=4 PV-Cre and n=2 Ai6 mice) injections AP -0.42, ML 0.375, DV 0.28. After 4 weeks of recovery, mice were transcardially perfused with 4% PFA in 0.1M PB for 30-40 minutes and PFC sections were prepared as described above.

3.3.4. Viral labelling of CaMKIIα-expressing neurons

Anaesthesia was induced with 125 mg/kg ketamine and 5 mg/kg xylazine. Male C57Bl6/J mice were secured in a stereotaxic frame and unilaterally injection of 200 nl distinct virus vectors (AAV5-CaMKIIa-ChR2(H134R)-mCherry-WPRE-hGH (Addgene: 26975) n=2 mice with full concentration and n=2 mice with 1:10 dilution (in physiological saline); AAV9-CaMKIIa-hChR2(E123T/T159C)-mCherry (Addgene: 35512, n=4 mice) and AAV9-CamKIIa-ArchT(PV2527)-GFP (Addgene: 99039, n=2 mice)) were performed at a 3 nl/sec flow rate at following coordinates from Bregma (in cm) for mPFC injection: AP +0.18, ML 0.3, DV -0.15. After 5-6 weeks mice were transcardially perfused with 4% PFA in 0.1M PB for 30-40 minutes, then the brain was removed and cut into 50 µm sections with a Vibratome (Leica VT1000S) and stored in 0.1M PB with 0.05% Na-azide until further processing. Sections ipsilateral to the injection side were used in the experiments.

3.4. Tissue processing and immunocytochemistry

All anatomical data, including those acquired with viruses and retrograde tracers, were obtained from immunostained brain slices. 50-100 µm thick sections were prepared from perfused brain or 30 µm thick sections were re-sectioned from immersion fixed *in vitro* slices using a Vibratome (Leica VT1000S). Sections were thoroughly washed in 0.1M

PB for several times (4-5 times for 10-15 minutes). For fluorescent labelling, sections were blocked with 10% Normal Donkey Serum (NDS, Vector Laboratories) or 10% Normal Goat Serum (NGS, Vector Laboratories) and 0.5% TritonX-100 in 0.1M PB for 30-60 minutes at room temperature. Then, sections were incubated in a mixture of different primary antibodies diluted in PB containing 2% NDS or 2% NGS, 0.5% or 2% TritonX-100 and 0.05% Na-azide overnight at room temperature for an additional 3-6 days at 4°C. The applied primary antibodies are detailed in Table 1 grouped and numbered according to the experimental objectives: determination of the borders of PFC layers (1); visualisation of GABAergic inputs on the perisomatic region (2); visualisation of inputs onto retrogradely labelled cells (3-6); validating the CCK- or PV-content in the transgenic mice (7-8); examination of CB1 receptor content of visualised CCKBCs (9); target distribution of CCKBCs and PVBCs on random PCs (10); target distribution of PVBCs on retrogradely labelled cells (11); visualisation of GABAergic inputs on AISs (12); postsynaptic target distribution of ChCs on AISs (13); visualisation of the monosynaptic input-receiving PV-containing cells (14-15). Immunostaining detailed in Table 2 were performed for the visualisation of INs labelled by CaMKIIα-promoter. After washing out primary antibodies several times, sections were treated with secondary antibodies diluted in 0.1M PB and 1% NDS or NGS for 2-4 hours (Table 1, 2). Following several washes in PB, sections were mounted on glass slides in Vectashield (Vector Laboratories).

Table1: Antibodies used in anatomical experiments Abbreviation of secondary antibodies: DAR: donkey anti rabbit, DARat: donkey anti rat, DAM: donkey anti mouse, DACh: donkey anti chicken, DAG: donkey anti goat, DAGp: donkey anti guinea pig. All the secondary antibodies were used in 1:500 dilution.

Immuno #	Thickness of slices	primary Ab	provider	catalog #	concentration	primary Ab incubation	secondary Ab	provider
1.	100 µm	rabbit anti-WFS1	Proteintech	11558-1-AP	1:500	4 day 4°C	Alexa647 DAR	Jackson
		rat anti- Ctip2	Abcam	ab18465	1:1000		Alexa488 DARat	Molecular Probes
		mouse anti-FoxP2	Sigma-Aldrich	MABE415	1:5000		Cy3 DAM	Jackson
		chicken anti-Calbindin	SYSY	214006	1:1000		Dyl405 DACh	Jackson
2.	50 µm	mouse anti-Kv2.1	Neuromab	75-014	1:1000	3 day 4°C	Alexa647 DAM	Jackson
		goat anti-CB1	Frontier Institute Co.Ltd	CB1-Go-Af450	1:1000		Dyl405 DAG	Jackson
		guinea pig anti-VGAT	SYSY	131004	1:1000		Alexa488 DAGp	Jackson
			Frontier Institute Co.Ltd	VGAT-GP-Af1000	1:1000			
		rabbit anti-PV	Swant	PV 25	1:5000		Cy3 DAR	Jackson
3.	50 µm	rabbit anti-PV	Swant	PV 25	1:5000	6 day 4°C	Cy3 DAR	Jackson
		goat anti-CB1	Frontier Institute Co.Ltd	CB1-Go-Af450	1:1000		Alexa488 DAG	Jackson
		guinea pig anti-Fluorogold	Protos Biotech	NM-101 FluGgp	1:5000		Dyl405 DAGp	Jackson
		mouse anti-Kv2.1	Neuromab	75-014	1:1000		Alexa647 DAM	Jackson
4.	50 µm	rabbit anti-PV	Swant	PV 25	1:5000	6 day 4°C	Cy3 DAR	Jackson
		goat anti-Coleratoxin B	List Biological Laboratories	703	1:20.000		Dyl405 DAG	Jackson
		guinea pig anti-CB1	Frontier Institute Co.Ltd	CB1-Go-Af530	1:1000		Alexa488 DAGp	Jackson
		mouse anti-Kv2.1	Neuromab	75-014	1:1000		Alexa647 DAM	Jackson
5.	50 µm	guinea pig anti-PV	SYSY	195004	1:10.000	6 day 4°C	Cy3 DAGp	Jackson
		goat anti-Coleratoxin B	List Biological Laboratories	703	1:20.000		Dyl405 DAG	Jackson
		rabbit anti-CB1	Cayman	10006590	1:1000		Alexa488 DAR	Jackson
		mouse anti-Kv2.1	Neuromab	75-014	1:1000		Alexa647 DAM	Jackson
6.	60 µm	guinea pig anti-PV	SYSY	195004	1:10.000	6 day 4°C	Cy5 DAG	Jackson
		goat anti-CB1	Frontier Institute Co.Ltd	CB1-Go-Af450	1:1000		Dyl405 DAG	Jackson
		rat RFP	Chromotec	5F8	1:1000		Cy3 DARat	Jackson
7.	50 µm	rabbit anti-proCCK	Frontier Institute Co.Ltd	CCK-pro-Rb-Af350	1:1000	3 day 4°C	Alexa488 DAR	Jackson
8.	50 µm	rabbit anti-PV	Swant	PV 25	1:5000	3 day 4°C	Cy3 DAR	Jackson
		goat anti-eGFP	Abcam	ab5450	1:5000		Alexa488 DAG	Jackson
9.	*in vitro* slices	goat anti-CB1	Frontier Institute Co.Ltd	CB1-Go-Af450	1:1000	6 day 4°C	Dyl405 DAG	Jackson
10.	*in vitro* slices	mouse anti-Kv2.1	Neuromab	75-014	1:1000	6 day 4°C	Alexa647 DAM	Jackson
11.	*in vitro* slices	goat anti-Coleratoxin B	List Biological Laboratories	703	1:20.000	6 day 4°C	Cy3 DAG	Jackson
		guinea pig anti-Fluorogold	Protos Biotech	NM-101 FluGgp	1:5000		DyL405 DAGp	Jackson
		mouse anti-Kv2.1	Neuromab	75-014	1:1000		A488 DAM	Molecular Probes
12.	50 µm	goat anti-PV	Swant	PVG-214	1:5000	3 day 4°C	Cy3 DAG	Jackson
		guinea pig anti-VGAT	SYSY	131004	1:1000		Cy5 DAGp	Jackson
		rabbit anti-AnkG	Santa Cruz	sc-28561	1:100		DyL05 DAR	Jackson
13.	30 µm	rabbit anti-AnkG	Santa Cruz	sc-28561	1:100	3 day 4°C	Cy3 DAR	Jackson
14.	100 µm	rabbit anti-PV	Swant	PV 25	1:5000	4 day 4°C	Cy3 DAR	Jackson
15.	100 µm	goat anti-PV	Swant	PVG-214	1:5000	4 day 4°C	Cy3 DAG	Jackson

Table2: Antibodies used for the visualisation of INs labelled by CaMKIIα-promoter

Abbreviation of secondary antibodies: DAR: donkey anti rabbit, DARat: donkey anti rat, DACh: donkey anti chicken, DAGp: donkey anti guinea pig. All the secondary antibodies were used in 1:500 dilution.

Immuno #	Thickness of slices	primary Ab	provider	catalog #	concentration	primary Ab incubation	secondary Ab	provider
mCherry expressing viruses								
1.	50 µm	rat anti-RFP	Chromotek	5F8	1:1000	6 day 4°C	Cy3 DARat	Jackson
		guinea pig anti-PV	SYSY	195004	1:10.000		Alexa488 DAGp	Jackson
2.	50 µm	rat anti-RFP	Chromotek	5F8	1:1000	6 day 4°C	Cy3 DARat	Jackson
		rabbit anti-proCCK	Frontier Institute	CCK-pro-Rb-Af350	1:1000		Alexa488 DAR	Jackson
GFP expressing virus								
3.	50 µm	chicken anti-GFP	SYSY	132006	1:1000	6 day 4°C	Alexa 488 DACh	Jackson
		guinea pig anti-PV	SYSY	195004	1:10.000		Alexa647 DAGp	Jackson
4.	50 µm	chicken anti-GFP	SYSY	132006	1:1000	6 day 4°C	Alexa 488 DACh	Jackson
		rabbit anti-proCCK	Frontier Institute	CCK-pro-Rb-Af350	1:1000		Alexa488 DAR	Jackson
CaMKIIα/GFP-FVB/AntF1 transgenic mice								
5.	50 µm	chicken anti-GFP	SYSY	132006	1:1000	6 day 4°C	Alexa 488 DACh	Jackson
		guinea pig anti-PV	SYSY	195004	1:10.000		Cy3 DAGp	Jackson

3.5. *In vitro* electrophysiology

In vitro biocytin labelling of INs was carried out as described earlier in detail (Veres et al., 2014). Briefly, BAC-CCK-DsRed, BAC-PV-eGFP and Nkx2.1-CreERT2:: LSL-Flpo mice were deeply anesthetized with isoflurane and decapitated. The brain was quickly removed and placed into ice-cold cutting solution containing (in mM): 252 sucrose, 2.5 KCl, 26 $NaHCO_3$, 1 $CaCl_2$, 5 $MgCl_2$, 1.25 NaH_2PO_4, 10 glucose, bubbled with 95% O_2 and 5% CO_2 (carbogen gas). Coronal slices of 200-µm thickness containing the PFC region were prepared with a Leica VT1200S Vibratome (Wetzlar, Germany), and kept in an interface-type holding chamber containing artificial cerebrospinal fluid (ACSF) at 36 °C that gradually cooled down to room temperature. ACSF contained (in mM) 126 NaCl, 2.5 KCl, 1.25 NaH_2PO_4, 2 $MgCl_2$, 2 $CaCl_2$, 26 $NaHCO_3$, and 10 glucose, bubbled with carbogen gas. INs were selected based on the presence of the fluorescent proteins (DsRed or eGFP) excited by an UV lamp and visualised by a CCD camera (Hamamatsu Photonics or Andor Zyla). Targeted cells were recorded under visual guidance using differential interference contrast microscopy (Olympus BX61W or Nikon FN-1) that laid 50–100 µm below the surface of the acute slice. INs were recorded in whole-cell mode using a K-gluconate based intrapipette solution containing biocytin to label their processes [intrapipette solution (in mM): 110 K-gluconate, 4 NaCl, 2 Mg-ATP, 20 HEPES, 0.1 EGTA, 0.3 GTP (sodium salt), 10 phosphocreatine, and 0.2% biocytin adjusted to pH 7.3 using KOH and with an osmolarity of 290mOsm/L]. After the recordings, slices were

fixed in 4% PFA and Alexa488-coupled streptavidin (1:10,000 in TBS, Molecular Probes), Cy3-coupled streptavidin (1:10,000 in TBS, Sigma-Aldrich) or Alexa647-coupled streptavidin (1:10,000 in TBS, Molecular Probes) was used to visualise the fine details of neurons in the entire slice.

3.6. Image acquisition and analysis

Fluorescent images were taken with a Nikon A1R and a Nikon C2 confocal laser scanning microscope (Nikon Europe, Amsterdam, The Netherlands) using distinct settings for different objectives: CFI Super Plan Fluor 20X, N.A. 0.45, z step size: 1 μm, xy: 0.62 μm/pixel for the cell reconstruction; CFI Plan Apo VC10X, N.A. 0.30, single plane, xy: 0.31 μm/pixel for the determination of the borders of layers within the mPFC and for the validation of reporter protein content of neurons; CFI Plan Apo VC60X Oil objective, N.A. 1.40, z step size: 0.13 μm, xy: 0.08 μm/pixel for the visualisation of GABAergic inputs on the perisomatic region and for the analysis of the density of CB1 and PV boutons on the retrogradely labelled cells; CFI Plan Apo VC60X Oil objective, N.A. 1.40, z step size: 0.2, xy: 0.21 μm/pixel for the analysis of target distribution of BCs on random PCs; CFI Plan Apo VC10X, N.A. 0.30, z step size: 3 μm, xy: 0.63 μm/pixel for the visualisation of the monosynaptic input receiving PV-containing cells; CFI Plan Apo VC60X Oil objective, N.A. 1.40, z step size: 0.13, xy: 0.09-0.10 μm/pixel for the analysis of postsynaptic target distribution of ChCs.

Reconstruction and analysis of the 3D confocal image stacks was performed with the Neurolucida 10.53 software (MBF Bioscience) and NIS Elements software (Nikon). The properties of axonal and dendritic arbours and surface analysis were performed with Neurolucida Explorer software (MBF Bioscience). Values were corrected for shrinkage and flattening of the tissue (x, y and z axis correction on pictures taken by using CFI Plan Apo VC60X Oil objective: 1.08; x, y axis correction was 1 and z axis correction was 2.5 on pictures taken from the biocytin-labelled BCs by using CFI Super Plan Fluor 20X objective). Schematic representation of brain slices from thalamus injection and PFC were achieved using Inkscape (Free Software Foundation Inc.) open access program.

3.7. Quantification of inputs targeting Kv2.1-immunolabelled somata and AnkG positive AISs

During quantification, different aspects were taken into account. Boutons were considered putative contacts if no apparent gap was visible between the labelled bouton and the surface of Kv2.1-stained somata or AnkG-immunolabelled AIS when examined in 3D view of confocal images. Varicosities located at branch points were not counted as putative contacts, as it has been shown by electron microscopy that these boutons do not form synapses (Veres et al., 2017; Veres et al., 2014). The surface of Kv2.1-stained cell bodies were calculated in 3D confocal image stacks by using Neurolucida Explorer software: the software calculated the superficies of cell bodies based on the drawn contours in every second stack, from which we subtracted the area of the top and bottom contours. Then, the bouton density was calculated by dividing the number of boutons with the calculated surface of cell bodies.

3.8. Statistical and Cluster Analysis

Normality was tested with the Shapiro-Wilk test. Two sample T-test and ANOVA were used for statistical analysis of data following normal distribution. For data with non-normal distribution the Mann-Whitney U test (M-W test), Wilcoxon Signed Rank test and Kruskal-Wallis ANOVA (K-W ANOVA) was used. For *post hoc* analysis Bonferroni test, Dunn's test or M-W test was used. For the comparison of distributions, the two sample Kolmogorov-Smirnov test (K-S test) and Chi-Square Homogeneity test were used. All statistics were performed using Origin 8.6 or 9.2 (Northampton, MA) or online LibreTexts statistical programs (www.stats.libretexts.org). Exact p values were indicated when p was higher than 0.001 considering the rounding rules. Data are presented as mean ± SEM, unless indicated otherwise. The cluster and principal component analysis (PCA) were performed using Origin 8.6 or 9.2. The PCA showed the main components from the 5 axonal and 5 dendritic distribution ratios between layers, and cluster analysis applying Ward methods was made based on these selected main components.

3.9. Personal contribution to the results

In case of chandelier cell labelling, the animal breeding was done mostly by me, the tamoxifen injections were made by my colleagues.

From different surgical procedures, I made the PAG injections, the other injections were made by my colleagues. The tissue processing of injected animals, from the perfusion through the cutting to the immunostaining, was mostly done by me, except some anterograde trans-synaptic labelled animals and BA-tracer injected animals, which were perfused by my colleagues.

The *in vitro* electrophysiology recordings and biocytin cell labelings were done by my colleague. Around two-third of BCs and all of the ChCs were reconstructed and analysed by me.

Most of the bouton counting, including the biocytin-labelled and immunostained boutons, were mostly done by me, except the counting of GABAergic inputs on perisomatic region of PCs and around half of target distribution of CCKBCs and PVBCs on random PCs, which were made one of my colleagues.

The analysis of the results were mostly carried out by me with the help and supervision of my colleagues.

4. Results

4.1. Defining the layers in the mPFC

Previous investigations showed (Anastasiades & Carter, 2021) that the inputs and outputs of PCs and INs located in distinct layers within the mPFC can be different, thereby they may contribute to network organization in a specific manner. Therefore, as a first step we needed to determine the borders of the layers, since we aimed to accomplish our analysis based on the defined layers in the following experiments. As previous studies defined boundaries of layers inconsistently (Anastasiades et al., 2018; Clarkson et al., 2017; Lu et al., 2017), an objective approach is needed to overcome this limitation. To outline the boundaries, we analysed the distribution of neurons in the PFC labelled with different types of antibodies developed against a calcium binding protein Calb and different transcriptional factors used as markers and compared with the well-defined layered structure of the somatosensory cortex (Figure 7).

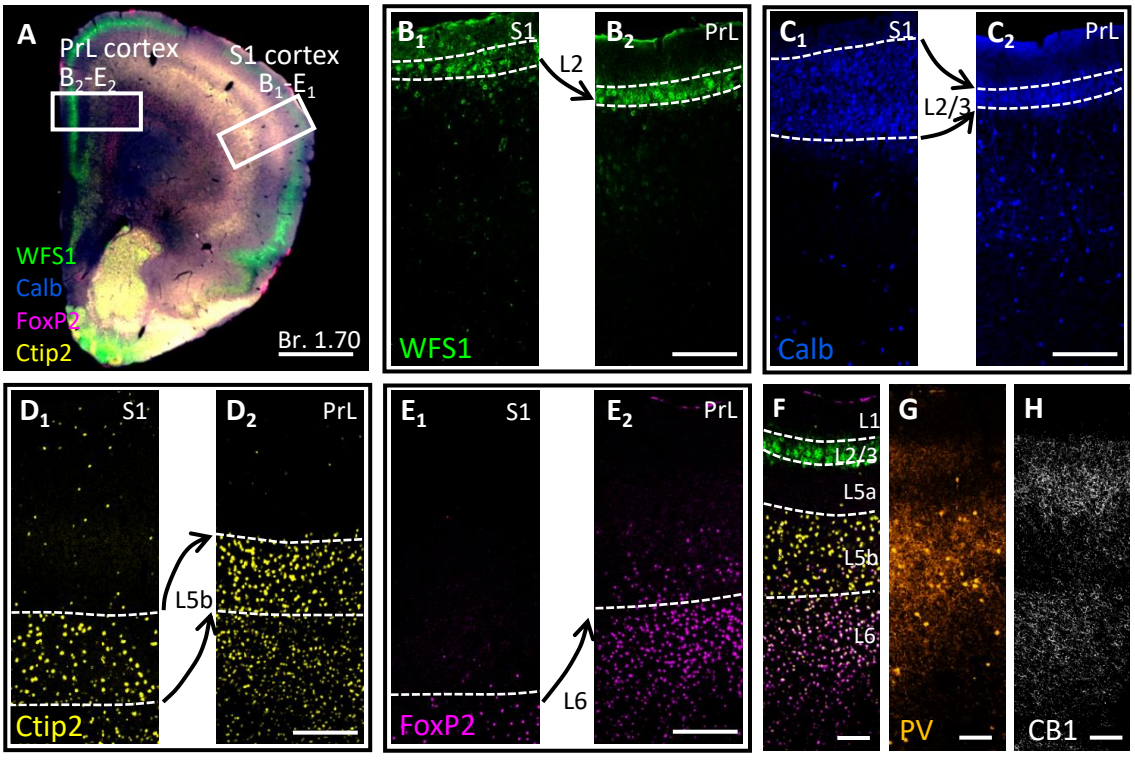

Figure 7: ***Defining layer boundaries in the mPFC by using different antibodies developed against the Ca^{2+} binding protein Calb and transcription factors (WFS1, Ctip2, FoxP2)*** *(A) A low magnification multicolour confocal image taken from a mPFC*

section immunostained against WFS1, Calb, Ctip2 and FoxP2. White empty rectangles indicate the PrL subregion of mPFC and S1 which are shown at a higher magnification in B-E. Scale bar: 1000 µm. (B-E) Higher magnification confocal images taken from the PrL and S1 regions, respectively, immunolabelled for WFS1, Calb, Ctip2, FoxP2. Dashed white lines indicate the boundaries of the layers defined by the immunolabeling. Scale bar: 200 µm. (F) A multicolour confocal image taken from a PrL region that was immunostained against WFS1 (green), Ctip2 (yellow) and FoxP2 (magenta), indicating the clear boundaries of the layers. Scale bar: 100 µm. (G-H) Immunostaining against PV and CB1 in the same PrL region of the mPFC. Scale bar: 100 µm.

In the superficial layers the transcription factor wolfram syndrome 1 protein (WFS1) visualized the neurons in layer 2 (Figure 7B_1-B_2, (Luuk et al., 2008)), while an antibody against the calcium-binding protein Calb marked the nerve cells in both superficial layers, i.e. in the layer 2 and 3 (Figure 7C_1-C_2, (Cruikshank et al., 2001)). As Figure 1 shows, these two layers in the PrL are fused and form a narrow layer 2/3, while in the somatosensory cortex these layers remain separated from each other. The transcription factors Ctip2 and Forkhead box protein P2 (FoxP2) were used to determine the borders in deep layers (Arlotta et al., 2005; Babiczky & Matyas, 2022; Hisaoka et al., 2010). Ctip2 was expressed in neurons located in layer 5b and layer 6 (Figure 7D_1-D_2), while FoxP2 was present only in layer 6 neurons (Figure 7E_1-E_2). Furthermore, since the layer 4 is missing in the PFC (Uylings et al., 2003), there was no need to use a distinct marker to reveal this layer. For determining layer 5a we did not need to apply any marker, because the borders of the surrounding layers have been already determined it by using WFS1/Calb and Ctip2 (Figure 7F). As we have defined the distinct layers of mPFC, the investigation of the features of INs can be achieved in a layer-specific manner.

4.2. Inhibitory inputs on the perisomatic region of PCs in the mPFC

In all cortical structures, the perisomatic region of PCs is strongly and exclusively innervated by GABAergic synapses, no excitatory inputs form synapses at this membrane compartment (Freund & Katona, 2007; Megias et al., 2001; Miles et al., 1996; Vereczki et al., 2016). To investigate the sources of the GABAergic inputs on the somata of PCs in the different layers of the mPFC, we visualized the perisomatic region of neurons by

using immunostaining against the voltage-gated potassium channel subunit Kv2.1 and the inhibitory terminals expressing vesicular GABA transporter (VGAT) (Figure 8A). As prior studies elucidated, these inhibitory axon terminals at the perisomatic regions originate mostly from PVBCs and CB1/CCKBCs (Freund & Katona, 2007; Vereczki et al., 2016). To confirm these findings in the mPFC, we examined the ratio of PV- and CB1-expressing boutons that were also immunopositive for VGAT and formed close appositions with Kv2.1-labelled somata (Figure 8A).

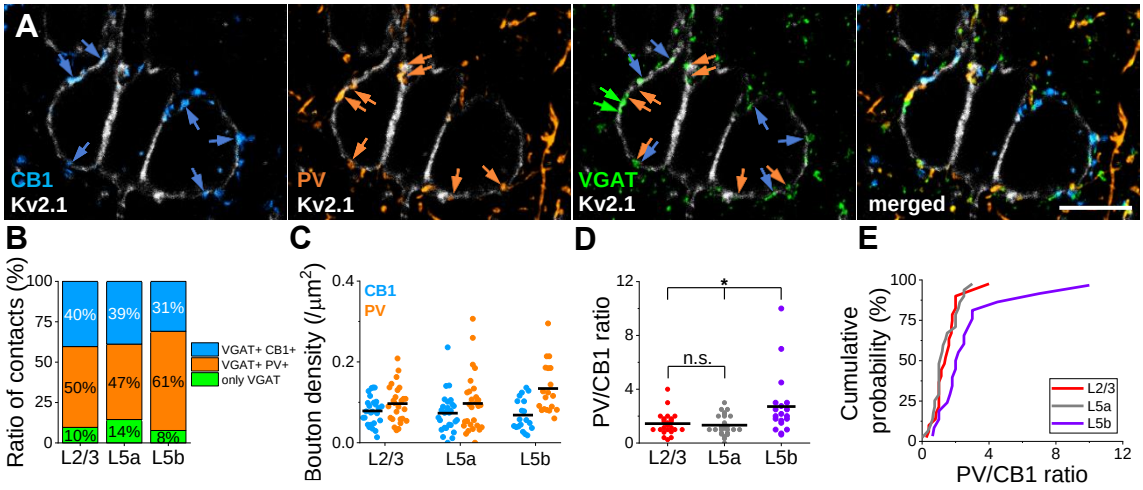

Figure 8. ***The vast majority of perisomatic GABAergic inputs originates from CB1- and PV-expressing boutons*** *(A) Multicolour maximum z-intensity projection confocal images taken of sections immunostained for Kv2.1, CB1, PV and VGAT. Blue arrows indicate the CB1- and VGAT-co-expressing boutons on Kv2.1-labelled profiles, orange arrows point to PV- and VGAT-co-expressing terminals that are in close appositions with Kv2.1-immunostained soma membranes, while green arrows show VGAT-immunpositive boutons on Kv2.1-labelled somata, axon terminals that lack PV or CB1 immunoreactivity. Scale bar: 10 µm. (B) The ratio of boutons expressing CB1, PV and VGAT only on the Kv2.1-immunostained somata in three different layers of the mPFC. (C) CB1 and PV bouton density on the surface of Kv2.1-labelled somata in different layers. Black lines represent the mean in each case. (D) The ratio of PV- and CB1-expressing boutons on Kv2.1- labelled membrane profiles in distinct layers. Each dot represents the ratio, which was determined on single PCs, while black lines show the mean. In layer 2/3 n=26 somata from 2 mice, in layer 5a n=28 somata from 2 mice, while in layer 5b n=19 somata from 3 mice were examined. (One way ANOVA: p=0.00217; Two sample t test: L2/3 vs. L5a:*

p=0.59345; L2/3 vs. L5b: p=0.01205; L5a vs. L5b: p=0.00612.) (E) Cumulative probability distributions of PV/CB1 ratios in different layers. Kolmogorov-Smirnov test confirmed that the ratio of PV/CB1 in L5b is different in comparison to other layers (K-S test: L2/3 vs. L5a: p= 0.72593; L2/3 vs. L5b: p<0.01; L5a vs. L5b: p<0.01).

We found that in layer 2/3 90%, in layer 5a 86%, while in layer 5b 92% of the VGAT-immunolabelled boutons were immunoposivite for PV or CB1 (Figure 8B). Moreover, we observed that PCs in different layers receive distinct ratio of PV+ and CB1+ perisomatic inputs, a ratio which was significantly larger in layer 5b than the upper layers (Figure 8C-E). Additionally, similar to previous neocortical studies, we have not found PV and CB1 co-expression in the examined boutons (Eggan et al., 2010). Collectively, these results suggest that CB1- and PV-containing inhibitory terminals are the major sources of perisomatic inhibition in the mPFC, GABAergic inputs that might originate from CCKBCs and PVBCs.

4.3. Inhibitory inputs on the perisomatic region of mPFC PCs that project to the BA, cPFC, DS and PAG

As our results showed, the ratio of PV+ and CB1+ boutons on PCs is different in distinct layers. Moreover, as previous studies have described PT neurons project subcortically, e.g. to the PAG, are located in deep layers of mPFC (Anastasiades & Carter, 2021; Gabbott et al., 2005; Kawaguchi, 2017). Therefore, we tested the hypothesis whether PCs projecting to distinct brain areas are innervated by various ratio of inhibitory boutons expressing PV and CB1. This assumption was based on other previous studies, showing that in other cortical regions a specific subset of PCs may receive perisomatic inhibitory inputs predominantly from PV-containing axon terminals (Bodor et al., 2005), or from CB1-expressing boutons (Varga et al., 2010). To investigate the potential target-selectivity, retrograde tracers (CTB and FG) and retrograde viruses (pAAVrg-CAG-GFP or AAVrg-EF1a-mCherry-IRES-Flpo) were injected into the following brain regions: BA, cPFC, DS and PAG.

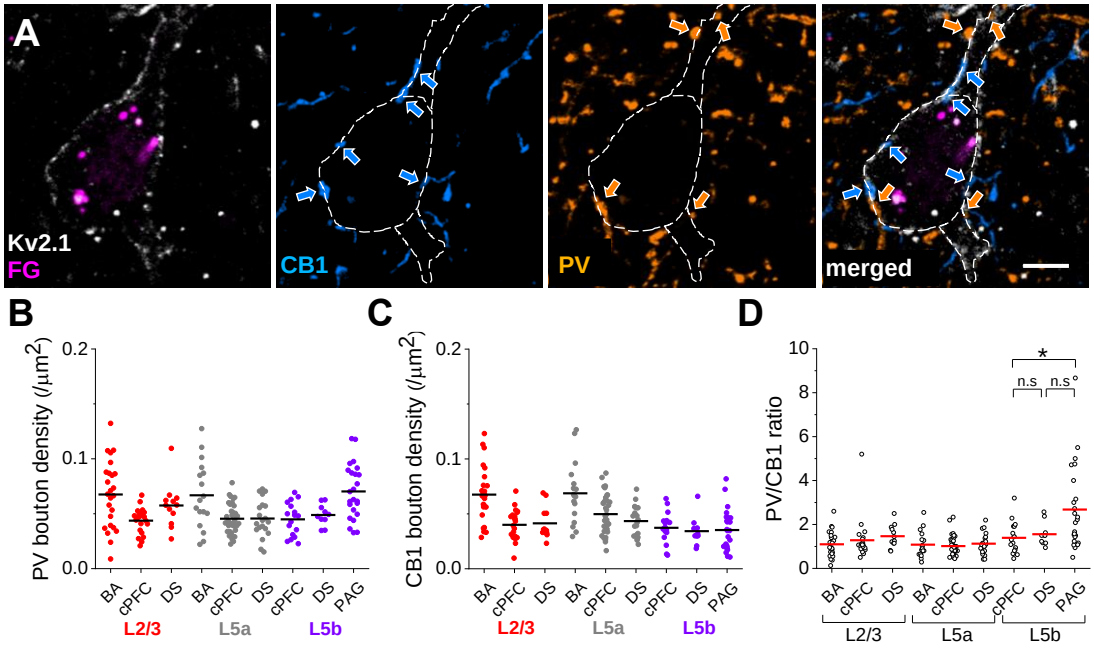

Figure 9. ***Inhibitory inputs on the perisomatic region of PCs projecting to different brain regions*** *(A) Multicolour maximum z-intensity projection confocal images taken from a section immunostained for Kv2.1, Fluorogold (FG), CB1 and PV to visualise the perisomatic CB1 and PV inputs on an FG-containing layer 5b PC labelled retrogradely from the DS. Scale bar: 5 µm. (B) PV bouton density on the perisomatic surface of PCs projecting to distinct brain regions. Red dots indicate cells located in L2/3, grey dots represent PCs located in L5a, while purple dots show PCs located in L5b. Each dot represents the PV bouton density on single PCs. Black lines indicate means. (C) CB1 bouton density on the perisomatic membrane surface of PCs projecting to distinct brain regions. Colours, lines, dots, and numbers are the same as in (B). (D) Perisomatic PV/CB1 ratio on PCs projecting to different brain areas and located in distinct layers. Red lines indicate means. (The number of examined cells by layers and by projection brain areas: L2/3: BA: n=25, cPFC: n=22, DS: n=12; L5a: BA: n=17, cPFC: n=36, DS: n=20; L5b: cPFC: n=17, DS: n=10, PAG: n=24. BA-projecting cells were counted in 6 slices from 2 mice, cPFC-projecting cells were counted in 10 slices from 4 mice, DS-projecting cells were counted in 6 slices from 2 mice and PAG-projecting cells were counted in 4 slices from 2 mice. K-W ANOVA in L2/3 p=0.104, in L5a p=0.633 and in L5b p=0.026. In L5b M-W test showed difference between cPFC- and PAG-projecting neurons: p=0.012; DS-PAG: p=0.121, cPFC-DS: p=0.303).*

The perisomatic region of the projecting PCs was labelled by using antibody developed against Kv2.1, while the two kinds of GABAergic inputs were visualized by immunostaining for PV and CB1 (Figure 9A). Our results uncovered that the ratio of PV+ and CB1+ boutons on the perisomatic regions of PCs was similar in layer 2/3 and 5a independently of the targeted areas (Figure 9B-D). This ratio, however, showed difference in layer 5b and was higher on PAG-projecting PCs compared to cPFC-projecting neurons. These findings demonstrate a higher ratio of PV+/CB1+ perisomatic inputs in deep layer PCs projecting to the PAG, indicating that the majority of perisomatic inhibition on PT cells originating from PV+ neurons.

4.4. Validation of reporter protein expression in two transgenic mouse lines

In the next set of experiments, we aimed to examine the characteristic of GABAergic INs that provide the perisomatic innervation onto PCs. To this end we performed whole-cell recordings in slice preparations from BAC-CCK-DsRed (Mate et al., 2013) and BAC-PV-eGFP (Meyer et al., 2002) transgenic mouse lines to target the CCK+ and PV+ INs, respectively. As a first step we validated the expression of reporter proteins in the mPFC of these two mouse lines (Figure 10).

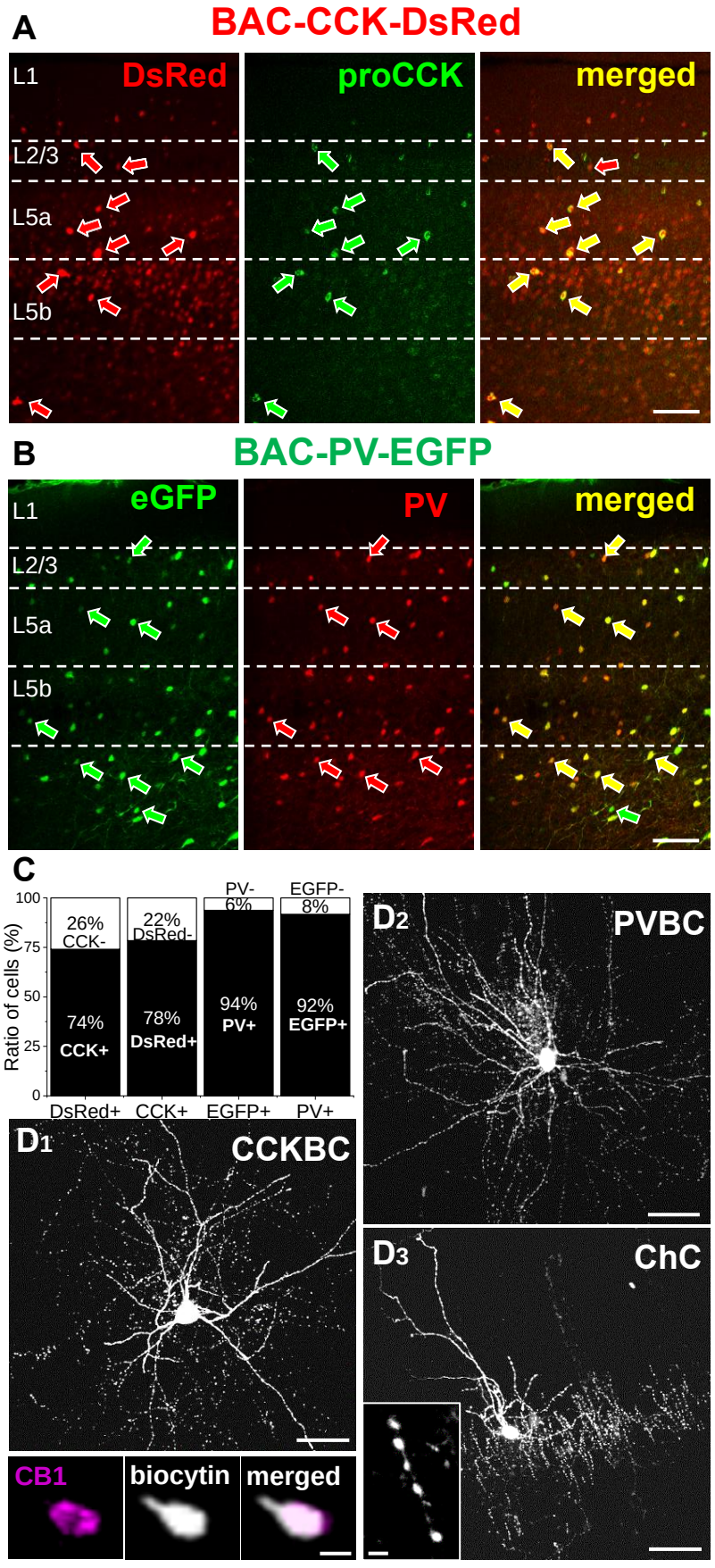
A
BAC-CCK-DsRed
L1
DsRed
proCCK
merged
L2/3
L5a
L5b
B
BAC-PV-EGFP
eGFP
PV
merged
C
Ratio of cells (%)
100
75
50
25
0
26%
CCK-
74%
CCK+
22%
DsRed-
78%
DsRed+
PV-
6%
94%
PV+
EGFP-
8%
92%
EGFP+
DsRed+
CCK+
EGFP+
PV+
D1
CCKBC
CB1
biocytin
merged
D2
PVBC
D3
ChC

Figure 10. ***Validation of reporter protein expression in two transgenic mouse lines*** *(A) Co-localization of antibody labelled proCCK and native DsRed signals in the mPFC of a BAC-CCK-DsRed mouse. Red arrows show DsRed expressing cells, green arrows point to proCCK-immunopositive cells, while yellow arrows indicate the co-localization of the two markers. Dashed white lines represent the boundaries of layers. Scale bar: 100 µm. (B) Co-localization of antibody labelled PV and native EGFP signals in the mPFC of BAC-PV-EGFP mouse. The green arrows show EGFP expressing cells, red arrows point to PV-immunolabelled neurons, while yellow arrows indicate the co-localization of the two markers. Dashed white lines represent the boundaries of layers. Scale bar: 100 µm. (C) The ratio of counted cells within the PrL (first two columns show DsRed/CCK cells (n=183 cell in 3 slices from 2 mice), second two columns show EGFP/PV cells (n=794 cells in 5 slices from 2 mice)). (D_1) Maximum z-intensity projection image taken of an in vitro biocytin-filled CCKBC. Scale bar: 50 µm. Small panels present the CB1-content of a biocytin-containing bouton of the same CCKBC. Scale bar: 1 µm. (D_2) Maximum z-intensity projection image taken of an in vitro biocytin-filled PVBC. Scale bar: 50 µm. (D_3) Maximum z-intensity projection image taken of an in vitro biocytin-filled ChC. Inset shows a characteristic bouton cartridge of ChCs. Scale bar: 50 µm, on the inset: 2 µm.*

We found that in both superficial and deep layers the majority of strongly DsRed+ cells showed immunopositivity for proCCK, while neurons expressing less or weaker DsRed signals were negative for this neuropeptide (Figure 10A, C). Based on these results we hypothesized that the strongly DsRed+ neurons may be INs, whereas lower DsRed signals may be present in a subset of PCs, as described earlier (Mate et al., 2013). To confirm this assumption, we performed whole-cell recordings in acute slices prepared from BAC-CCK-DsRed mice. In line with our prediction, all strong DsRed+ neurons were found to be INs. We revealed in our earlier studies that in this mouse line CCKBCs expressing CB1 on their axon terminals could be sampled both in the hippocampus and BLA (Andrasi et al., 2017; Szabo et al., 2010; Veres et al., 2017). To test, whether the strong DsRed+ neurons in the mPFC also express CB1 on their boutons, we performed CB1 immunostaining on the biocytin-containing neurons (n = 20 cells). Our biocytin-filled INs in the mPFC indeed expressed CB1 on their axon terminals (n = 20 CB1+ out of 20 biocytin filled neurons), i.e. strong DsRed+ INs are CB1/CCKBCs (Figure 10D_1). To sample the PV+ INs, we used the BAC-PV-eGFP mouse line. A similar analysis was

executed to prove the good correspondence between the PV content and eGFP expression (Figure 10B, C). As it is known from previous studies, a various percentage of PV-expressing neurons is ChC in cortical structures (Baude et al., 2007; Vereczki et al., 2016), so we separated them from the PVBCs based on the typical morphological feature of ChCs, i.e. the presence of the characteristic axonal cartridges along their axonal collaterals (Somogyi, 1977; Szentagothai & Arbib, 1974) (Figure 10D_2-D_3). Thus, our results show that these two mouse lines can be used to selectively identify and study CCK/CB1BCs, PVBCs and ChCs in the mPFC.

4.5. Morphological features of basket cells

As biocytin was added in the intrapipette solution during whole-cell recordings obtained in acute brain slices containing the mPFC, using fluorescent dye conjugated streptavidin we visualized the dendritic and axonal arborisation of recorded cells and compared the characteristics of their input and output properties. Using Neurolucida (11.1) software, we reconstructed the dendritic tree and axonal arbour of individual biocytin-labelled INs within the entire *in vitro* slices and compared the different morphological features of BCs. First, we correlated the total axonal length with the total dendritic length for CCKBCs and PVBCs (Figure 11A_1-A_2). We found a significant correlation in case of PVBCs, indicating that PVBCs with larger dendritic tree have larger axonal tree (Figure 11A_2).

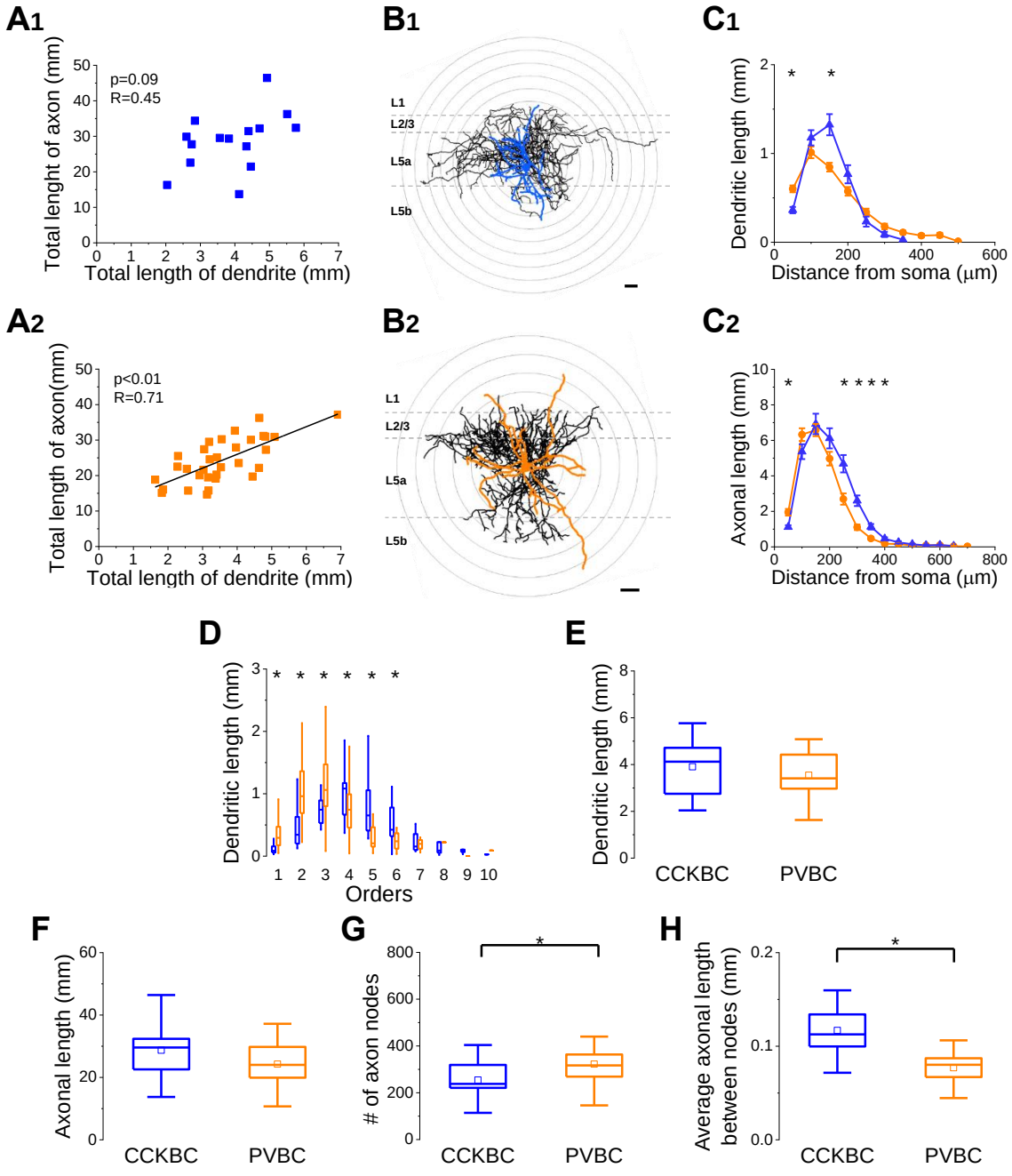

Figure 11. ***Comparison of the dendritic and axonal arborisations of CCKBCs and PVBCs*** *(A_1-A_2) Total axonal length as a function of the total dendritic length. Each dot corresponds to the values of a reconstructed BC. A significant relationship was found between these two values in case of PVBCs (Pearson's r: R=0.71; p<0.01). (B_1-B_2) Neurolucida reconstructions of dendritic and axonal tree of two exampled BCs labelled in slice preparations. Black lines represent the axons, while coloured lines show the dendritic trees. Concentric grey circles drawn on the reconstructions illustrate the 50 µm*

radii used for Sholl analysis. Dashed gray lines represent the boundaries of the layers in the mPFC. (C_1) The dendritic length as a function of the distance from the soma. (M-W test showed differences at 0-50 µm distance from the soma ($p<0.001$) and at 100-150 µm ($p=0.001$)). (C_2) The axonal length as a function of the distance from the soma. (M-W test showed differences at 0-50 µm distance from the soma ($p=0.002$), at 200-250 µm ($p<0.001$), at 250-300 µm ($p<0.001$), at 300-350 µm ($p<0.001$) and at 350-400 µm ($p=0.002$)). (D) Comparison of the dendritic length as a function of the dendritic order. (K-W ANOVA: 1. order: $p<0.01$; 2. order: $p<0.01$; 3. order: $p=0.01874$; 4. order: $p=0.02201$; 5. order: $p<0.01$; 6. order: $p=0.0162$) (E-H) Box chart comparison of the total axonal length, total number of axonal nodes, total axonal length/ total number of nodes and total dendritic length. The mean (small open square), the median (continuous line within the box), the interquartile range (box) and the 5-95% values (ends of whiskers bar) are plotted. (Statistical comparisons were performed with M-W test (G) $p=0.02181$; (H) $p<0.01$.)

The comparison of the total dendritic lengths between the two BC types showed no difference (Figure 11E) though the PVBCs emitted longer dendrites measured from soma than CCKBCs (Figure 11C_1). In addition, we observed differences also in the structure of their dendritic trees. PVBCs had longer primary, secondary and tertiary dendrites than CCKBCs, while CCKBCs had longer higher-order dendritic segments (Figure 11D). Next, we compared the features of the axonal arborisations that again showed several differences. Although both cell types possessed similar axonal length (Figure 11F), the axon of CCKBCs had significantly less axonal nodes (Figure 11G) that resulted in a higher length/nodes ratio (Figure 11H). In contrast to the dendrites, the axon length from the soma was similar in both BC types (Figure 11C_2).

To evaluate whether there are morphologically distinct subpopulations of CCKBCs and PVBCs in the mPFC, principal component and cluster analysis were used to reveal any differences among BCs (Figure 12A-B).

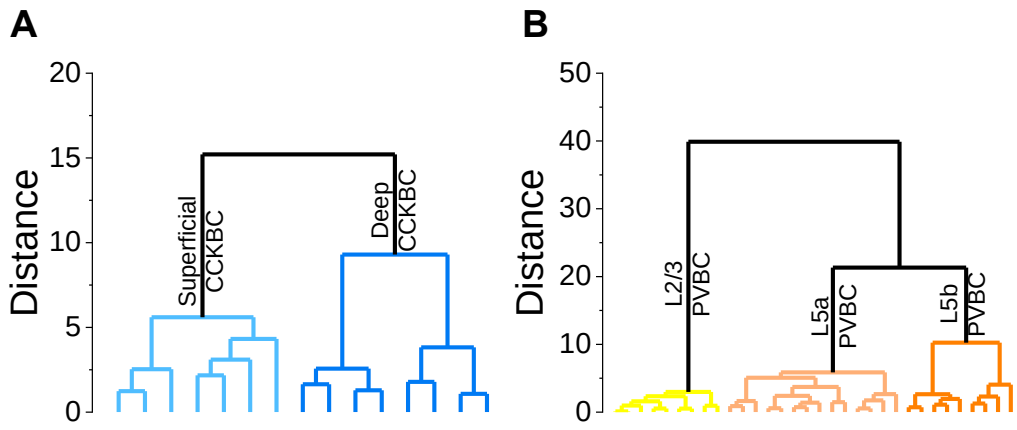

Figure 12. ***Cluster analysis of the two basket cell types*** *(A) Cluster analysis of CCKBCs segregated superficial and deep groups based on the location of their dendrites. Different subgroups are defined by distinct colors: light blue shows the superficial CCKBCs, while dark blue presents the deep CCKBCs. Distance reflects to the accuracy of cluster analysis. (B) Cluster analysis separated PVBCs into three subgroups based on the location of their dendrites and axons. Different subgroups are defined by distinct colors: in yellow L2/3 PVBCs are presented, light orange shows L5a PVBCs, while dark orange defines L5b PVBCs. Distance reflects to the accuracy of cluster analysis.*

Based on their soma and dendritic localization, CCKBCs could be divided into two morphological subgroups (Figure 12A): BCs in the 'superficial group' located in layer 2/3 (Figure 13A_1-B_1) and spread their dendrites predominantly into the upper layers, while the soma and dendrites of the 'deep layer' group were found mostly in layer 5a (Figure 13A_2-B_2). Interestingly, the axonal arborisation of both CCKBCs subgroups were similar and restricted mainly to the layer 5a (Figure 13C_1, C_2). Thus, based on the location of dendritic tree, CCKBCs may be divided into two morphological subgroups, however they may innervate the same populations of PCs within the mPFC based on the distribution of their axonal collaterals.

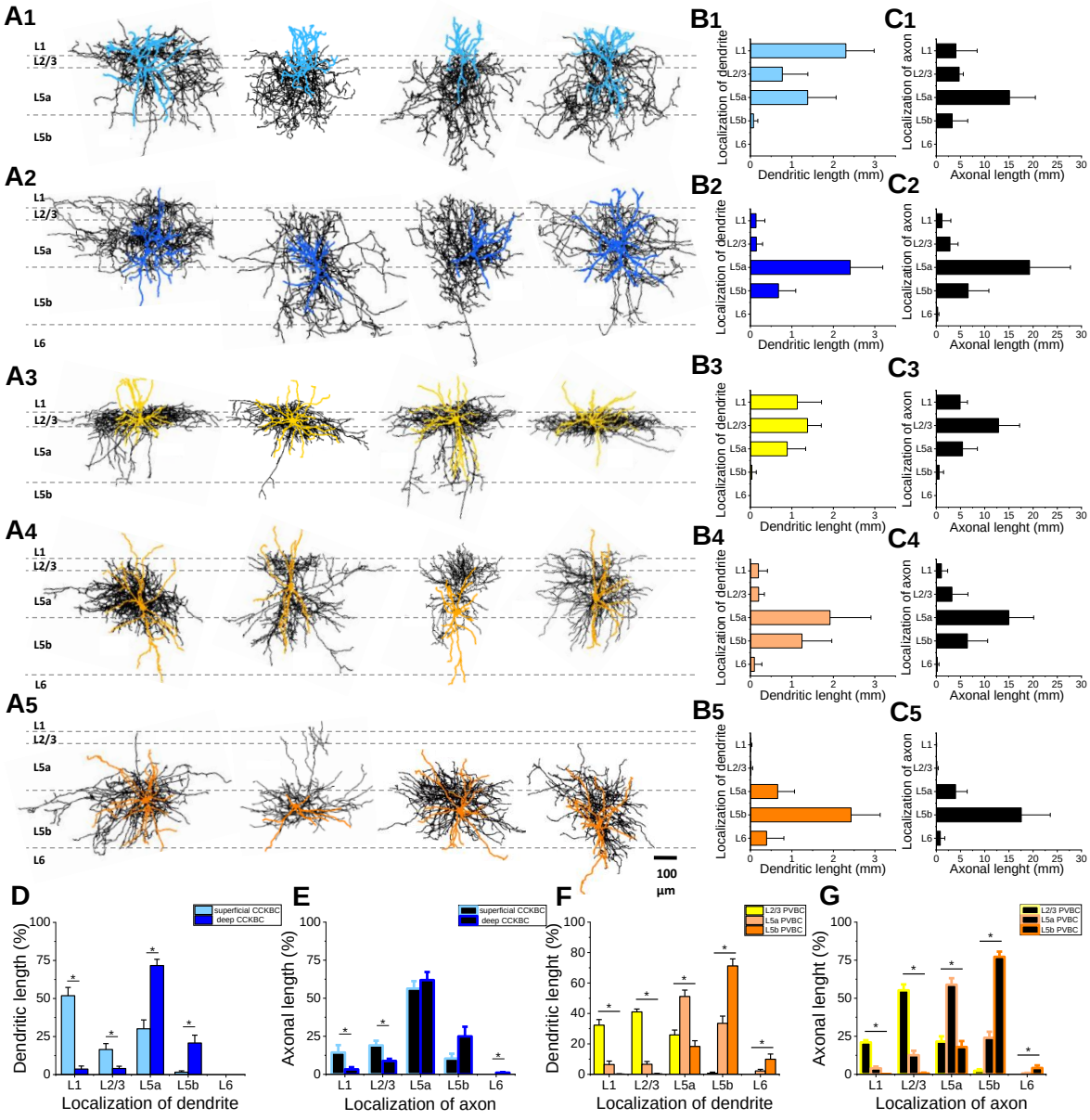

Figure 13. ***Distribution of dendritic and axonal arbour of different BC types within the layers of the mPFC*** *(A1-A5) Neurolucida reconstructions of dendritic and axonal arbour of different BCs labelled in slice preparations. Black lines represent the axons, while coloured lines show the dendritic trees. In light blue the dendrites of 'superficial' CCKBCs are presented (n=7), while the dendrites of 'deep' CCKBCs are shown in dark blue (n=8). With yellow the dendrites of L2/3 PVBCs (n=9), with light orange the dendrites of L5a PVBCs (n=14), while with dark orange the dendrites of L5b PVBCs (n=9) are shown. Dashed dark gray lines represent the boundaries of the layers. Scale bar: 100 µm. (B1-B5) The ratio of the dendritic length in the different layers. (C1-C5)*

The ratio of axons in of the different layers. (D) Comparison of the distribution of the dendritic length in different layers for the two CCKBC subgroups. (M-W tests by layers: L1: p=0.00132, L2/3: p=0.01276, L5a: p=0.00146, L5b: p=0.01569) (E) Comparison of the distribution of the axons of the two CCKBC subgroups in different layers. (M-W tests by layers: L1: p=0.01284, L2/3: p=0.00317, L6: p=0.01915) (F) Comparison of the distribution of dendritic length of the three PVBCs subgroups in different layers. (K-W ANOVA by layers: L1: p<0.01, L2/3: p<0.01, L5a: p<0.01, L5b: p<0.01, L6: p=0.00663.) (G) Comparison of the distribution of axons of the three PVBCs subgroups in different layers. (K-W ANOVA by layers: L1: p<0.01, L2/3: p<0.01, L5a: p<0.01, L5b: p<0.01, L6: p=0.00517.)

In contrast to the similarity of axonal arbour location of the two distinct subgroups of CCKBCs, a larger heterogeneity was observed in case of PVBCs. Cluster analysis separated PVBCs into three subgroups mainly by the dominant location of their axons (Figure 12B). The layer 2/3 PVBCs spread approximately half of their axons along the layer 2/3, while their dendrites located in layer 1, 2/3 and 5a with a similar ratio (Figure 13A_3-C_3). The layer 5a PVBCs and layer 5b PVBCs extended the majority of their dendrites and axons in layer 5a (Figure 13A_4-C_4) and layer 5b, respectively (Figure 13A_5-C_5). These observations indicate that i) the input-output properties of the two BCs are different and ii) there are morphological subgroups of BCs in the mPFC. Our results may imply that the different BCs might contribute to the network operation of mPFC in a distinct manner.

4.6. Postsynaptic target distribution of BCs in the mPFC

To verify that interneurons sampled in the BAC-CCK-DsRed and BAC-PV-eGFP mice are indeed BCs, we examined their postsynaptic target distribution. BCs are defined by preferentially targeting the perisomatic region of their postsynaptic partners. Therefore, we investigated the ratio of axonal boutons of BCs that contacted the perisomatic region revealed by Kv2.1 immunostaining using confocal microscopy (Figure 14A, B). If a biocytin-filled bouton of a BC was in a close apposition with a Kv2.1-labelled soma or a proximal dendritic segment, then we considered this bouton to target the perisomatic region (Figure 14A, B, coloured arrows). If the biocytin-filled bouton avoided any Kv2.1-

immunostained profile, then it was assumed as this boutons targeted a distal dendritic segment (Figure 14A, B, white triangles). With considering these classifications, we estimated the target distribution of BCs by counting 150-200 boutons per biocytin-filled cell.

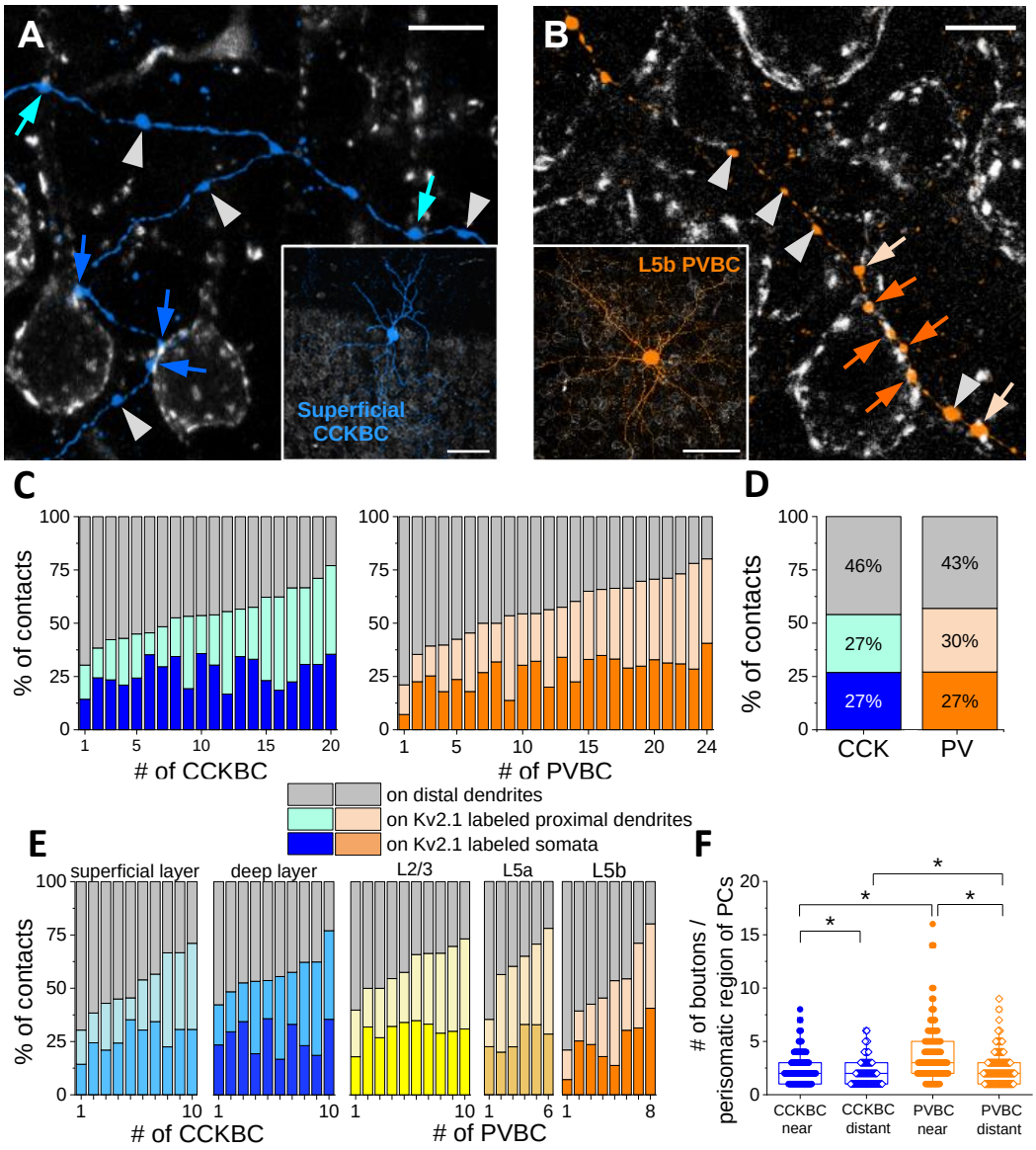

Figure 14. ***Postsynaptic target distribution of BCs within the mPFC*** *(A) High magnification multicolour maximum z-intensity projection confocal image shows biocytin-filled boutons around Kv2.1-labelled neurons, dark blue arrows point to boutons forming contacts on the somata, light blue arrows indicate the proximal dendrite-targeting boutons, while greyish arrows show varicosities that presumably target distal*

dendrites. Scale bar: 10 µm. Inset shows an in vitro biocytin-filled 'superficial' CCKBC. Scale bar: 100 µm. (B) High magnification multicolour maximum z-intensity projection confocal image shows biocytin-filled boutons around Kv2.1-labelled neurons, dark orange arrows point to boutons forming close contacts on a soma, light orange arrows indicate the proximal dendrite-targeting boutons, while greyish arrows show varicosities that likely target distal dendrites. Scale bar: 10 µm. Inset shows an in vitro biocytin-filled L5b PVBC. Scale bar: 100 µm. (C) Ratio of the boutons of CCKBCs and PVBCs forming close contacts on Kv2.1-immunostained perisomatic regions of neurons. Each column represents a single BC (n=20 CCKBC and n=24 PVBC were examined). (D) Average ratio of biocytin-filled boutons forming contacts on Kv2.1-immunolabelled profiles or on unlabelled targets (pooled data from C). (E) Ratio of the boutons of the BC subgroups. Each column represents a single BC (n=3560 boutons of 10 'superficial', n=3518 boutons of 10 'deep' CCKBC and n=2838 boutons of 10 L2/3, n=1986 boutons of 6 L5a and n=1995 boutons of 8 L5b PVBC were examined). (F) Box chart comparison of the number of the perisomatic contacts received by a single neuron from an individual CCKBC and PVBC. Filled circles present the number of perisomatic contacts within 200 µm (near), while open diamonds show number of perisomatic contacts outside the circle with 200 µm radius (distant)., The median (continuous line within the box), the interquartile range (box) and the 5/95% values (ends of whiskers bar) are plotted. 211 and 172 Kv2.1-labelled neurons innervated by 520 and 350 boutons, respectively, from 10 CCKBCs; 199 and 182 Kv2.1-labelled neurons innervated by 761 and 457 boutons, respectively, from 10 PVBCs were examined (K-W ANOVA: $p<0.001$, post hoc Dunn's test: CCKBC near vs. CCKBC distant: $p=0.007$; CCKBC near vs. PVBC near: $p<0.001$; CCKBC distant vs. PVBC distant: $p=0.009$; PVBC near vs. PVBC distant: $p<0.001$).

We found that the boutons of CCKBCs (Figure 14C) and PVBCs (Figure 14D) innervated the perisomatic region with a similar ratio. Overall, around 55% of the boutons targeted the soma and proximal dendrites in both cases (Figure 14E). This high ratio of perisomatic innervation provides evidence that our recorded and biocytin-filled cells are indeed BCs. Importantly, although the ratio of boutons contacting the soma was fairly similar between the BC types and between the subpopulations of CCKBCs and PVBCs, there was a substantial variance in the ratio of boutons innervating the proximal dendritic segments

(Figure 14C, E). The variance in the overall ratio of perisomatic boutons may reflect the difference in the efficacy of synaptic inhibition originated from individual BCs.

Next, we asked the question whether there is a difference in the number of perisomatic boutons from CCKBCs and PVBCs at the single cell level. Therefore, we compared the number of boutons received by Kv2.1-labelled neurons from a CCKBC or PVBC. We selected approximately 20 Kv2.1-labelled neurons per BCs which were located inside or outside of a circle with a radius of 150-200 µm from the somata of BCs and their perisomatic region was clearly distinguishable. We found that individual Kv2.1-labelled neurons receive more boutons from a PVBC than from a CCKBC irrespective of the distance (Figure 14F). These observation implies that PVBCs may provide a stronger synaptic inhibition on their postsynaptic partners than CCKBCs in the mPFC, as the number of perisomatic contacts has been shown to correlate with the magnitude of the postsynaptic responses (Veres et al., 2017).

4.7. Target distribution of PVBCs on PCs projecting to different brain regions

Based on the morphological differences of PVBCs that innervate mostly the PCs in that layers in which they have the most dendrites, we were wondering whether PVBCs innervate distinctly their postsynaptic partners projecting to different regions but located in the same layer. To this end, two different retrograde tracers were injected into two distinct brain regions of BAC-PV-eGFP mice and individual PVBCs from layer 5a and 5b were recorded and filled up by biocytin in *in vitro* slices prepared from the brain of these mice (Figure 15A_1-A_3). CTB was injected into the nucleus accumbens or BA (Figure 15A_2), while FG into the DS, respectively (Figure 15A_3).

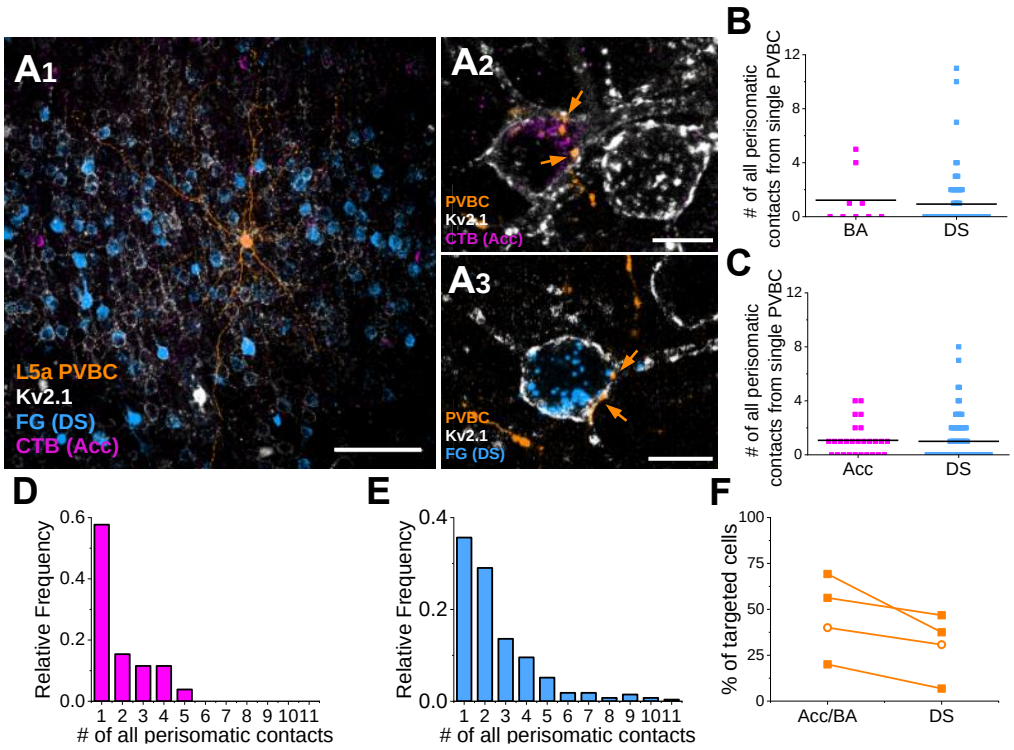

Figure 15. ***Target distribution of PVBCs on PCs projecting to distinct brain areas*** *(A1-A3) Multicolour maximum z-intensity projection images taken from an in vitro biocytin-filled PVBC and PCs projecting to DS or nucleus accumbens. Besides the biocytin-filled and retrogradely labelled cells, immunostaining against Kv2.1 was applied to visualize the perisomatic membranes. Scale bar: 100 µm and 10 µm. (B-C) The number of perisomatic contacts of single PVBCs innervating individual PCs that project to the BA and DS or to the nucleus accumbens and DS. Magenta dots present the number of boutons on BA or nucleus accumbens projecting cells, blue dots show the number of boutons on DS projecting neurons, while black lines indicate the corresponding mean. (D-E) Relative frequency of perisomatic contacts given rise by PVBCs on BA/nucleus accumbent-(magenta) and DS (blue)-projecting PCs. (F) Ratio of innervated PCs projecting to different brain areas (boutons of n=3 PVBCs were examined on PCs projecting to nucleus accumbens and DS (filled square) and boutons of n=1 PVBC were counted on PCs projecting to BA and DS (open circle)).*

By counting the biocytin-filled boutons in a close apposition with Kv2.1-immunolabelled profiles of retrogradely labelled PCs, the following observations were made. First, we found that a single PVBC innervated PCs projecting to different regions with a similar boutons number (Figure 15B, C). Second, we observed that only 10% of all perisomatic

contacts was formed by more than 4 boutons (Figure 15D, E, n=272), indicating that only a small ratio of PCs received a significant innervation from a single PVBC. Finally, we compared the single PVBC-provided innervation of PC populations that project to different areas but their somata were located in the same layer. We found that ~45% of PCs projecting to BA or nucleus accumbens were innervated by a single PVBC in addition to PCs that projected to the DS (Figure 15F). Overall, we concluded based on these observations that single PVBCs did not show target preference and innervate their postsynaptic PCs irrespectively of their projecting area.

4.8. Morphological characterization of ChCs

In addition to BCs, we also recorded and characterized ChCs that expressed eGFP in BAC-PV-eGFP mice (Figure 16A_1). Moreover, a different strategy was applied to visualize almost exclusively ChCs in the mPFC. Here, AAV-fDIO-GFP virus was injected into the mPFC of Nkx2.1-CreERT2::LSL-Flpo mice, resulted in labelling of ChCs in line with the original study (He et al., 2016) (Figure 16A_2). Similarly to BCs, we reconstructed the dendritic and axonal arbour of biocytin-filled ChCs by using Neurolucida software. The morphology of ChCs differed substantially from the BCs: their dendrites spread into the layer 1, reached the pia where they turned and ran parallel with the surface, their soma was located in layer 2/3, while their axons were mostly located in layer 5a (Figure 16A_1-A_2, B, C) and formed so-called cartridges.

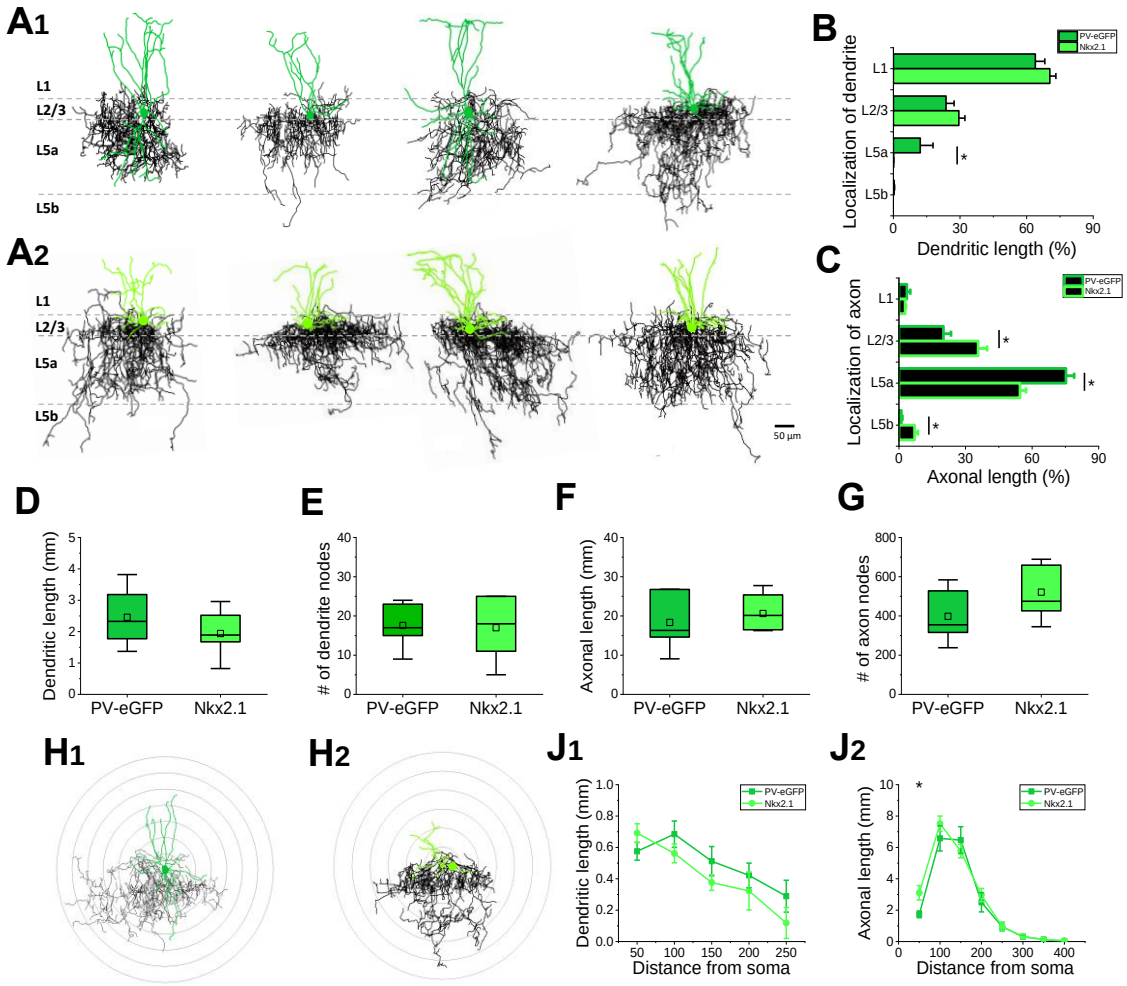

Figure 16. ***Comparison of the morphological features of ChCs recorded in two transgenic mouse lines*** *(A_1-A_2) Neurolucida reconstructions of dendritic and axonal arbours of ChCs labelled in slice preparations prepared from two different genetically-modified mouse lines. Black lines represent the axons, while coloured lines show the dendritic trees, respectively. In dark green the dendrites of PV-eGFP ChCs are presented (n=7), while the dendrites of Nkx2.1 ChCs are shown in light green (n=7). Scale bar: 50 µm. (B) Comparison of the dendritic length of two types of ChCs in different layers. (M-W tests by layers: L5a: p=0.02357.). (C) Comparison of the axonal length of two types of ChCs in different layers. (M-W test by layers: L2/3: p=0.0106, L5a: p=0.00217, L5b: p=0.01684.). (D-E, F-G) Comparison of the total dendritic length (D), number of dendritic nodes (E), total axonal length (F) and number of axonal nodes (G). The mean (small open square), the median (continuous line within the box), the interquartile range (box) and the 5/95% values (ends of whiskers bar) are plotted. Statistical comparisons*

were performed with M-W test. No significant difference was found (D: p= 0.30669; E: p= 0.84751; G: p= 0.37109; H: p= 0.0967). (H_1-H_2) Neurolucida reconstructions of dendritic and axonal trees of two example ChCs labelled in slice preparations. Black lines represent the axons, while coloured lines show the dendritic trees. Concentric grey circles drawn on the reconstructions illustrate the 50 µm radii used for Sholl analysis. (J_1) The dendritic length as a function of the distance from the soma. (K-S test: n.s). (J_2) The axonal length as a function of the distance from the soma. (K-S test: n.s., M-W test in 0-50 µm from soma: p=0.01519.)

The axonal distribution of ChCs implies that these INs mostly innervate their postsynaptic PCs in a different layer than they receive their inputs. Neither the total dendritic and axonal length (Figure 16D, F) nor the total number of dendritic and axonal nodes (Figure 16E, G) showed difference between the two ChC types, however, their dendritic and axonal distribution between the layers differed in some points. We observed that approximately half of PV-eGFP ChCs extended their dendrites into layer 5a, while only a minority (<0.5%) of dendrites of Nkx2.1 ChCs were found in this layer (Figure 16B). Interestingly, the dendritic length from the soma did not differ significantly (Figure 16H_1-H_2, J_1). Comparison of their axonal distributions showed that Nkx2.1 ChCs had more axons in layer 2/3 and 5b and less in layer 5a than PV-eGFP ChCs (Figure 16A_1, A_2, C). The difference in the axonal distribution in layer 2/3 could be observed in results of Sholl analysis, too: Nkx2.1 ChCs possessed more axons in the first 100 µm from the soma, which was located in layer 2/3 (Figure 16H_1-H_2, J_2). These findings suggest that ChCs in the mPFC are morphologically diverse, a variability which might be an important factor in controlling the local network operations.

4.9. Postsynaptic target distribution of ChCs in the mPFC

Next, we examined the target distribution of ChCs. Here, the investigations were conducted on AnkyrinG (AnkG)-immunostained profiles. AnkG expresses in the AIS at the highest level, therefore it is a good tool to visualize the postsynaptic elements of ChCs (Gulyas et al., 2010). First, we applied a triple immunostaining against AnkG, PV and VGAT in the mPFC of wild type animals to examine the GABAergic bouton distribution along the AISs (Figure 17A). A VGAT- or PV-immunolabeled bouton was considered to

contact an AIS if it formed a close apposition with an AnkG-immunolabelled profile. Our analyses revealed that around half of the VGAT+ boutons were PV+ also on the AISs in these mice (Figure 17B, C).

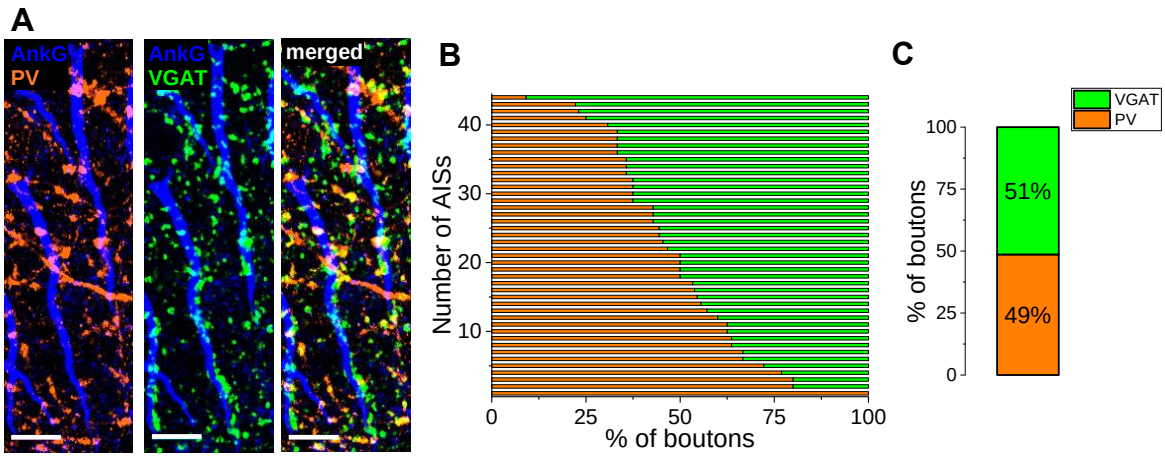

Figure 17: Distribution of immunolabelled PV- and VGAT-expressing boutons along the AISs. *(A) Multicolour maximum z-intensity projection confocal images taken of PrL sections immunostained for AnkG, PV and VGAT. Scale bar: 5 µm. (B) Ratio of immunolabelled PV- and VGAT-expressing boutons forming contacts on AnkG-immunostained profiles. Each row represents a single AIS. (C) Pooled data from B.*

Then we examined the AIS innervation of biocytin-filled ChCs originating from the two transgenic mouse lines. A biocytin-filled bouton was considered to contact an AIS (Figure 18A1-A2), if it overlapped or formed close apposition with an AnkG-immunostained profile (Veres et al., 2014).

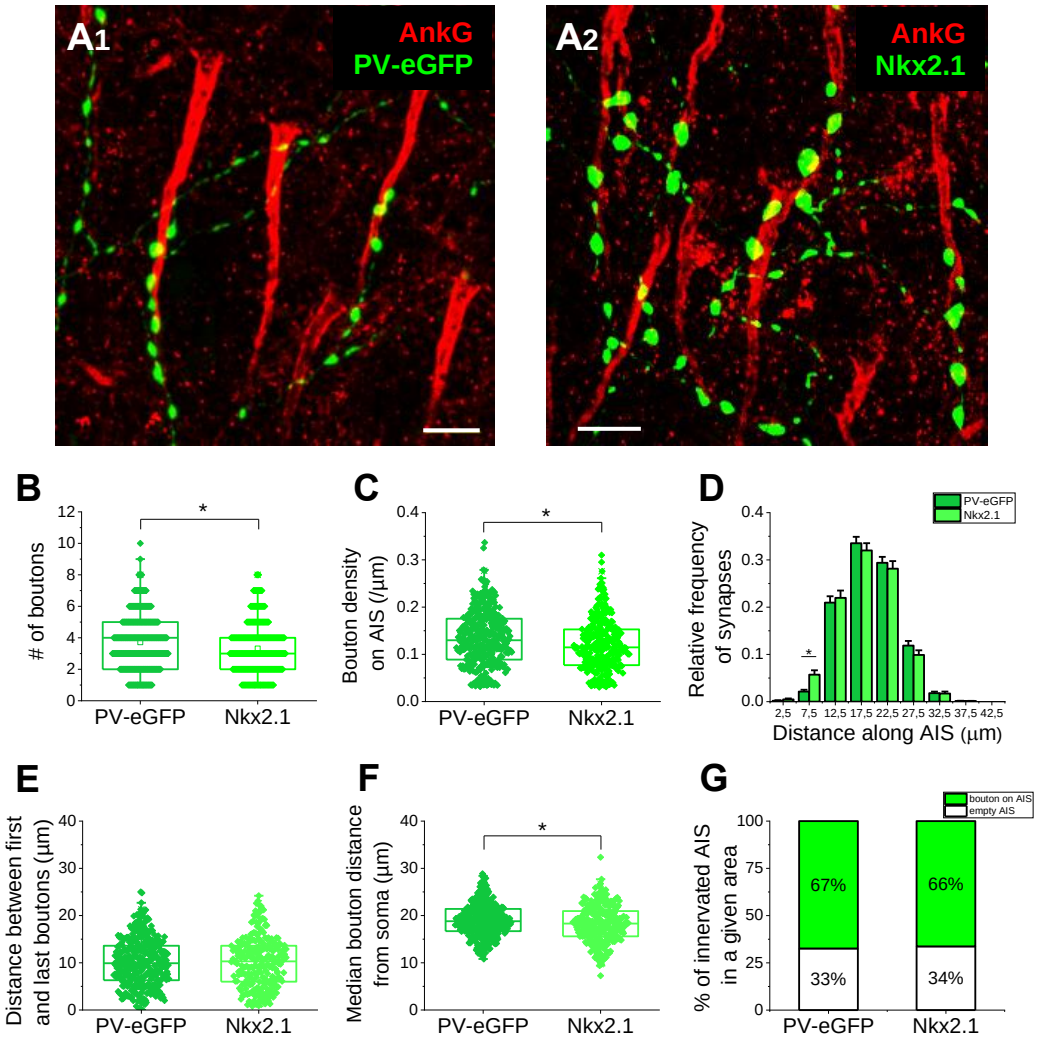

Figure 18. Distribution of boutons of the two types of ChCs along the AISs *(A1-A2) Multicolour maximum z-intensity projection confocal images taken from in vitro biocytin-filled ChCs from the two transgenic mouse lines. Immunostaining against AnkG visualized the AISs. The left image represents boutons of a PV-eGFP ChC, while the right image shows boutons of an Nkx2.1 ChC. Note that both cases the biocytin-labelled boutons form multiple contacts along the AISs. Scale bar: 5µm. (B-C, E-F) Box chart comparison of the number of biocytin-filled boutons along the AISs (B, M-W test: p=0.0028), bouton density on the AISs (C, M-W test: p=0.00126), the distance between first and last boutons along individual AISs (E, M-W test: n.s., p=0.9498) and median bouton distance measured from the soma (F, M-W test: p=0.01929) in the two transgenic mouse lines. Each dot represents data obtained on a single AIS (PV-eGFP: n=8 ChCs, n=1361 boutons on n=366 AISs and Nkx2.1: n=8 ChCs, n=969 boutons on n=292 AISs were examined). The mean (small open square), the median (continuous line within the*

*box), the interquartile range (box) and the 5/95% values (whiskers) are plotted. (D) Comparison of the relative frequency distribution of synapses along the AISs. Bin size: 5 µm (K-S test: n.s., M-W test in 5-10 µm distance: p=0.00242). (G) Ratio of the innervated AISs in a given area (Size of area: 100*100*12 µm; PV-eGFP: n=6 ChCs and n=279 AISs, Nkx2.1: n=6 ChCs and n=347 AISs were counted).*

Counting the boutons along the AISs revealed some differences in the innervation characteristics of the two types of ChCs. We observed that PV-eGFP ChCs innervated their postsynaptic elements with significantly more boutons (Figure 18B) and higher density (Figure 18C) than Nkx2.1 ChCs. Although the distance of the innervated segments along the AISs was similar for both ChCs (Figure 18E), the distribution of single boutons along AIS was distinct: Nkx2.1 ChCs innervated the AISs closer to the soma (Figure 18D, F). Notably, we did not find any difference in the ratio of the innervated AISs in the area occupied by the ChC axon collaterals (Figure 18G). Taken together, these results indicate that the morphologically distinct ChCs show differences in their inhibitory connections, which supports the idea that ChCs from the two transgenic mouse lines could differentially modulate the local network activity.

4.10. Neurochemical content of mPFC INs targeted by BA inputs

To understand the logic of information transfer between brain regions, the identity of neuron types receiving the inputs and, therefore, contributing to shaping the circuit operation is needed to be revealed. One of the key areas, which projects to the mPFC is the BA. Previous studies have shown that the communication via strong bidirectional connections with the BA is an important component of PFC functions (Marek et al., 2018; Peters et al., 2009). Therefore, we examined which types of INs are innervated directly by BA afferents. To achieve this aim, we combined viral tracing with immunostaining. We injected AAV1-hSyn-Cre vectors into the BA of transgenic mice (CAG-LSL-ZsGreen1). The genome of this mouse line contains a gene of the reporter protein ZsGreen1, expression of which is under the control of Cre recombinase. Thus, the expression of ZsGreen1 in a cell reports the operation of the Cre. We used AAV1 to deliver the Cre, as it has been shown that viruses with this capsid effectively jump one synapse, infecting the cells in an anterograde manner (Zingg et al., 2017). Thus, this

anterograde trans-synaptic labelling approach allows us to visualize all neurons in the BA target areas, including the mPFC that are innervated by BA afferents (Figure 19A). To identify the IN types that receive BA inputs, the neurochemical content of ZsGreen1-expressing cells was examined using immunocytochemistry. We used antibodies developed against PV, SST, NPY, VIP and CCK, neurochemical markers that visualize largely non-overlapping IN populations in cortical networks. (Figure 19B$_1$-B$_2$).

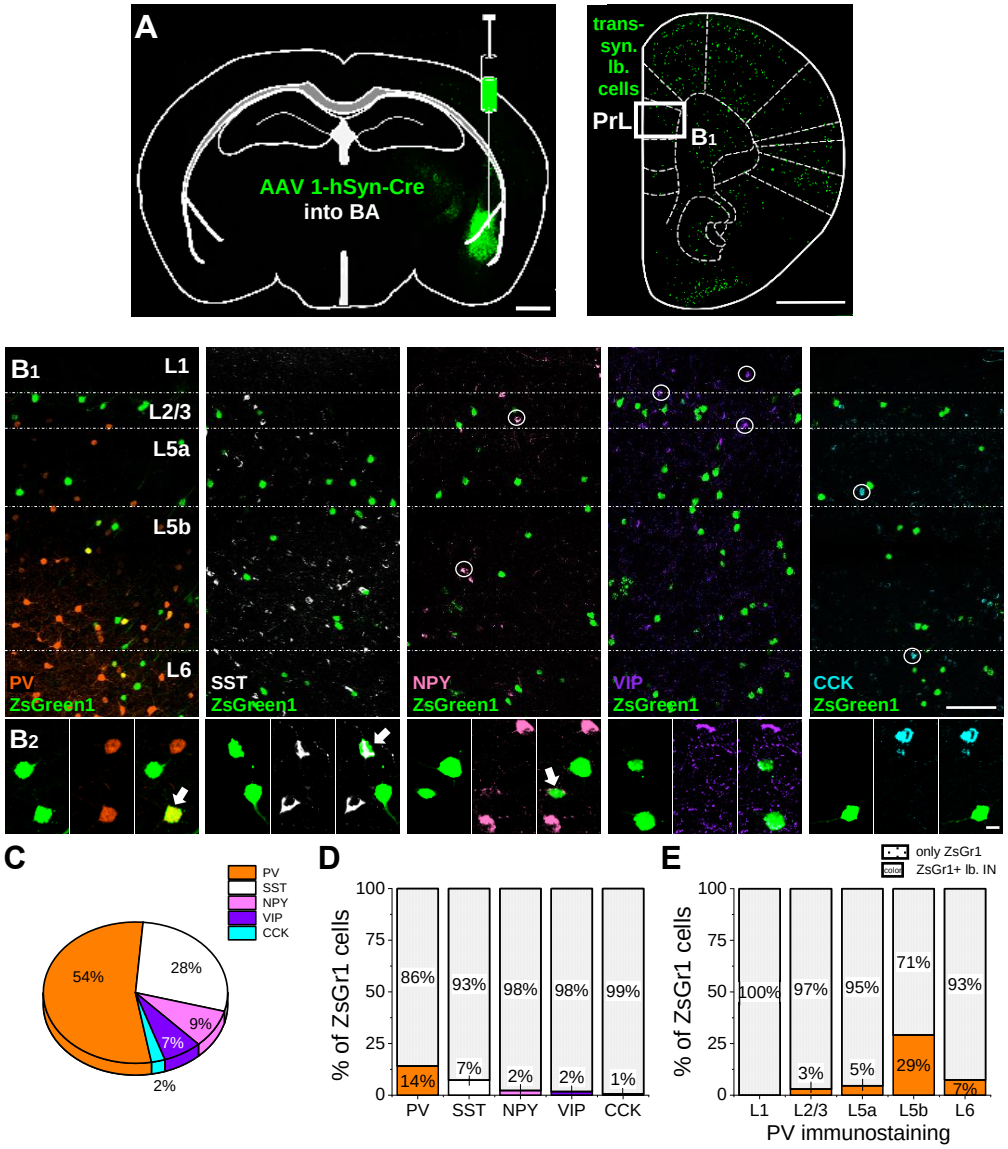

Figure 19. ***Neurochemical content of BA input receiving INs within the PrL*** *(A) Left panel shows the schematic representation of AAV1-hSyn-Cre virus injection into the amygdala. Right panel represents the localization of trans-synaptically labelled neurons within the mPFC. Scale bar: 1000 µm. (B$_1$) Multicolour maximum z-intensity projection*

confocal images taken from the PrL subregion of a ZsGreen1 mouse that was injected with AAV1-hSyn-Cre into the amygdala. From left to right the following immunostaining were applied on the sections: PV is presented in orange, SST in white, NPY in pink, VIP in purple, pro-CCK in light blue, while ZsGreen1-expressing neurons in green. Scale bar: 100 µm. (B_2) Enlarged images from B_1. White arrows indicate those ZsGreen1 neurons that express the given neurochemical marker. Scale bar: 10 µm. (C) Normalised ratio of different neurochemical marker containing ZsGreen cells. (D) The ratio of immunolabelled ZsGreen1neurons (83 cells were PV+ from 565 ZsGreen1 cells, 18 cells were SST+ from 287 ZsGreen1 cells, 10 cells were NPY+ from 397 ZsGreen1 cells, 4 cells were VIP+ from 236 ZsGreen1 cells and 2 cells were CCK+ from 565 ZsGreen1 cells). (E) The ratio of PV-immunolabelled INs that expressed ZsGreen1 in different layers.

We observed that 54% of the immunolabelled, BA input receiving ZsGreen1-expressing INs were positive for PV, the second largest group (28%) expressed SST, while NPY-, VIP- and CCK-positive INs gave rise to smaller fractions of INs containing ZsGreen1 (Figure 19C). However, the ratio of all INs receiving inputs from the BA (~26%) was relatively small compared to the whole ZsGreen1-expressing cell population (Figure 19D), this ratio was slightly higher than the average ratio of INs in the mPFC, indicating that BA afferents might innervate INs with a higher preference. Based on our findings that PV- and SST-expressing INs are the two largest groups of BA-targeted GABAergic cells in the mPFC and the fact that one of the main focuses of this thesis is the PVBCs, we further analysed the distribution of PV-immunolabelled neurons within the different layers. We found that the majority of ZsGreen1-expressing PV+ INs were in layer 5b (Figure 19 E). Thus, these results suggest that BA inputs might preferentially innervate these INs that locate in layer 5b in comparison to other layers.

4.11. PV-expressing INs are preferentially targeted by thalamic and amygdalar inputs in layer 5a and 5b, respectively

As the main IN type that was innervated by BA afferents in the mPFC contained PV, we examined further their innervation. First, we asked whether the proportion of PV+/ ZsGreen1+ INs in layer 5b corresponds to the ratio of PV INs in this layer, or the ratio of

BA-input targeted PV INs deviates from the fraction of these INs occurring normally in distinct layers. Second, we examined whether the inputs arriving from the thalamus (Thal) and lateral entorhinal cortex (LEnt), two additional excitatory inputs of the mPFC, innervate PV-expressing INs in different layers in a similar or distinct manner. To investigate these questions, we made similar anterograde trans-synaptic labelling like in the previous experiments (Figure 19). To confirm that the labelling is not dependent on the AAV type used in these investigations, two approaches were used. In the first set of experiments, we injected AAV1-hSyn-Cre into ZsGreen1 mice as above, revealing all neurons in the mPFC that received monosynaptic innervation, followed by immunostaining to identify PV-expressing INs. In the other set of experiments, we used PV-Cre mice, in which a Cre-dependent construct packed into AAV1 (AAV1-DIO-ChETA-EYFP) was injected into the regions of interest. As the distribution of the labelled PV-expressing neurons in the different layers was similar in both approaches, we merged the data (Figure 20C).

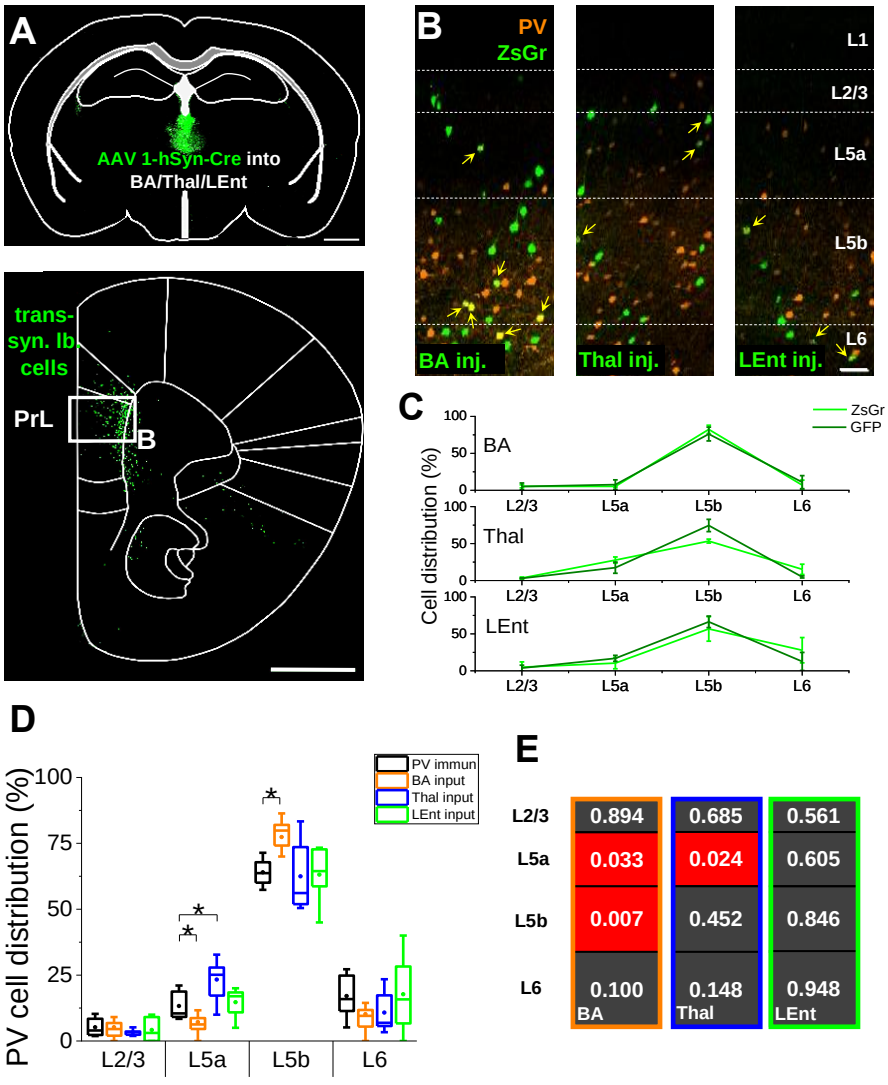

Figure 20. ***PV-expressing INs in the mPFC are preferentially innervated by thalamic and amygdalar afferents in layer 5a and 5b, respectively.*** *(A) Upper panel shows the schematic representation of AAV1-hSyn-Cre virus injection into the Thal. Bottom panel represents the localization of trans-synaptically labelled cells within the mPFC. Scale bar: 1000 µm. (B) Multicolour maximum z-intensity projection confocal images taken from the PrL subregion of ZsGreen1 mice injected with AAVs into the BA, Thal and LEnt. Immunostaining was used to visualize PV INs. Arrows point to the PV positive ZsGreen1 cells. (C) Comparison of PV cell distribution in ZsGreen1 and PV-Cre mouse lines upon AAV injections into different areas. Chi-Square Homogeneity test showed no differences between mouse lines. (BA: χ2=0.09, p=0.99; Thal: χ2=1.86, p=0.6; LEnt: χ2=0.2,*

p=0.98) (D) Box chart comparison of PV cell ratios in different layers. PV-immunolabelled INs are shown in black, the BA input receiving PV cells in orange (n=680), Thal input receiving PV cells in blue (n=737), while LEnt input receiving PV cells in green (n=178). The mean (small open square), the median (continuous line within the box), the interquartile range (box) and the 5/95% values (ends of whiskers bar) are plotted. (E) p values of M-W test comparison between the ratios of PV cells receiving a given extra-mPFC inputs versus PV-immunolabelled cells in a given layer (Black versus coloured bars in panel (D). Red colours indicate significant differences.

By counting the BA, Thal and LEnt input receiving PV-containing INs in different layers and comparing their distribution to all PV-immunostained INs, we found that inputs from the BA and Thal innervate PV-expressing GABAergic cells in a layer specific manner. A higher ratio of PV-positive INs was labelled with AAVs in layer 5b in case of BA inputs and layer 5a in case of Thal inputs, respectively (Figure 20B$_1$, D, E), in comparison to the relative distribution of all immunostained PV INs would indicate. These results show that PV-expressing INs are disproportionally innervated in layer 5a and 5b by thalamic and amygdalar inputs, respectively, while afferents from the lateral entorhinal cortex make no preference in the innervation of PV-containing INs. These data may imply that excitation from the thalamus and amygdala may control the mPFC function in a layer specific manner via feedforward inhibition.

4.12. Visualizing INs in the mPFC by CaMKIIα promoter

Previously we found that PV-containing INs receive layer-specific inputs from remote brain regions, but to better understand the exact role of these cells in circuit operation, we need to explore their local inputs. To unravel the structural and functional connectivity between cells and regions, viral vectors are used typically. CaMKIIα-driven protein expression is often a choice aiming to specifically target or manipulate PCs in cortical networks (Basu et al., 2008; Egashira et al., 2018; Fenno et al., 2014; Huang, 2014; Scheyltjens et al., 2015; Song & Palmiter, 2018). This approach is based on the observations that immunostaining against CaMKIIα labelled PCs, but not INs (Liu & Jones, 1996; Sik et al., 1998). However, recent studies have reported that CaMKIIα promoter was able to visualize GABAergic INs too (Radhiyanti et al., 2021; Watakabe et

al., 2015). To clarify this contradiction, we examined whether CaMKIIα promoter-controlled protein expression can be identified in different GABAergic cell types in distinct cortical areas including the mPFC. Therefore, we injected three different viruses into the mPFC using the same CaMKIIα promoter to express different genetic constructs (AAV2/5-CaMKIIα-ChR2-mCherry, AAV9-hChR2-CaMKII-mCherry, AAV9-CaMKII-ArchT-GFP) and performed immunostaining on fixed slices containing the virus infected area. We observed that 88% of PV-immunolabelled neurons (Figure 21 A, C, E) and 26% of CCK-immunolabelled neurons (Figure 21 B, D, E) co-expressed the mCherry or GFP signals in the mPFC. These observations revealed that in addition to the PCs, AAVs carrying CaMKIIα-promoter-driven constructs can infect distinct types of cortical INs to a different extent.

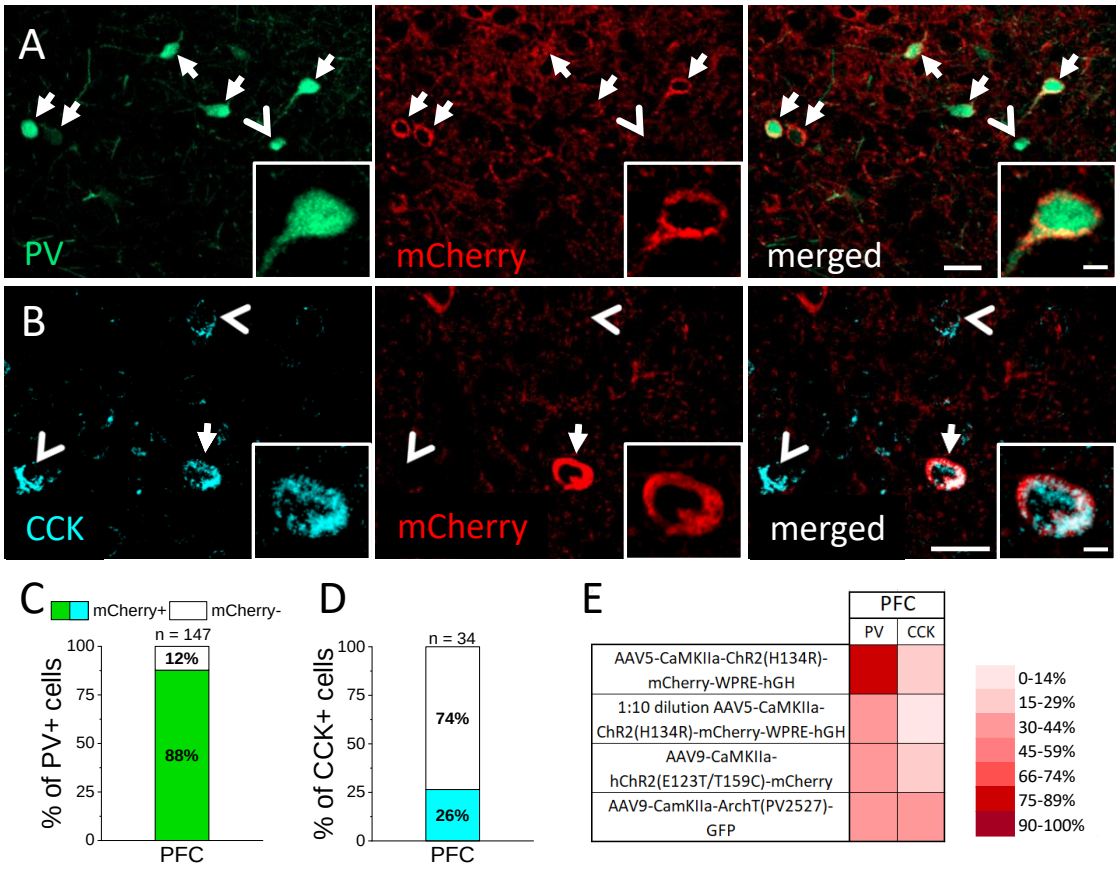

Figure 21. ***CaMKIIα promoter-driven expression of reporter proteins visualizes a substantial portion of INs expressing PV and CCK.*** *(A, B) Multicolour confocal microscopic images taken of fluorescently immunolabelled PV (green) and CCK (light*

blue) containing INs, respectively, together with mCherry (red) expression in neurons infecting by AAV5-CaMKIIα-ChR2-mCherry construct. Arrows point to mCherry containing INs, arrowheads label those lacking mCherry signal. Scale bars: 25 µm and 5 µm (insets). (C, D) Ratio of mCherry expression in the different IN types in the mPFC. (n=2 mice, number of examined cells is indicated above the bar.) (E) Heat map showing the percentage of reporter protein expressing INs using different virus constructs or dilution injected into the mPFC.

5. Discussion

We have examined the GABAergic inputs arriving to the perisomatic region of PCs in the PrL subregion of mouse mPFC, identified the sources of these inputs and compared the morphological features of INs that provide the vast majority of perisomatic inhibitory inputs. In addition to the layer definition in mouse mPFC our main findings are the followings: (1) the perisomatic region of PCs in the mPFC is innervated mostly by CB1- or PV-expressing GABAergic inputs. These inhibitory inputs on the somata and proximal dendrites of PCs originate from morphologically different BC types expressing CCK/CB1 or PV. At the population level, more than 50% of boutons of both BC types innervated the perisomatic region of PCs. However, at the single cell level, PVBCs innervated the perisomatic region via more boutons than CCKBCs. (2) The AISs of PCs are innervated by distinct ChCs, which differed in their morphological features. Notably, the distinct ChC types contacted their postsynaptic AISs in a different manner. (3) Additionally, we found that PVBCs are innervated by inputs arriving from the BA and Thal in a layer-specific manner. (4) CaMKIIα promoter containing constructs packed into AAVs infect both PV and CCK-expressing INs, albeit with different efficacy.

5.1. Layer definition in the mPFC

Although several studies have examined the cytoarchitectural and connectivity features of the mPFC, the layers in this cortical area are still ill-defined and show inconsistency among studies (Anastasiades et al., 2018; Clarkson et al., 2017; Lu et al., 2017). Recent studies have been established a molecular definition of layers by using spatial and single-cell transcriptomics (Ortiz et al., 2020; Tasic et al., 2018; Wang et al., 2018). Examining several hundred genes, distinct molecular cell types in cortical areas could be defined that were used to delineate the layers in these studies. However, defining a layer using gene expression appears the most precise method, it is more complicated and expensive method than using for example immunohistochemistry. Moreover, the widely used approach to define the layers based on measurements of the distance from the brain surface does not seem to be the best way, because the layers in the mPFC do not run parallel with the *pia*. Therefore, we defined the layers of the mPFC by using a combination of antibodies developed against WFS1, Calb, Ctip2 and FoxP2 (Figure 7).

The visualization of these markers makes the layer definition easier, cheaper, and more reliable than previously mentioned approaches.

5.2. GABAergic inputs on the perisomatic region of PCs in the mouse mPFC

The perisomatic region of cortical PCs is innervated mostly, if not exclusively by GABAergic inputs (Freund & Katona, 2007; Megias et al., 2001; Vereczki et al., 2016). This functional domain of PCs is composed of the AIS, soma and proximal dendrites. These distinct parts can be visualized by using different immunostaining: Kv2.1-labbeling visualized the soma and around the first 50 µm of proximal dendrites of the PCs, while it provides only a weak labelling on the AIS (Bishop et al., 2015; Newkirk et al., 2022). To visualize the AISs, we applied AnkG staining which labels around the first 10-60 µm of the AISs. Additionally, prior studies elucidated that if a labelled bouton forms a close apposition to Kv2.1 or AnkG visualized profile, we can identify this bouton as a contact on these parts, as electron microscopic analyses showed that such a bouton gives rise to a synaptic contact with its postsynaptic elements with more than 80% probability (Veres et al., 2017; Veres et al., 2014). Collectively, these results and tools provide the opportunity to examine thoroughly the perisomatic inhibition in the mouse mPFC. It is important to note that Kv2.1 immunostaining visualizes not only the perisomatic region of PCs, but also some GABAergic neurons in cortical networks. As about 20% of all neurons are GABAergic cells in the mouse neocortex (Le Merre et al., 2021; Tremblay et al., 2016), the majority of Kv2.1-immunoreactive neurons examined in this thesis should be PCs. Similarly, AnkG visualizes the AISs of both PCs and INs, but as previously it has been shown that ChCs form synapses only on the AISs of PCs (Somogyi, 1977; Szentagothai & Arbib, 1974), it is safe to assume that we examined the PC inputs from ChCs,

Our findings revealed that altogether around 90% of the GABAergic somatic inputs contain PV or CB1, however, the ratio of two types of inputs showed small differences in distinct layers (Figure 8C). This difference between layers, especially difference between upper (layer 2/3 and 5a) and deep (layer 5b) layers was also observed, when we analysed the inputs on PCs projecting to distinct brain regions: PAG projecting PT cells received significantly higher ratio of PV/CB1 inputs compared to other PCs projecting to

different regions (Figure 9). These data suggest that perisomatic innervation of PCs in the mPFC depends on the projection area of PCs. (Figure 9). Noticeable that the high ratio of GABAergic somatic inputs containing either PV or CB1 was comparable to that found in other brain regions: in the BLA 71% of perisomatic inhibitory inputs express PV or CB1 (Vereczki et al., 2016), while in the hippocampus this ratio reached the 95% (Takacs et al., 2015). Moreover, a similar variability between layers was found in hippocampal CA1 region, too: PCs located in deeper CA1 *stratum pyramidale* received more PV inputs than PCs located in superficial CA1 (S. H. Lee et al., 2014). Thus, additionally to the findings that two types of BCs contribute mainly to perisomatic inhibition in the mPFC as well as in other cortical structures (Freund & Katona, 2007; Vereczki et al., 2016), PVBCs provide more numerous inputs on PCs in deeper layers. These results support the hypothesis that INs are able to selectively modulate various populations of PCs and may strongly influence the excitation/inhibition balance across layers, shaping the information transfer from the PFC towards other brain regions.

The third part of perisomatic region of PCs, the AISs are also densely innervated by GABAergic inputs, and the vast majority, if not all, of these boutons originates from ChCs in the cortical structures (Schneider-Mizell et al., 2021; Vereczki et al., 2016; Veres et al., 2014). When we examined the GABAergic boutons that form close appositions with the AIS in the layer 2/3 and layer 5a of mPFC, we found that around half of these inputs contains PV (Figure 18). Although our result seem to contradict to previous findings obtained in the mPFC, where only 15% of ChC were found to be immunopositive for PV (Inan & Anderson, 2014; Taniguchi et al., 2013). The fact that these studies examined the PV content of ChCs at the soma level, whereas we investigated the axonal boutons may explain, at least partially the disagreement, as the PV level of a given cell is a subject of changes (Baimbridge et al., 1992).

5.3. Morphologically distinct PTIs are present in the microcircuits of the mPFC

Our results showed that inputs on the somata and proximal dendrites of PCs in the mPFC arrived almost exclusively from PV- and CB1-expressing GABAergic terminals. Previous studies revealed that these boutons originated from PV-and CCKBCs (Freund & Katona, 2007; Kawaguchi & Kubota, 1998). Our previous studies in the amygdala and

hippocampus showed that BAC-PV-eGFP and BAC-CCK-DsRed transgenic mouse lines are appropriate to examine these BCs selectively (Gulyas et al., 2010; Szabo et al., 2014; Vereczki et al., 2016). Similarly to the amygdala, in the mPFC we also did not find a full correspondence between the reporter protein expression and immunocytochemically labelled cells (Vereczki et al., 2016). The minor difference in BAC-PV-eGFP can be caused by protein expression level, which may vary during the lifespan (Baimbridge et al., 1992) Thus, using these transgenic mouse lines, which allow us to selectively target the different IN types, we examined the morphological characteristics of BCs. Though the morphological features of these two BC types have not been compared in the mouse mPFC yet, there are some studies that examined separately these cells in mouse and rat neocortex or made comparative studies in other brain regions, like BA and hippocampus (Freund & Katona, 2007; Kawaguchi & Kubota, 1998; Lagler et al., 2016; Vereczki et al., 2016). In accordance with previous findings in rat frontal cortex, we observed that both BC types possessed multipolar dendritic trees, their main axon originated mostly from the soma, shortly branched and emitted collaterals in all directions (Kawaguchi & Kubota, 1998; Lagler et al., 2016; Miyamae et al., 2017). Additionally, axon collaterals of PVBCs were mainly restricted to the layers of the soma and neighbouring layers (Lagler et al., 2016). Although, the non-layered structure of BA is the exact opposite to the layered structure of mPFC, the features of BCs were similar in both region (Vereczki et al., 2016). For instance, the comparison of total dendritic and axonal length did not show any difference either in the mPFC or BA. Moreover, the structural differences of dendrites were also similar: PVBCs possess more primary and secondary dendrites than CCKBCs, whereas CCKBCs have more higher-order dendritic segments than PVBCs in both brain regions. The distinct number of axonal nodes was also noticeable in both areas (Vereczki et al., 2016). These similarities suggest that BCs do not have brain region- or species-specific morphological characteristics, which predicts that these INs play similar role in distinct brain regions. It is worth noting that for the reconstructions, we selected those cells which located in the middle of the slices and whose dendrites were mostly intact. Moreover, the reconstruction of several BCs makes possible to reveal the differences between BC types. In contrast of the non-layered structure of BA, mPFC possesses well-defined layered structure (Figure 7), thus different BC types could be divided to further subgroups in the mPFC based on the localization of their somata,

dendrites and axons. These morphological differences might have an important role, because distinct layers in the mPFC are innervated by inputs arriving from different brain regions. Therefore, BCs in distinct layers may receive inputs from different brain areas and if these inputs arrive separated in times, then they can influence the PC activity in a temporarily altered manner. On the other hand, PCs located in distinct layers project to different brain regions, therefore, BCs are able to modulate the intrinsic and extrinsic connectivity of mPFC, too.

The third type of examined PTIs is the ChCs, cells which possess unique morphology in the neocortex. Similarly to our observations, the somata of these INs mostly located at the border of layer 1 and 2, their dendrites were extended in layer 1 and 2 and their axons exhibited chandelier-like cartridges (Inan et al., 2013; Taniguchi et al., 2013). Moreover, combining a transgenic approach with viral technique, we were able to compare the features of ChCs originating from two different genetically modified mouse lines. Our results revealed that morphologically distinct ChCs exist in the mPFC, although the overlap between these cell populations is not known at present. Our analysis showed that, although the total dendritic and axonal lengths of distinct ChCs were similar, a different distribution of their processes between layers was observed that might endow them to control PC networks distinctly. Taken together, our results suggest that beside the two distinct BC types, different ChCs can contribute to physiological network operation in the mPFC.

Although no comparative morphological studies have been published about BCs or ChCs in mouse and human cortices, it is worth highlighting some similarities and differences obtained in these species. For instance, in human motor cortex BCs extend their dendrites across several layers, while in mouse mPFC the dendrites localized in the layers where their soma located (Marin-Padilla, 1969). The dendrites of ChCs also showed ascending or descending vertical orientation in human visual cortex, similarly to our observations. Additionally, similarly to ChCs in the mPFC, human ChCs also possess recurving dendritic ends (Marin-Padilla, 1987). The more detailed comparison of these cell types between species in the future might help us to understand better the pathological conditions underlying different neuropsychiatric disorders.

5.4. Postsynaptic target distribution of distinct PTIs

Multicolour labelling allowed us to analyse the innervation pattern of distinct PTIs. We observed that on average 56% of the boutons of both BC types contacted the somatic and proximal dendritic regions of neurons. Additionally, the ratio of the innervation showed a great variability in both BC types, meaning that there were cells, which targeted rather more distal dendritic parts of PCs than their perisomatic region, while other cells innervated preferentially the perisomatic membrane surface. Interestingly, this observed variance was due to the difference in the innervation of the proximal dendrites, as the ratio of boutons on the somata was fairly similar within and between the BC types (Figure 8D). Moreover, between the two extreme values, the ratio of the perisomatic contacts varied continuously, which means that the target distribution of BCs did not reflect their morphologically distinguished subgroups (Figure 8E). When we counted the number of boutons received by single PCs in the neighbourhood of BCs, we observed that PVBCs innervated individual PCs with significantly more boutons than CCKBCs, which suggest that PVBCs may provide stronger synaptic inhibition (Figure 8F). These observations show resemblances to findings in the BA, where a similarly great and continuous variability were found in the target distribution for both BC types (Veres et al., 2017), and the difference between the number of boutons received by single PCs was also noticed (Vereczki et al., 2016).

In addition to the BCs, we compared the target distribution of ChCs sampled in different transgenic mouse lines. Similar to the visual cortex and BA, a great variability was observed in the number of synaptic contacts in both ChC types (Schneider-Mizell et al., 2021; Veres et al., 2014). Although the variability was similar between brain regions, the average number of synapses originated from individual ChCs on single PCs shows clear differences: in the BA around 35% more synapses was found on the AISs compared to those found in the somatosensory cortex and the present study (Inan et al., 2013; Veres et al., 2014). Interestingly, when we compared the target distribution of ChCs sampled in the two mouse lines, a small but significant difference was observed in the number and position of the boutons along the AIS, which may indicate a difference in their capability to control the function of their target PCs.

5.5. Layer-specific innervation of PV-expressing INs

Our morphological analysis of PVBCs revealed that most of their dendrites and axons were restricted to the same layer where their cell bodies were found (Figure 6). Moreover, previous findings (Oh et al., 2014) and our unpublished data demonstrated that axons from distinct brain regions projecting to the mPFC also show a layer-specific distribution. Namely, BA afferents target layer 2/3 and layer 5b, thalamic inputs terminate preferentially in layer 1 and 5a, whereas the projection from the lateral entorhinal cortex occupies layer 2/3 and layer 5b. Based on these observations, we investigated whether PV-expressing INs in the given layer of the mPFC are preferentially innervated by the extra-PFC inputs where they terminate. We found that thalamic and amygdalar inputs provided indeed a layer-dependent innervation. The BA-innervated PVBCs are disproportionally more abundant in layer 5b and less numerous in layer 5a in comparison to the ratio of PV-expressing INs revealed by immunostaining. In contrast, PVBCs innervated by the thalamus are more abundant in layer 5a as it would be predicted by PV immunostaining. These anatomical findings support the hypothesis that excitatory inputs from the BA and thalamus can mediate profound feedforward inhibition via PVBCs in the mPFC in a layer-specific manner. Although, there is no study which directly investigated the impact of extra-mPFC driven, PVBC-mediated layer-specific feedforward inhibition in the mPFC, several studies examined the role of PVBCs in distinct afferent-driven circuit operation (Delevich et al., 2015; Ferguson & Gao, 2018b; McGarry & Carter, 2016; Yang et al., 2021). In these studies, e.g., the authors showed that thalamic inputs driven PV INs play a crucial role in social preference and working memory (Delevich et al., 2015; Ferguson & Gao, 2018b), while BA inputs innervated PV cells have a role in regulation of social and fear behaviour (McGarry & Carter, 2016). Based on these observation it is safe to assume that the layer-specific feedforward inhibition might play a critical role in various cognitive processes via altering the function of PCs located in distinct layers. Notably, there is evidence obtained in the primary visual cortex which supports the hypothesis regarding the functional operation of layer-specific inhibition. A layer-specific and brain state dependent gamma oscillations in the visual cortex were observed in awake and sleeping animals, oscillations that are dependent on the activity of PVBCs (Buzsaki & Wang, 2012; Gulyas et al., 2010; Klausberger et al., 2003; Senzai et al., 2019). Thus, taken together, similarly to other cortical regions,

laminar specific inputs from remote areas and morphology of PVBCs might enable these GABAergic cells to convey a layer-specific inhibition onto mPFC network.

5.6. CaMKIIα promoter-driven expression of reporter proteins in cortical INs

Previous study in marmoset cerebral cortex showed that PV-expressing INs can be infected by a CaMKIIα promoter-driven AAV construct (Watakabe et al., 2015). Our findings in mouse mPFC are consistent with this observation, but we extended these findings, showing that other neurochemical marker expressing GABAergic cell types – e.g. CCK-expressing interneurons – could be infected also by AAV carrying CaMKIIα promoter-driven virus constructs. Although, there is no clear explanation for this phenomenon yet, it has been known that another isoform of CaMKII– namely γCaMKII – is specifically expressed in cortical INs (He et al., 2021). This fact raises the possibility that the promoter of CaMKIIα might interact with the gene sequence of γCaMKII, thereby providing the opportunity to miss-express proteins driven by the CaMKIIα promoter in GABAergic cells. In summary, our findings revealed that CaMKIIα promoter-driven expression of different virus constructs is not specific for cortical excitatory neurons, but also infect distinct GABAergic cell types, constraining the use of CaMKIIα promoter in studying PC functions specifically.

6. Conclusion

The perisomatic inhibition is one of the most powerful way to regulate the inhibition-excitation balance in a given microcircuit. In the mouse mPFC two main types of inhibitory neurons are responsible for innervating the perisomatic region of PCs: the different neurochemical marker-expressing BCs and at least two distinct types of ChCs.

The soma and proximal dendrites targeting CCK- or PV-expressing BCs showed morphological diversity within the mPFC. CCKBCs could be divided into two subgroups based on their soma and dendritic location, however, they possessed similar axonal distribution between layers. PVBCs could be separated into three morphological subgroups based on their predominant location of their axons and dendrites, thereby they possessed a layer-restricted arborisation. These differences in their axonal distribution suggest that these cells play distinct role in the microcircuit of mPFC. Additionally, we found that PVBC innervated their postsynaptic partners with more boutons at single cell level, than CCKBCs, therefore might provide stronger inhibition on them. We observed also that PV-expressing INs in different layers are preferentially innervated by extra-PFC inputs. This innervation combined with the layer-restricted axonal arborisation of PVBCs might enable them to provide layer-specific feedforward inhibition in the mPFC.

The AIS of PCs is innervated mostly, if not exclusively by ChCs. Due to the transgenic approach combined with viral labelling, we were able to compare the features of two types of ChCs originating from distinct mouse lines. The two types of ChCs showed morphological differences in their dendritic and axonal distribution between layers: some of the PV-eGFP ChCs spread their dendrites in layer 5a, while Nkx2.1 ChCs had denser axonal arborisation around their soma resulting more axons in layer 2/3 and 5a. Additionally, the number and distribution of postsynaptic boutons on the AISs of distinct ChCs also showed differences, which might indicate that these cells contribute to the network organisation in a distinct manner.

In summary, our findings revealed that morphologically heterogeneous inhibitory neurons provide the perisomatic inhibition in the mFPC. The diversity of PTIs might enable them to influence the operation of mPFC in functionally specific manner.

7. Summary

Perisomatic inhibition provided by local GABAergic neurons can efficiently control the spiking of postsynaptic neurons, thereby they can play a critical role in different cortical functions. Despite the importance of these inhibitory circuits, their details are still largely elusive especially in associative cortices, like the medial prefrontal cortex (mPFC). Therefore, in this thesis, we determined the sources of inhibitory inputs on the perisomatic region of pyramidal cells (PCs) in the mPFC, compared the morphological features and postsynaptic target distribution of these interneurons (INs) and examined their inputs arriving from distinct brain region. As these perisomatic region targeting interneurons (PTIs) could be divided into basket cells (BCs) and chandelier cells (ChCs), we examined the two groups separately.

Our results showed that the somato-dendritic part of the perisomatic region of PCs is innervated mostly by cholecystokinin- and parvalbumin-containing BCs (CCKBC and PVBC). Although, both BC groups could be divided further into distinct morphological subgroups based on their soma location, dendritic or axonal distributions between layers, their postsynaptic target distribution at population level did not show difference. However, comparison of the target distribution at single cell level revealed that PVBCs innervate their postsynaptic partners via more boutons. By using trans-synaptic viral labelling approach we observed that PV-expressing cells located in a given layer are preferentially innervated by thalamic and amygdalar inputs.

Combined transgenic techniques and viral labelling allowed us to examine and compare the features of different types of ChCs originating from two distinct mouse lines. We found that these two types of ChCs differed both in their morphological features and postsynaptic target distribution along the AISs.

At the end we examined the specificity of widely applied viral labelling technique by using CamKIIα promoter to target local PCs, thereby providing the opportunity to determine the local inputs of the PTIs. Our results showed that distinct IN types could be infected also by this virus construct, precluding to study the local PC inputs on these INs.

Our findings revealed that distinct types of PTIs contribute to the perisomatic inhibition in the mPFC. Their morphological variability suggest that these cells contribute to the network organization in a distinct manner.

8. Összefoglalás

A lokális GABAerg neuronok által biztosított periszomatikus gátlás hatékonyan képes szabályozni a posztszinaptikus sejtek tüzelését, így jelentősen befolyásolva a különböző kérgi funkciókat. Ezen gátló hálózat jelentőségének ellenére a részleteik még mindig kevéssé ismertek különösen az olyan asszociatív kérgi régiókban, mint a mediális prefrontális agykéreg (mPFC). Ezért megvizsgáltuk a mPFC-ben található piramissejtek periszomatikus régiójára érkező gátló bemenetek forrásait, összehasonlítottuk az interneuronok (IN) morfológiai tulajdonságait, célsejtekre adott bemeneteinek eloszlását és végül megvizsgáltuk a különböző agyterületekről rájuk érkező bemeneteket.

Eredményeink megmutatták, hogy a piramissejtek szomato-dendritikus részeit parvalbumint (PV) és kolecisztokinint kifejező kosársejtek idegzik be. Habár mind a két kosársejt-típust további alcsoportokra lehetett bontani különböző morfológiai tulajdonságaik alapján, populációs szinten mégsem mutattak különbséget a célsejtek beidegzésében. Egy-sejt szinten viszont azt figyeltük meg, hogy a PV-t kifejező kosársejtek több kontaktust adtak a célsejtekre. Emellett transz-szinaptikus vírus jelölő technikát alkalmazva azt találtuk, hogy az egy bizonyos rétegben elhelyezkedő PV-s sejteket előszeretettel idegzik be az amygdalából és thalamuszból érkező bemenetek.

Transzgenikus technikákat vírus jelöléssel kombinálva lehetőségünk volt megvizsgálni és összehasonlítani olyan kandelláber sejtek tulajdonságait, amelyek különböző egérvonalakból származtak. Azt figyeltük meg, hogy mind a morfológiai tulajdonságokban, mind az axon-iniciális szegmentumra adott kontaktusok eloszlásában különbözött a két kandelláber sejt.

Végül megvizsgáltuk a széles körben alkalmazott CamKIIα promótert használó vírus jelölő technika specifikusságát a lokális piramissejtekre nézve, ezáltal megteremtve a lehetőséget a periszomatikus gátlósejtek lokális bemeneteinek a vizsgálatára. Eredményeink megmutatták, hogy a használt víruskonstrukció képes volt a különböző IN-kat is megfertőzni, ami így nem teszi lehetővé ezen eszköz használatát erre a célra.

Eredményeink megmutatták, hogy a periszomatikus gátlásért különböző típusú IN-k felelnek a mPFC területén. Morfológiai variabilitásuk azt feltételezi, hogy ezek a sejtek különböző módon járulnak hozzá a hálózat szerveződéséhez és működéséhez.

9. References

Acsady, L., Gorcs, T. J., & Freund, T. F. (1996). Different populations of vasoactive intestinal polypeptide-immunoreactive interneurons are specialized to control pyramidal cells or interneurons in the hippocampus. *Neuroscience*, *73*(2), 317-334. https://doi.org/10.1016/0306-4522(95)00609-5

Adhikari, A., Topiwala, M. A., & Gordon, J. A. (2010). Synchronized activity between the ventral hippocampus and the medial prefrontal cortex during anxiety. *Neuron*, *65*(2), 257-269. https://doi.org/10.1016/j.neuron.2009.12.002

Ahrlund-Richter, S., Xuan, Y., van Lunteren, J. A., Kim, H., Ortiz, C., Pollak Dorocic, I., Meletis, K., & Carlen, M. (2019). A whole-brain atlas of monosynaptic input targeting four different cell types in the medial prefrontal cortex of the mouse. *Nat Neurosci*, *22*(4), 657-668. https://doi.org/10.1038/s41593-019-0354-y

Akirav, I., & Maroun, M. (2006). Ventromedial prefrontal cortex is obligatory for consolidation and reconsolidation of object recognition memory. *Cereb Cortex*, *16*(12), 1759-1765. https://doi.org/10.1093/cercor/bhj114

Anastasiades, P. G., & Carter, A. G. (2021). Circuit organization of the rodent medial prefrontal cortex. *Trends Neurosci*, *44*(7), 550-563. https://doi.org/10.1016/j.tins.2021.03.006

Anastasiades, P. G., Marlin, J. J., & Carter, A. G. (2018). Cell-Type Specificity of Callosally Evoked Excitation and Feedforward Inhibition in the Prefrontal Cortex. *Cell Rep*, *22*(3), 679-692. https://doi.org/10.1016/j.celrep.2017.12.073

Andrasi, T., Veres, J. M., Rovira-Esteban, L., Kozma, R., Vikor, A., Gregori, E., & Hajos, N. (2017). Differential excitatory control of 2 parallel basket cell networks in amygdala microcircuits. *PLoS Biol*, *15*(5), e2001421. https://doi.org/10.1371/journal.pbio.2001421

Arlotta, P., Molyneaux, B. J., Chen, J., Inoue, J., Kominami, R., & Macklis, J. D. (2005). Neuronal subtype-specific genes that control corticospinal motor neuron development in vivo. *Neuron*, *45*(2), 207-221. https://doi.org/10.1016/j.neuron.2004.12.036

Arnsten, A. F., Wang, M. J., & Paspalas, C. D. (2012). Neuromodulation of thought: flexibilities and vulnerabilities in prefrontal cortical network synapses. *Neuron*, *76*(1), 223-239. https://doi.org/10.1016/j.neuron.2012.08.038

Atallah, B. V., & Scanziani, M. (2009). Instantaneous modulation of gamma oscillation frequency by balancing excitation with inhibition. *Neuron*, *62*(4), 566-577. https://doi.org/10.1016/j.neuron.2009.04.027

Babiczky, A., & Matyas, F. (2022). Molecular characteristics and laminar distribution of prefrontal neurons projecting to the mesolimbic system. *Elife*, *11*. https://doi.org/10.7554/eLife.78813

Baddeley, A. (1992). Working memory. *Science*, *255*(5044), 556-559. https://doi.org/10.1126/science.1736359

Baimbridge, K. G., Celio, M. R., & Rogers, J. H. (1992). Calcium-binding proteins in the nervous system. *Trends Neurosci*, *15*(8), 303-308. https://doi.org/10.1016/0166-2236(92)90081-i

Balleine, B. W., Delgado, M. R., & Hikosaka, O. (2007). The role of the dorsal striatum in reward and decision-making. *J Neurosci*, *27*(31), 8161-8165. https://doi.org/10.1523/JNEUROSCI.1554-07.2007

Barsy, B., Szabo, G. G., Andrasi, T., Vikor, A., & Hajos, N. (2017). Different output properties of perisomatic region-targeting interneurons in the basal amygdala. *Eur J Neurosci*, *45*(4), 548-558. https://doi.org/10.1111/ejn.13498

Basu, J., Srinivas, K. V., Cheung, S. K., Taniguchi, H., Huang, Z. J., & Siegelbaum, S. A. (2013). A cortico-hippocampal learning rule shapes inhibitory microcircuit activity to enhance hippocampal information flow. *Neuron*, *79*(6), 1208-1221. https://doi.org/10.1016/j.neuron.2013.07.001

Basu, K., Gravel, C., Tomioka, R., Kaneko, T., Tamamaki, N., & Sik, A. (2008). Novel strategy to selectively label excitatory and inhibitory neurons in the cerebral cortex of mice. *J Neurosci Methods*, *170*(2), 212-219. https://doi.org/10.1016/j.jneumeth.2008.01.016

Batiuk, M. Y., Tyler, T., Dragicevic, K., Mei, S., Rydbirk, R., Petukhov, V., Deviatiiarov, R., Sedmak, D., Frank, E., Feher, V., Habek, N., Hu, Q., Igolkina, A., Roszik, L., Pfisterer, U., Garcia-Gonzalez, D., Petanjek, Z., Adorjan, I., Kharchenko, P. V., & Khodosevich, K. (2022). Upper cortical layer-driven network impairment in schizophrenia. *Sci Adv*, *8*(41), eabn8367. https://doi.org/10.1126/sciadv.abn8367

Battaglia, F. P., Sutherland, G. R., & McNaughton, B. L. (2004). Hippocampal sharp wave bursts coincide with neocortical "up-state" transitions. *Learn Mem*, *11*(6), 697-704. https://doi.org/10.1101/lm.73504

Baude, A., Bleasdale, C., Dalezios, Y., Somogyi, P., & Klausberger, T. (2007). Immunoreactivity for the GABAA receptor alpha1 subunit, somatostatin and Connexin36 distinguishes axoaxonic, basket, and bistratified interneurons of the rat hippocampus. *Cereb Cortex*, *17*(9), 2094-2107. https://doi.org/10.1093/cercor/bhl117

Benchenane, K., Peyrache, A., Khamassi, M., Tierney, P. L., Gioanni, Y., Battaglia, F. P., & Wiener, S. I. (2010). Coherent theta oscillations and reorganization of spike timing in the hippocampal- prefrontal network upon learning. *Neuron*, *66*(6), 921-936. https://doi.org/10.1016/j.neuron.2010.05.013

Bienvenu, T. C., Busti, D., Magill, P. J., Ferraguti, F., & Capogna, M. (2012). Cell-type-specific recruitment of amygdala interneurons to hippocampal theta rhythm and noxious stimuli in vivo. *Neuron*, *74*(6), 1059-1074. https://doi.org/10.1016/j.neuron.2012.04.022

Bishop, H. I., Guan, D., Bocksteins, E., Parajuli, L. K., Murray, K. D., Cobb, M. M., Misonou, H., Zito, K., Foehring, R. C., & Trimmer, J. S. (2015). Distinct Cell- and Layer-Specific Expression Patterns and Independent Regulation of Kv2 Channel Subtypes in Cortical Pyramidal Neurons. *J Neurosci*, *35*(44), 14922-14942. https://doi.org/10.1523/JNEUROSCI.1897-15.2015

Blackstad, T. W., & Flood, P. R. (1963). Ultrastructure of hippocampal axo-somatic synapses. *Nature*, *198*, 542-543. https://doi.org/10.1038/198542a0

Blum, S., Hebert, A. E., & Dash, P. K. (2006). A role for the prefrontal cortex in recall of recent and remote memories. *Neuroreport*, *17*(3), 341-344. https://doi.org/10.1097/01.wnr.0000201509.53750.bc

Bodor, A. L., Katona, I., Nyiri, G., Mackie, K., Ledent, C., Hajos, N., & Freund, T. F. (2005). Endocannabinoid signaling in rat somatosensory cortex: laminar differences and involvement of specific interneuron types. *J Neurosci*, *25*(29), 6845-6856. https://doi.org/10.1523/JNEUROSCI.0442-05.2005

Bolkan, S. S., Stujenske, J. M., Parnaudeau, S., Spellman, T. J., Rauffenbart, C., Abbas, A. I., Harris, A. Z., Gordon, J. A., & Kellendonk, C. (2017). Thalamic projections sustain prefrontal activity during working memory maintenance. *Nat Neurosci*, *20*(7), 987-996. https://doi.org/10.1038/nn.4568

Bontempi, B., Laurent-Demir, C., Destrade, C., & Jaffard, R. (1999). Time-dependent reorganization of brain circuitry underlying long-term memory storage. *Nature*, *400*(6745), 671-675. https://doi.org/10.1038/23270

BrainMesh: A Matlab GUI for rendering 3D mouse brain structures. (2020). https://github.com/Yaoyao-Hao/BrainMesh/

Brodmann, K. (1909). *Vergleichende Lokalisationslehre der Grosshirnrinde in ihren Prinzipien dargestellt auf Grund des Zellenbaues*. Barth.

Brown, S. P., & Hestrin, S. (2009). Intracortical circuits of pyramidal neurons reflect their long-range axonal targets. *Nature*, *457*(7233), 1133-1136. https://doi.org/10.1038/nature07658

Buhl, E. H., Tamas, G., Szilagyi, T., Stricker, C., Paulsen, O., & Somogyi, P. (1997). Effect, number and location of synapses made by single pyramidal cells onto aspiny interneurones of cat visual cortex. *J Physiol*, *500 (Pt 3)*(Pt 3), 689-713. https://doi.org/10.1113/jphysiol.1997.sp022053

Buzsaki, G., & Chrobak, J. J. (1995). Temporal structure in spatially organized neuronal ensembles: a role for interneuronal networks. *Curr Opin Neurobiol*, *5*(4), 504-510. https://doi.org/10.1016/0959-4388(95)80012-3

Buzsaki, G., & Wang, X. J. (2012). Mechanisms of gamma oscillations. *Annu Rev Neurosci*, *35*, 203-225. https://doi.org/10.1146/annurev-neuro-062111-150444

Capogna, M., Gahwiler, B. H., & Thompson, S. M. (1993). Mechanism of mu-opioid receptor-mediated presynaptic inhibition in the rat hippocampus in vitro. *J Physiol*, *470*, 539-558. https://doi.org/10.1113/jphysiol.1993.sp019874

Carballo-Marquez, A., Vale-Martinez, A., Guillazo-Blanch, G., Torras-Garcia, M., Boix-Trelis, N., & Marti-Nicolovius, M. (2007). Differential effects of muscarinic receptor blockade in prelimbic cortex on acquisition and memory formation of an odor-reward task. *Learn Mem*, *14*(9), 616-624. https://doi.org/10.1101/lm.597507

Carlen, M. (2017). What constitutes the prefrontal cortex? *Science*, *358*(6362), 478-482. https://doi.org/10.1126/science.aan8868

Cheriyan, J., & Sheets, P. L. (2018). Altered Excitability and Local Connectivity of mPFC-PAG Neurons in a Mouse Model of Neuropathic Pain. *J Neurosci*, *38*(20), 4829-4839. https://doi.org/10.1523/JNEUROSCI.2731-17.2018

Clarkson, R. L., Liptak, A. T., Gee, S. M., Sohal, V. S., & Bender, K. J. (2017). D3 Receptors Regulate Excitability in a Unique Class of Prefrontal Pyramidal Cells. *J Neurosci*, *37*(24), 5846-5860. https://doi.org/10.1523/JNEUROSCI.0310-17.2017

Cobb, S. R., Buhl, E. H., Halasy, K., Paulsen, O., & Somogyi, P. (1995). Synchronization of neuronal activity in hippocampus by individual GABAergic interneurons. *Nature*, *378*(6552), 75-78. https://doi.org/10.1038/378075a0

Cohen, J. D., Braver, T. S., & O'Reilly, R. C. (1996). A computational approach to prefrontal cortex, cognitive control and schizophrenia: recent developments and current challenges. *Philos Trans R Soc Lond B Biol Sci*, *351*(1346), 1515-1527. https://doi.org/10.1098/rstb.1996.0138

Colgin, L. L. (2011). Oscillations and hippocampal-prefrontal synchrony. *Curr Opin Neurobiol*, *21*(3), 467-474. https://doi.org/10.1016/j.conb.2011.04.006

Collins, D. P., Anastasiades, P. G., Marlin, J. J., & Carter, A. G. (2018). Reciprocal Circuits Linking the Prefrontal Cortex with Dorsal and Ventral Thalamic Nuclei. *Neuron*, *98*(2), 366-379 e364. https://doi.org/10.1016/j.neuron.2018.03.024

Connors, B. W., Malenka, R. C., & Silva, L. R. (1988). Two inhibitory postsynaptic potentials, and GABAA and GABAB receptor-mediated responses in neocortex of rat and cat. *J Physiol*, *406*, 443-468. https://doi.org/10.1113/jphysiol.1988.sp017390

Cruikshank, S. J., Killackey, H. P., & Metherate, R. (2001). Parvalbumin and calbindin are differentially distributed within primary and secondary subregions of the mouse auditory forebrain. *Neuroscience*, *105*(3), 553-569. https://doi.org/10.1016/s0306-4522(01)00226-3

Curley, A. A., Arion, D., Volk, D. W., Asafu-Adjei, J. K., Sampson, A. R., Fish, K. N., & Lewis, D. A. (2011). Cortical deficits of glutamic acid decarboxylase 67 expression in schizophrenia:

clinical, protein, and cell type-specific features. *Am J Psychiatry*, *168*(9), 921-929. https://doi.org/10.1176/appi.ajp.2011.11010052

Curley, A. A., & Lewis, D. A. (2012). Cortical basket cell dysfunction in schizophrenia. *J Physiol*, *590*(4), 715-724. https://doi.org/10.1113/jphysiol.2011.224659

DeFelipe, J., & Farinas, I. (1992). The pyramidal neuron of the cerebral cortex: morphological and chemical characteristics of the synaptic inputs. *Prog Neurobiol*, *39*(6), 563-607. https://doi.org/10.1016/0301-0082(92)90015-7

DeFelipe, J., Lopez-Cruz, P. L., Benavides-Piccione, R., Bielza, C., Larranaga, P., Anderson, S., Burkhalter, A., Cauli, B., Fairen, A., Feldmeyer, D., Fishell, G., Fitzpatrick, D., Freund, T. F., Gonzalez-Burgos, G., Hestrin, S., Hill, S., Hof, P. R., Huang, J., Jones, E. G., Kawaguchi, Y., Kisvarday, Z., Kubota, Y., Lewis, D. A., Marin, O., Markram, H., McBain, C. J., Meyer, H. S., Monyer, H., Nelson, S. B., Rockland, K., Rossier, J., Rubenstein, J. L., Rudy, B., Scanziani, M., Shepherd, G. M., Sherwood, C. C., Staiger, J. F., Tamas, G., Thomson, A., Wang, Y., Yuste, R., & Ascoli, G. A. (2013). New insights into the classification and nomenclature of cortical GABAergic interneurons. *Nat Rev Neurosci*, *14*(3), 202-216. https://doi.org/10.1038/nrn3444

del Rio, M. R., & DeFelipe, J. (1997). Colocalization of parvalbumin and calbindin D-28k in neurons including chandelier cells of the human temporal neocortex. *J Chem Neuroanat*, *12*(3), 165-173. https://doi.org/10.1016/s0891-0618(96)00191-3

Delevich, K., Tucciarone, J., Huang, Z. J., & Li, B. (2015). The mediodorsal thalamus drives feedforward inhibition in the anterior cingulate cortex via parvalbumin interneurons. *J Neurosci*, *35*(14), 5743-5753. https://doi.org/10.1523/JNEUROSCI.4565-14.2015

DeNicola, A. L., Park, M. Y., Crowe, D. A., MacDonald, A. W., 3rd, & Chafee, M. V. (2020). Differential Roles of Mediodorsal Nucleus of the Thalamus and Prefrontal Cortex in Decision-Making and State Representation in a Cognitive Control Task Measuring Deficits in Schizophrenia. *J Neurosci*, *40*(8), 1650-1667. https://doi.org/10.1523/JNEUROSCI.1703-19.2020

Dienel, S. J., Fish, K. N., & Lewis, D. A. (2023). The Nature of Prefrontal Cortical GABA Neuron Alterations in Schizophrenia: Markedly Lower Somatostatin and Parvalbumin Gene Expression Without Missing Neurons. *Am J Psychiatry*, *180*(7), 495-507. https://doi.org/10.1176/appi.ajp.20220676

Dilgen, J., Tejeda, H. A., & O'Donnell, P. (2013). Amygdala inputs drive feedforward inhibition in the medial prefrontal cortex. *J Neurophysiol*, *110*(1), 221-229. https://doi.org/10.1152/jn.00531.2012

Dudok, B., Klein, P. M., Hwaun, E., Lee, B. R., Yao, Z., Fong, O., Bowler, J. C., Terada, S., Sparks, F. T., Szabo, G. G., Farrell, J. S., Berg, J., Daigle, T. L., Tasic, B., Dimidschstein, J., Fishell, G., Losonczy, A., Zeng, H., & Soltesz, I. (2021). Alternating sources of perisomatic inhibition during behavior. *Neuron*, *109*(6), 997-1012 e1019. https://doi.org/10.1016/j.neuron.2021.01.003

Dudok, B., Szoboszlay, M., Paul, A., Klein, P. M., Liao, Z., Hwaun, E., Szabo, G. G., Geiller, T., Vancura, B., Wang, B. S., McKenzie, S., Homidan, J., Klaver, L. M. F., English, D. F., Huang, Z. J., Buzsaki, G., Losonczy, A., & Soltesz, I. (2021). Recruitment and inhibitory action of hippocampal axo-axonic cells during behavior. *Neuron*, *109*(23), 3838-3850 e3838. https://doi.org/10.1016/j.neuron.2021.09.033

Duncan, J. (2001). An adaptive coding model of neural function in prefrontal cortex. *Nat Rev Neurosci*, *2*(11), 820-829. https://doi.org/10.1038/35097575

Egashira, Y., Mori, Y., Yanagawa, Y., & Takamori, S. (2018). Development of lentiviral vectors for efficient glutamatergic-selective gene expression in cultured hippocampal neurons. *Sci Rep*, *8*(1), 15156. https://doi.org/10.1038/s41598-018-33509-5

Eggan, S. M., Hashimoto, T., & Lewis, D. A. (2008). Reduced cortical cannabinoid 1 receptor messenger RNA and protein expression in schizophrenia. *Arch Gen Psychiatry*, *65*(7), 772-784. https://doi.org/10.1001/archpsyc.65.7.772

Eggan, S. M., Stoyak, S. R., Verrico, C. D., & Lewis, D. A. (2010). Cannabinoid CB1 receptor immunoreactivity in the prefrontal cortex: Comparison of schizophrenia and major depressive disorder. *Neuropsychopharmacology*, *35*(10), 2060-2071. https://doi.org/10.1038/npp.2010.75

Euston, D. R., Gruber, A. J., & McNaughton, B. L. (2012). The role of medial prefrontal cortex in memory and decision making. *Neuron*, *76*(6), 1057-1070. https://doi.org/10.1016/j.neuron.2012.12.002

Fanselow, E. E., Richardson, K. A., & Connors, B. W. (2008). Selective, state-dependent activation of somatostatin-expressing inhibitory interneurons in mouse neocortex. *J Neurophysiol*, *100*(5), 2640-2652. https://doi.org/10.1152/jn.90691.2008

Fenno, L. E., Mattis, J., Ramakrishnan, C., Hyun, M., Lee, S. Y., He, M., Tucciarone, J., Selimbeyoglu, A., Berndt, A., Grosenick, L., Zalocusky, K. A., Bernstein, H., Swanson, H., Perry, C., Diester, I., Boyce, F. M., Bass, C. E., Neve, R., Huang, Z. J., & Deisseroth, K. (2014). Targeting cells with single vectors using multiple-feature Boolean logic. *Nat Methods*, *11*(7), 763-772. https://doi.org/10.1038/nmeth.2996

Ferguson, B. R., & Gao, W. J. (2018a). PV Interneurons: Critical Regulators of E/I Balance for Prefrontal Cortex-Dependent Behavior and Psychiatric Disorders. *Front Neural Circuits*, *12*, 37. https://doi.org/10.3389/fncir.2018.00037

Ferguson, B. R., & Gao, W. J. (2018b). Thalamic Control of Cognition and Social Behavior Via Regulation of Gamma-Aminobutyric Acidergic Signaling and Excitation/Inhibition Balance in the Medial Prefrontal Cortex. *Biol Psychiatry*, *83*(8), 657-669. https://doi.org/10.1016/j.biopsych.2017.11.033

Ferrier, D. (1884). Cerebral Localisation. A Review and Forecast. Being the Marshall Hall Prize Oration. *Med Chir Trans*, *67*, 33-49. https://doi.org/10.1177/095952878406700103

Folke, J., Pakkenberg, B., & Brudek, T. (2019). Impaired Wnt Signaling in the Prefrontal Cortex of Alzheimer's Disease. *Mol Neurobiol*, *56*(2), 873-891. https://doi.org/10.1007/s12035-018-1103-z

Frankland, P. W., & Bontempi, B. (2005). The organization of recent and remote memories. *Nat Rev Neurosci*, *6*(2), 119-130. https://doi.org/10.1038/nrn1607

Freund, T. F. (2003). Interneuron Diversity series: Rhythm and mood in perisomatic inhibition. *Trends Neurosci*, *26*(9), 489-495. https://doi.org/10.1016/S0166-2236(03)00227-3

Freund, T. F., & Buzsaki, G. (1996). Interneurons of the hippocampus. *Hippocampus*, *6*(4), 347-470. https://doi.org/10.1002/(SICI)1098-1063(1996)6:4<347::AID-HIPO1>3.0.CO;2-I

Freund, T. F., & Katona, I. (2007). Perisomatic inhibition. *Neuron*, *56*(1), 33-42. https://doi.org/10.1016/j.neuron.2007.09.012

Fuster, J. M. (2006). The cognit: a network model of cortical representation. *Int J Psychophysiol*, *60*(2), 125-132. https://doi.org/10.1016/j.ijpsycho.2005.12.015

Gabbott, P. L., Warner, T. A., & Busby, S. J. (2006). Amygdala input monosynaptically innervates parvalbumin immunoreactive local circuit neurons in rat medial prefrontal cortex. *Neuroscience*, *139*(3), 1039-1048. https://doi.org/10.1016/j.neuroscience.2006.01.026

Gabbott, P. L., Warner, T. A., Jays, P. R., Salway, P., & Busby, S. J. (2005). Prefrontal cortex in the rat: projections to subcortical autonomic, motor, and limbic centers. *J Comp Neurol*, *492*(2), 145-177. https://doi.org/10.1002/cne.20738

Geiger, J. R., Melcher, T., Koh, D. S., Sakmann, B., Seeburg, P. H., Jonas, P., & Monyer, H. (1995). Relative abundance of subunit mRNAs determines gating and Ca2+ permeability of AMPA receptors in principal neurons and interneurons in rat CNS. *Neuron*, *15*(1), 193-204. https://doi.org/10.1016/0896-6273(95)90076-4

Gilmartin, M. R., & McEchron, M. D. (2005). Single neurons in the medial prefrontal cortex of the rat exhibit tonic and phasic coding during trace fear conditioning. *Behav Neurosci*, *119*(6), 1496-1510. https://doi.org/10.1037/0735-7044.119.6.1496

Gilmartin, M. R., Miyawaki, H., Helmstetter, F. J., & Diba, K. (2013). Prefrontal activity links nonoverlapping events in memory. *J Neurosci*, *33*(26), 10910-10914. https://doi.org/10.1523/JNEUROSCI.0144-13.2013

Glantz, L. A., & Lewis, D. A. (2000). Decreased dendritic spine density on prefrontal cortical pyramidal neurons in schizophrenia. *Arch Gen Psychiatry*, *57*(1), 65-73. https://doi.org/10.1001/archpsyc.57.1.65

Glickfeld, L. L., Atallah, B. V., & Scanziani, M. (2008). Complementary modulation of somatic inhibition by opioids and cannabinoids. *J Neurosci*, *28*(8), 1824-1832. https://doi.org/10.1523/JNEUROSCI.4700-07.2008

Glickfeld, L. L., Roberts, J. D., Somogyi, P., & Scanziani, M. (2009). Interneurons hyperpolarize pyramidal cells along their entire somatodendritic axis. *Nat Neurosci*, *12*(1), 21-23. https://doi.org/10.1038/nn.2230

Glickfeld, L. L., & Scanziani, M. (2006). Distinct timing in the activity of cannabinoid-sensitive and cannabinoid-insensitive basket cells. *Nat Neurosci*, *9*(6), 807-815. https://doi.org/10.1038/nn1688

Goldman-Rakic, P. S. (1988). Topography of cognition: parallel distributed networks in primate association cortex. *Annu Rev Neurosci*, *11*, 137-156. https://doi.org/10.1146/annurev.ne.11.030188.001033

Goldman-Rakic, P. S. (1995). Cellular basis of working memory. *Neuron*, *14*(3), 477-485. https://doi.org/10.1016/0896-6273(95)90304-6

Gonzalez-Burgos, G., Cho, R. Y., & Lewis, D. A. (2015). Alterations in cortical network oscillations and parvalbumin neurons in schizophrenia. *Biol Psychiatry*, *77*(12), 1031-1040. https://doi.org/10.1016/j.biopsych.2015.03.010

Gouwens, N. W., Sorensen, S. A., Baftizadeh, F., Budzillo, A., Lee, B. R., Jarsky, T., Alfiler, L., Baker, K., Barkan, E., Berry, K., Bertagnolli, D., Bickley, K., Bomben, J., Braun, T., Brouner, K., Casper, T., Crichton, K., Daigle, T. L., Dalley, R., de Frates, R. A., Dee, N., Desta, T., Lee, S. D., Dotson, N., Egdorf, T., Ellingwood, L., Enstrom, R., Esposito, L., Farrell, C., Feng, D., Fong, O., Gala, R., Gamlin, C., Gary, A., Glandon, A., Goldy, J., Gorham, M., Graybuck, L., Gu, H., Hadley, K., Hawrylycz, M. J., Henry, A. M., Hill, D., Hupp, M., Kebede, S., Kim, T. K., Kim, L., Kroll, M., Lee, C., Link, K. E., Mallory, M., Mann, R., Maxwell, M., McGraw, M., McMillen, D., Mukora, A., Ng, L., Ng, L., Ngo, K., Nicovich, P. R., Oldre, A., Park, D., Peng, H., Penn, O., Pham, T., Pom, A., Popovic, Z., Potekhina, L., Rajanbabu, R., Ransford, S., Reid, D., Rimorin, C., Robertson, M., Ronellenfitch, K., Ruiz, A., Sandman, D., Smith, K., Sulc, J., Sunkin, S. M., Szafer, A., Tieu, M., Torkelson, A., Trinh, J., Tung, H., Wakeman, W., Ward, K., Williams, G., Zhou, Z., Ting, J. T., Arkhipov, A., Sumbul, U., Lein, E. S., Koch, C., Yao, Z., Tasic, B., Berg, J., Murphy, G. J., & Zeng, H. (2020). Integrated Morphoelectric and Transcriptomic Classification of Cortical GABAergic Cells. *Cell*, *183*(4), 935-953 e919. https://doi.org/10.1016/j.cell.2020.09.057

Gulyas, A. I., Hajos, N., & Freund, T. F. (1996). Interneurons containing calretinin are specialized to control other interneurons in the rat hippocampus. *J Neurosci*, *16*(10), 3397-3411. https://doi.org/10.1523/JNEUROSCI.16-10-03397.1996

Gulyas, A. I., Hajos, N., Katona, I., & Freund, T. F. (2003). Interneurons are the local targets of hippocampal inhibitory cells which project to the medial septum. *Eur J Neurosci*, *17*(9), 1861-1872. https://doi.org/10.1046/j.1460-9568.2003.02630.x

Gulyas, A. I., Megias, M., Emri, Z., & Freund, T. F. (1999). Total number and ratio of excitatory and inhibitory synapses converging onto single interneurons of different types in the

CA1 area of the rat hippocampus. *J Neurosci*, *19*(22), 10082-10097. https://doi.org/10.1523/JNEUROSCI.19-22-10082.1999

Gulyas, A. I., Miles, R., Hajos, N., & Freund, T. F. (1993). Precision and variability in postsynaptic target selection of inhibitory cells in the hippocampal CA3 region. *Eur J Neurosci*, *5*(12), 1729-1751. https://doi.org/10.1111/j.1460-9568.1993.tb00240.x

Gulyas, A. I., Miles, R., Sik, A., Toth, K., Tamamaki, N., & Freund, T. F. (1993). Hippocampal pyramidal cells excite inhibitory neurons through a single release site. *Nature*, *366*(6456), 683-687. https://doi.org/10.1038/366683a0

Gulyas, A. I., Szabo, G. G., Ulbert, I., Holderith, N., Monyer, H., Erdelyi, F., Szabo, G., Freund, T. F., & Hajos, N. (2010). Parvalbumin-containing fast-spiking basket cells generate the field potential oscillations induced by cholinergic receptor activation in the hippocampus. *J Neurosci*, *30*(45), 15134-15145. https://doi.org/10.1523/JNEUROSCI.4104-10.2010

Hajos, N., Acsady, L., & Freund, T. F. (1996). Target selectivity and neurochemical characteristics of VIP-immunoreactive interneurons in the rat dentate gyrus. *Eur J Neurosci*, *8*(7), 1415-1431. https://doi.org/10.1111/j.1460-9568.1996.tb01604.x

Hajos, N., Karlocai, M. R., Nemeth, B., Ulbert, I., Monyer, H., Szabo, G., Erdelyi, F., Freund, T. F., & Gulyas, A. I. (2013). Input-output features of anatomically identified CA3 neurons during hippocampal sharp wave/ripple oscillation in vitro. *J Neurosci*, *33*(28), 11677-11691. https://doi.org/10.1523/JNEUROSCI.5729-12.2013

Harris, K. D., & Shepherd, G. M. (2015). The neocortical circuit: themes and variations. *Nat Neurosci*, *18*(2), 170-181. https://doi.org/10.1038/nn.3917

Harris, R. M., & Woolsey, T. A. (1983). Computer-assisted analyses of barrel neuron axons and their putative synaptic contacts. *J Comp Neurol*, *220*(1), 63-79. https://doi.org/10.1002/cne.902200107

Hartwich, K., Pollak, T., & Klausberger, T. (2009). Distinct firing patterns of identified basket and dendrite-targeting interneurons in the prefrontal cortex during hippocampal theta and local spindle oscillations. *J Neurosci*, *29*(30), 9563-9574. https://doi.org/10.1523/JNEUROSCI.1397-09.2009

Hattox, A. M., & Nelson, S. B. (2007). Layer V neurons in mouse cortex projecting to different targets have distinct physiological properties. *J Neurophysiol*, *98*(6), 3330-3340. https://doi.org/10.1152/jn.00397.2007

He, M., Tucciarone, J., Lee, S., Nigro, M. J., Kim, Y., Levine, J. M., Kelly, S. M., Krugikov, I., Wu, P., Chen, Y., Gong, L., Hou, Y., Osten, P., Rudy, B., & Huang, Z. J. (2016). Strategies and Tools for Combinatorial Targeting of GABAergic Neurons in Mouse Cerebral Cortex. *Neuron*, *91*(6), 1228-1243. https://doi.org/10.1016/j.neuron.2016.08.021

He, X., Li, J., Zhou, G., Yang, J., McKenzie, S., Li, Y., Li, W., Yu, J., Wang, Y., Qu, J., Wu, Z., Hu, H., Duan, S., & Ma, H. (2021). Gating of hippocampal rhythms and memory by synaptic plasticity in inhibitory interneurons. *Neuron*, *109*(6), 1013-1028 e1019. https://doi.org/10.1016/j.neuron.2021.01.014

Hefft, S., & Jonas, P. (2005). Asynchronous GABA release generates long-lasting inhibition at a hippocampal interneuron-principal neuron synapse. *Nat Neurosci*, *8*(10), 1319-1328. https://doi.org/10.1038/nn1542

Heidbreder, C. A., & Groenewegen, H. J. (2003). The medial prefrontal cortex in the rat: evidence for a dorso-ventral distinction based upon functional and anatomical characteristics. *Neurosci Biobehav Rev*, *27*(6), 555-579. https://doi.org/10.1016/j.neubiorev.2003.09.003

Higo, S., Akashi, K., Sakimura, K., & Tamamaki, N. (2009). Subtypes of GABAergic neurons project axons in the neocortex. *Front Neuroanat*, *3*, 25. https://doi.org/10.3389/neuro.05.025.2009

Hioki, H., Okamoto, S., Konno, M., Kameda, H., Sohn, J., Kuramoto, E., Fujiyama, F., & Kaneko, T. (2013). Cell type-specific inhibitory inputs to dendritic and somatic compartments of parvalbumin-expressing neocortical interneuron. *J Neurosci*, *33*(2), 544-555. https://doi.org/10.1523/JNEUROSCI.2255-12.2013

Hirai, Y., Morishima, M., Karube, F., & Kawaguchi, Y. (2012). Specialized cortical subnetworks differentially connect frontal cortex to parahippocampal areas. *J Neurosci*, *32*(5), 1898-1913. https://doi.org/10.1523/JNEUROSCI.2810-11.2012

Hisaoka, T., Nakamura, Y., Senba, E., & Morikawa, Y. (2010). The forkhead transcription factors, Foxp1 and Foxp2, identify different subpopulations of projection neurons in the mouse cerebral cortex. *Neuroscience*, *166*(2), 551-563. https://doi.org/10.1016/j.neuroscience.2009.12.055

Holmes, A., & Wellman, C. L. (2009). Stress-induced prefrontal reorganization and executive dysfunction in rodents. *Neurosci Biobehav Rev*, *33*(6), 773-783. https://doi.org/10.1016/j.neubiorev.2008.11.005

Hoover, W. B., & Vertes, R. P. (2007). Anatomical analysis of afferent projections to the medial prefrontal cortex in the rat. *Brain Struct Funct*, *212*(2), 149-179. https://doi.org/10.1007/s00429-007-0150-4

Huang, C. Y., & Rasband, M. N. (2018). Axon initial segments: structure, function, and disease. *Ann N Y Acad Sci*, *1420*(1), 46-61. https://doi.org/10.1111/nyas.13718

Huang, Z., Li, T., & Xu, M. (2020). Are There Heterogeneous Impacts of National Income on Mental Health? *Int J Environ Res Public Health*, *17*(20). https://doi.org/10.3390/ijerph17207530

Huang, Z. J. (2014). Toward a genetic dissection of cortical circuits in the mouse. *Neuron*, *83*(6), 1284-1302. https://doi.org/10.1016/j.neuron.2014.08.041

Inan, M., & Anderson, S. A. (2014). The chandelier cell, form and function. *Curr Opin Neurobiol*, *26*, 142-148. https://doi.org/10.1016/j.conb.2014.01.009

Inan, M., Blazquez-Llorca, L., Merchan-Perez, A., Anderson, S. A., DeFelipe, J., & Yuste, R. (2013). Dense and overlapping innervation of pyramidal neurons by chandelier cells. *J Neurosci*, *33*(5), 1907-1914. https://doi.org/10.1523/JNEUROSCI.4049-12.2013

Insel, N., & Barnes, C. A. (2015). Differential Activation of Fast-Spiking and Regular-Firing Neuron Populations During Movement and Reward in the Dorsal Medial Frontal Cortex. *Cereb Cortex*, *25*(9), 2631-2647. https://doi.org/10.1093/cercor/bhu062

Isaacson, J. S., & Scanziani, M. (2011). How inhibition shapes cortical activity. *Neuron*, *72*(2), 231-243. https://doi.org/10.1016/j.neuron.2011.09.027

Ishino, Y., Yetman, M. J., Sossi, S. M., Steinecke, A., Hayano, Y., & Taniguchi, H. (2017). Regional Cellular Environment Shapes Phenotypic Variations of Hippocampal and Neocortical Chandelier Cells. *J Neurosci*, *37*(41), 9901-9916. https://doi.org/10.1523/JNEUROSCI.0047-17.2017

Jackson, J., Karnani, M. M., Zemelman, B. V., Burdakov, D., & Lee, A. K. (2018). Inhibitory Control of Prefrontal Cortex by the Claustrum. *Neuron*, *99*(5), 1029-1039 e1024. https://doi.org/10.1016/j.neuron.2018.07.031

Jasmin, L., Burkey, A. R., Granato, A., & Ohara, P. T. (2004). Rostral agranular insular cortex and pain areas of the central nervous system: a tract-tracing study in the rat. *J Comp Neurol*, *468*(3), 425-440. https://doi.org/10.1002/cne.10978

Jinno, S., Klausberger, T., Marton, L. F., Dalezios, Y., Roberts, J. D., Fuentealba, P., Bushong, E. A., Henze, D., Buzsaki, G., & Somogyi, P. (2007). Neuronal diversity in GABAergic long-range projections from the hippocampus. *J Neurosci*, *27*(33), 8790-8804. https://doi.org/10.1523/JNEUROSCI.1847-07.2007

Johnston, D., Magee, J. C., Colbert, C. M., & Cristie, B. R. (1996). Active properties of neuronal dendrites. *Annu Rev Neurosci*, *19*, 165-186. https://doi.org/10.1146/annurev.ne.19.030196.001121

Jones, R. T., Faas, G. C., & Mody, I. (2014). Intracellular bicarbonate regulates action potential generation via KCNQ channel modulation. *J Neurosci*, *34*(12), 4409-4417. https://doi.org/10.1523/JNEUROSCI.3836-13.2014

Joshi, A., Salib, M., Viney, T. J., Dupret, D., & Somogyi, P. (2017). Behavior-Dependent Activity and Synaptic Organization of Septo-hippocampal GABAergic Neurons Selectively Targeting the Hippocampal CA3 Area. *Neuron*, *96*(6), 1342-1357 e1345. https://doi.org/10.1016/j.neuron.2017.10.033

Jung, M. W., Qin, Y., McNaughton, B. L., & Barnes, C. A. (1998). Firing characteristics of deep layer neurons in prefrontal cortex in rats performing spatial working memory tasks. *Cereb Cortex*, *8*(5), 437-450. https://doi.org/10.1093/cercor/8.5.437

Karlocai, M. R., Heredi, J., Benedek, T., Holderith, N., Lorincz, A., & Nusser, Z. (2021). Variability in the Munc13-1 content of excitatory release sites. *Elife*, *10*. https://doi.org/10.7554/eLife.67468

Karube, F., Kubota, Y., & Kawaguchi, Y. (2004). Axon branching and synaptic bouton phenotypes in GABAergic nonpyramidal cell subtypes. *J Neurosci*, *24*(12), 2853-2865. https://doi.org/10.1523/JNEUROSCI.4814-03.2004

Katona, I., & Freund, T. F. (2008). Endocannabinoid signaling as a synaptic circuit breaker in neurological disease. *Nat Med*, *14*(9), 923-930. https://doi.org/10.1038/nm.f.1869

Kawaguchi, Y. (1995). Physiological subgroups of nonpyramidal cells with specific morphological characteristics in layer II/III of rat frontal cortex. *J Neurosci*, *15*(4), 2638-2655. https://doi.org/10.1523/JNEUROSCI.15-04-02638.1995

Kawaguchi, Y. (2017). Pyramidal Cell Subtypes and Their Synaptic Connections in Layer 5 of Rat Frontal Cortex. *Cereb Cortex*, *27*(12), 5755-5771. https://doi.org/10.1093/cercor/bhx252

Kawaguchi, Y., & Kondo, S. (2002). Parvalbumin, somatostatin and cholecystokinin as chemical markers for specific GABAergic interneuron types in the rat frontal cortex. *J Neurocytol*, *31*(3-5), 277-287. https://doi.org/10.1023/a:1024126110356

Kawaguchi, Y., & Kubota, Y. (1997). GABAergic cell subtypes and their synaptic connections in rat frontal cortex. *Cereb Cortex*, *7*(6), 476-486. https://doi.org/10.1093/cercor/7.6.476

Kawaguchi, Y., & Kubota, Y. (1998). Neurochemical features and synaptic connections of large physiologically-identified GABAergic cells in the rat frontal cortex. *Neuroscience*, *85*(3), 677-701. https://doi.org/10.1016/s0306-4522(97)00685-4

Kepecs, A., & Fishell, G. (2014). Interneuron cell types are fit to function. *Nature*, *505*(7483), 318-326. https://doi.org/10.1038/nature12983

Kim, D., Jeong, H., Lee, J., Ghim, J. W., Her, E. S., Lee, S. H., & Jung, M. W. (2016). Distinct Roles of Parvalbumin- and Somatostatin-Expressing Interneurons in Working Memory. *Neuron*, *92*(4), 902-915. https://doi.org/10.1016/j.neuron.2016.09.023

Kisvarday, Z. F., Adams, C. B., & Smith, A. D. (1986). Synaptic connections of axo-axonic (chandelier) cells in human epileptic temporal cortex. *Neuroscience*, *19*(4), 1179-1186. https://doi.org/10.1016/0306-4522(86)90131-4

Klausberger, T., Magill, P. J., Marton, L. F., Roberts, J. D., Cobden, P. M., Buzsaki, G., & Somogyi, P. (2003). Brain-state- and cell-type-specific firing of hippocampal interneurons in vivo. *Nature*, *421*(6925), 844-848. https://doi.org/10.1038/nature01374

Klausberger, T., Marton, L. F., Baude, A., Roberts, J. D., Magill, P. J., & Somogyi, P. (2004). Spike timing of dendrite-targeting bistratified cells during hippocampal network oscillations in vivo. *Nat Neurosci*, *7*(1), 41-47. https://doi.org/10.1038/nn1159

Klausberger, T., Marton, L. F., O'Neill, J., Huck, J. H., Dalezios, Y., Fuentealba, P., Suen, W. Y., Papp, E., Kaneko, T., Watanabe, M., Csicsvari, J., & Somogyi, P. (2005). Complementary roles of cholecystokinin- and parvalbumin-expressing GABAergic neurons in hippocampal network oscillations. *J Neurosci*, *25*(42), 9782-9793. https://doi.org/10.1523/JNEUROSCI.3269-05.2005

Klausberger, T., & Somogyi, P. (2008). Neuronal diversity and temporal dynamics: the unity of hippocampal circuit operations. *Science*, *321*(5885), 53-57. https://doi.org/10.1126/science.1149381

Knowles, W. D., & Schwartzkroin, P. A. (1981). Local circuit synaptic interactions in hippocampal brain slices. *J Neurosci*, *1*(3), 318-322. https://doi.org/10.1523/JNEUROSCI.01-03-00318.1981

Koenigs, M., & Grafman, J. (2009). The functional neuroanatomy of depression: distinct roles for ventromedial and dorsolateral prefrontal cortex. *Behav Brain Res*, *201*(2), 239-243. https://doi.org/10.1016/j.bbr.2009.03.004

Kohus, Z., Kali, S., Rovira-Esteban, L., Schlingloff, D., Papp, O., Freund, T. F., Hajos, N., & Gulyas, A. I. (2016). Properties and dynamics of inhibitory synaptic communication within the CA3 microcircuits of pyramidal cells and interneurons expressing parvalbumin or cholecystokinin. *J Physiol*, *594*(13), 3745-3774. https://doi.org/10.1113/JP272231

Kole, M. H., Ilschner, S. U., Kampa, B. M., Williams, S. R., Ruben, P. C., & Stuart, G. J. (2008). Action potential generation requires a high sodium channel density in the axon initial segment. *Nat Neurosci*, *11*(2), 178-186. https://doi.org/10.1038/nn2040

Kole, M. H., & Stuart, G. J. (2012). Signal processing in the axon initial segment. *Neuron*, *73*(2), 235-247. https://doi.org/10.1016/j.neuron.2012.01.007

Kranz, G. S., Kasper, S., & Lanzenberger, R. (2010). Reward and the serotonergic system. *Neuroscience*, *166*(4), 1023-1035. https://doi.org/10.1016/j.neuroscience.2010.01.036

Kubota, Y., Karube, F., Nomura, M., & Kawaguchi, Y. (2016). The Diversity of Cortical Inhibitory Synapses. *Front Neural Circuits*, *10*, 27. https://doi.org/10.3389/fncir.2016.00027

Kubota, Y., & Kawaguchi, Y. (1997). Two distinct subgroups of cholecystokinin-immunoreactive cortical interneurons. *Brain Res*, *752*(1-2), 175-183. https://doi.org/10.1016/s0006-8993(96)01446-1

Kubota, Y., Kondo, S., Nomura, M., Hatada, S., Yamaguchi, N., Mohamed, A. A., Karube, F., Lubke, J., & Kawaguchi, Y. (2015). Functional effects of distinct innervation styles of pyramidal cells by fast spiking cortical interneurons. *Elife*, *4*. https://doi.org/10.7554/eLife.07919

Kuramoto, E., Tanaka, Y. R., Hioki, H., Goto, T., & Kaneko, T. (2022). Local Connections of Pyramidal Neurons to Parvalbumin-Producing Interneurons in Motor-Associated Cortical Areas of Mice. *eNeuro*, *9*(1). https://doi.org/10.1523/ENEURO.0567-20.2021

Lagler, M., Ozdemir, A. T., Lagoun, S., Malagon-Vina, H., Borhegyi, Z., Hauer, R., Jelem, A., & Klausberger, T. (2016). Divisions of Identified Parvalbumin-Expressing Basket Cells during Working Memory-Guided Decision Making. *Neuron*, *91*(6), 1390-1401. https://doi.org/10.1016/j.neuron.2016.08.010

Larkum, M. E., Zhu, J. J., & Sakmann, B. (1999). A new cellular mechanism for coupling inputs arriving at different cortical layers. *Nature*, *398*(6725), 338-341. https://doi.org/10.1038/18686

Lasztoczi, B., Tukker, J. J., Somogyi, P., & Klausberger, T. (2011). Terminal field and firing selectivity of cholecystokinin-expressing interneurons in the hippocampal CA3 area. *J Neurosci*, *31*(49), 18073-18093. https://doi.org/10.1523/JNEUROSCI.3573-11.2011

Le Be, J. V., Silberberg, G., Wang, Y., & Markram, H. (2007). Morphological, electrophysiological, and synaptic properties of corticocallosal pyramidal cells in the neonatal rat neocortex. *Cereb Cortex*, *17*(9), 2204-2213. https://doi.org/10.1093/cercor/bhl127

Le Merre, P., Ahrlund-Richter, S., & Carlen, M. (2021). The mouse prefrontal cortex: Unity in diversity. *Neuron*, *109*(12), 1925-1944. https://doi.org/10.1016/j.neuron.2021.03.035

Lee, A. T., Gee, S. M., Vogt, D., Patel, T., Rubenstein, J. L., & Sohal, V. S. (2014). Pyramidal neurons in prefrontal cortex receive subtype-specific forms of excitation and inhibition. *Neuron*, *81*(1), 61-68. https://doi.org/10.1016/j.neuron.2013.10.031

Lee, S. H., Marchionni, I., Bezaire, M., Varga, C., Danielson, N., Lovett-Barron, M., Losonczy, A., & Soltesz, I. (2014). Parvalbumin-positive basket cells differentiate among hippocampal pyramidal cells. *Neuron*, *82*(5), 1129-1144. https://doi.org/10.1016/j.neuron.2014.03.034

Lee, S. Y., & Soltesz, I. (2011). Cholecystokinin: a multi-functional molecular switch of neuronal circuits. *Dev Neurobiol*, *71*(1), 83-91. https://doi.org/10.1002/dneu.20815

Lein, E. S., Hawrylycz, M. J., Ao, N., Ayres, M., Bensinger, A., Bernard, A., Boe, A. F., Boguski, M. S., Brockway, K. S., Byrnes, E. J., Chen, L., Chen, L., Chen, T. M., Chin, M. C., Chong, J., Crook, B. E., Czaplinska, A., Dang, C. N., Datta, S., Dee, N. R., Desaki, A. L., Desta, T., Diep, E., Dolbeare, T. A., Donelan, M. J., Dong, H. W., Dougherty, J. G., Duncan, B. J., Ebbert, A. J., Eichele, G., Estin, L. K., Faber, C., Facer, B. A., Fields, R., Fischer, S. R., Fliss, T. P., Frensley, C., Gates, S. N., Glattfelder, K. J., Halverson, K. R., Hart, M. R., Hohmann, J. G., Howell, M. P., Jeung, D. P., Johnson, R. A., Karr, P. T., Kawal, R., Kidney, J. M., Knapik, R. H., Kuan, C. L., Lake, J. H., Laramee, A. R., Larsen, K. D., Lau, C., Lemon, T. A., Liang, A. J., Liu, Y., Luong, L. T., Michaels, J., Morgan, J. J., Morgan, R. J., Mortrud, M. T., Mosqueda, N. F., Ng, L. L., Ng, R., Orta, G. J., Overly, C. C., Pak, T. H., Parry, S. E., Pathak, S. D., Pearson, O. C., Puchalski, R. B., Riley, Z. L., Rockett, H. R., Rowland, S. A., Royall, J. J., Ruiz, M. J., Sarno, N. R., Schaffnit, K., Shapovalova, N. V., Sivisay, T., Slaughterbeck, C. R., Smith, S. C., Smith, K. A., Smith, B. I., Sodt, A. J., Stewart, N. N., Stumpf, K. R., Sunkin, S. M., Sutram, M., Tam, A., Teemer, C. D., Thaller, C., Thompson, C. L., Varnam, L. R., Visel, A., Whitlock, R. M., Wohnoutka, P. E., Wolkey, C. K., Wong, V. Y., Wood, M., Yaylaoglu, M. B., Young, R. C., Youngstrom, B. L., Yuan, X. F., Zhang, B., Zwingman, T. A., & Jones, A. R. (2007). Genome-wide atlas of gene expression in the adult mouse brain. *Nature*, *445*(7124), 168-176. https://doi.org/10.1038/nature05453

Leon, W. C., Bruno, M. A., Allard, S., Nader, K., & Cuello, A. C. (2010). Engagement of the PFC in consolidation and recall of recent spatial memory. *Learn Mem*, *17*(6), 297-305. https://doi.org/10.1101/lm.1804410

Leterrier, C. (2018). The Axon Initial Segment: An Updated Viewpoint. *J Neurosci*, *38*(9), 2135-2145. https://doi.org/10.1523/JNEUROSCI.1922-17.2018

Lewis, D. A., Hashimoto, T., & Volk, D. W. (2005). Cortical inhibitory neurons and schizophrenia. *Nat Rev Neurosci*, *6*(4), 312-324. https://doi.org/10.1038/nrn1648

Little, J. P., & Carter, A. G. (2013). Synaptic mechanisms underlying strong reciprocal connectivity between the medial prefrontal cortex and basolateral amygdala. *J Neurosci*, *33*(39), 15333-15342. https://doi.org/10.1523/JNEUROSCI.2385-13.2013

Liu, X. B., & Jones, E. G. (1996). Localization of alpha type II calcium calmodulin-dependent protein kinase at glutamatergic but not gamma-aminobutyric acid (GABAergic) synapses in thalamus and cerebral cortex. *Proc Natl Acad Sci U S A*, *93*(14), 7332-7336. https://doi.org/10.1073/pnas.93.14.7332

Lorincz, A., & Nusser, Z. (2010). Molecular identity of dendritic voltage-gated sodium channels. *Science*, *328*(5980), 906-909. https://doi.org/10.1126/science.1187958

Lovett-Barron, M., Turi, G. F., Kaifosh, P., Lee, P. H., Bolze, F., Sun, X. H., Nicoud, J. F., Zemelman, B. V., Sternson, S. M., & Losonczy, A. (2012). Regulation of neuronal input transformations by tunable dendritic inhibition. *Nat Neurosci*, *15*(3), 423-430, S421-423. https://doi.org/10.1038/nn.3024

Lu, J., Tucciarone, J., Padilla-Coreano, N., He, M., Gordon, J. A., & Huang, Z. J. (2017). Selective inhibitory control of pyramidal neuron ensembles and cortical subnetworks by chandelier cells. *Nat Neurosci*, *20*(10), 1377-1383. https://doi.org/10.1038/nn.4624

Luuk, H., Koks, S., Plaas, M., Hannibal, J., Rehfeld, J. F., & Vasar, E. (2008). Distribution of Wfs1 protein in the central nervous system of the mouse and its relation to clinical symptoms of the Wolfram syndrome. *J Comp Neurol*, *509*(6), 642-660. https://doi.org/10.1002/cne.21777

Magee, J. C. (2000). Dendritic integration of excitatory synaptic input. *Nat Rev Neurosci*, *1*(3), 181-190. https://doi.org/10.1038/35044552

Mahanty, N. K., & Sah, P. (1998). Calcium-permeable AMPA receptors mediate long-term potentiation in interneurons in the amygdala. *Nature*, *394*(6694), 683-687. https://doi.org/10.1038/29312

Maier, S. F., & Watkins, L. R. (2005). Stressor controllability and learned helplessness: the roles of the dorsal raphe nucleus, serotonin, and corticotropin-releasing factor. *Neurosci Biobehav Rev*, *29*(4-5), 829-841. https://doi.org/10.1016/j.neubiorev.2005.03.021

Marek, R., Xu, L., Sullivan, R. K. P., & Sah, P. (2018). Excitatory connections between the prelimbic and infralimbic medial prefrontal cortex show a role for the prelimbic cortex in fear extinction. *Nat Neurosci*, *21*(5), 654-658. https://doi.org/10.1038/s41593-018-0137-x

Marin-Padilla, M. (1969). Origin of the pericellular baskets of the pyramidal cells of the human motor cortex: a Golgi study. *Brain Res*, *14*(3), 633-646. https://doi.org/10.1016/0006-8993(69)90204-2

Marin-Padilla, M. (1987). The chandelier cell of the human visual cortex: a Golgi study. *J Comp Neurol*, *256*(1), 61-70. https://doi.org/10.1002/cne.902560106

Markham, J. A., Morris, J. R., & Juraska, J. M. (2007). Neuron number decreases in the rat ventral, but not dorsal, medial prefrontal cortex between adolescence and adulthood. *Neuroscience*, *144*(3), 961-968. https://doi.org/10.1016/j.neuroscience.2006.10.015

Mascagni, F., & McDonald, A. J. (2003). Immunohistochemical characterization of cholecystokinin containing neurons in the rat basolateral amygdala. *Brain Res*, *976*(2), 171-184. https://doi.org/10.1016/s0006-8993(03)02625-8

Massi, L., Lagler, M., Hartwich, K., Borhegyi, Z., Somogyi, P., & Klausberger, T. (2012). Temporal dynamics of parvalbumin-expressing axo-axonic and basket cells in the rat medial prefrontal cortex in vivo. *J Neurosci*, *32*(46), 16496-16502. https://doi.org/10.1523/JNEUROSCI.3475-12.2012

Mate, Z., Poles, M. Z., Szabo, G., Bagyanszki, M., Talapka, P., Fekete, E., & Bodi, N. (2013). Spatiotemporal expression pattern of DsRedT3/CCK gene construct during postnatal development of myenteric plexus in transgenic mice. *Cell Tissue Res*, *352*(2), 199-206. https://doi.org/10.1007/s00441-013-1552-7

Matyas, F., Freund, T. F., & Gulyas, A. I. (2004). Convergence of excitatory and inhibitory inputs onto CCK-containing basket cells in the CA1 area of the rat hippocampus. *Eur J Neurosci*, *19*(5), 1243-1256. https://doi.org/10.1111/j.1460-9568.2004.03225.x

Matyas, F., Lee, J., Shin, H. S., & Acsady, L. (2014). The fear circuit of the mouse forebrain: connections between the mediodorsal thalamus, frontal cortices and basolateral amygdala. *Eur J Neurosci*, *39*(11), 1810-1823. https://doi.org/10.1111/ejn.12610

Maviel, T., Durkin, T. P., Menzaghi, F., & Bontempi, B. (2004). Sites of neocortical reorganization critical for remote spatial memory. *Science*, *305*(5680), 96-99. https://doi.org/10.1126/science.1098180

McClelland, J. L., McNaughton, B. L., & O'Reilly, R. C. (1995). Why there are complementary learning systems in the hippocampus and neocortex: insights from the successes and failures of connectionist models of learning and memory. *Psychol Rev*, *102*(3), 419-457. https://doi.org/10.1037/0033-295X.102.3.419

McGarry, L. M., & Carter, A. G. (2016). Inhibitory Gating of Basolateral Amygdala Inputs to the Prefrontal Cortex. *J Neurosci*, *36*(36), 9391-9406. https://doi.org/10.1523/JNEUROSCI.0874-16.2016

Megias, M., Emri, Z., Freund, T. F., & Gulyas, A. I. (2001). Total number and distribution of inhibitory and excitatory synapses on hippocampal CA1 pyramidal cells. *Neuroscience*, *102*(3), 527-540. https://doi.org/10.1016/s0306-4522(00)00496-6

Mesulam, M. M. (1998). From sensation to cognition. *Brain*, *121 (Pt 6)*, 1013-1052. https://doi.org/10.1093/brain/121.6.1013

Meyer-Lindenberg, A. (2010). From maps to mechanisms through neuroimaging of schizophrenia. *Nature*, *468*(7321), 194-202. https://doi.org/10.1038/nature09569

Meyer, A. H., Katona, I., Blatow, M., Rozov, A., & Monyer, H. (2002). In vivo labeling of parvalbumin-positive interneurons and analysis of electrical coupling in identified neurons. *J Neurosci*, *22*(16), 7055-7064. https://doi.org/10.1523/JNEUROSCI.22-16-07055.2002

Mihaljevic, B., Benavides-Piccione, R., Bielza, C., Larranaga, P., & DeFelipe, J. (2019). Classification of GABAergic interneurons by leading neuroscientists. *Sci Data*, *6*(1), 221. https://doi.org/10.1038/s41597-019-0246-8

Miles, R., Toth, K., Gulyas, A. I., Hajos, N., & Freund, T. F. (1996). Differences between somatic and dendritic inhibition in the hippocampus. *Neuron*, *16*(4), 815-823. https://doi.org/10.1016/s0896-6273(00)80101-4

Miller, E. K. (2000). The prefrontal cortex and cognitive control. *Nat Rev Neurosci*, *1*(1), 59-65. https://doi.org/10.1038/35036228

Miyamae, T., Chen, K., Lewis, D. A., & Gonzalez-Burgos, G. (2017). Distinct Physiological Maturation of Parvalbumin-Positive Neuron Subtypes in Mouse Prefrontal Cortex. *J Neurosci*, *37*(19), 4883-4902. https://doi.org/10.1523/JNEUROSCI.3325-16.2017

Mody, I., De Koninck, Y., Otis, T. S., & Soltesz, I. (1994). Bridging the cleft at GABA synapses in the brain. *Trends Neurosci*, *17*(12), 517-525. https://doi.org/10.1016/0166-2236(94)90155-4

Molle, M., Yeshenko, O., Marshall, L., Sara, S. J., & Born, J. (2006). Hippocampal sharp wave-ripples linked to slow oscillations in rat slow-wave sleep. *J Neurophysiol*, *96*(1), 62-70. https://doi.org/10.1152/jn.00014.2006

Molnar, Z., & Cheung, A. F. (2006). Towards the classification of subpopulations of layer V pyramidal projection neurons. *Neurosci Res*, *55*(2), 105-115. https://doi.org/10.1016/j.neures.2006.02.008

Murayama, M., Perez-Garci, E., Nevian, T., Bock, T., Senn, W., & Larkum, M. E. (2009). Dendritic encoding of sensory stimuli controlled by deep cortical interneurons. *Nature*, *457*(7233), 1137-1141. https://doi.org/10.1038/nature07663

Musazzi, L., Milanese, M., Farisello, P., Zappettini, S., Tardito, D., Barbiero, V. S., Bonifacino, T., Mallei, A., Baldelli, P., Racagni, G., Raiteri, M., Benfenati, F., Bonanno, G., & Popoli, M. (2010). Acute stress increases depolarization-evoked glutamate release in the rat prefrontal/frontal cortex: the dampening action of antidepressants. *PLoS One*, *5*(1), e8566. https://doi.org/10.1371/journal.pone.0008566

Nelson, R. J., & Trainor, B. C. (2007). Neural mechanisms of aggression. *Nat Rev Neurosci*, *8*(7), 536-546. https://doi.org/10.1038/nrn2174

Newkirk, G. S., Guan, D., Dembrow, N., Armstrong, W. E., Foehring, R. C., & Spain, W. J. (2022). Kv2.1 Potassium Channels Regulate Repetitive Burst Firing in Extratelencephalic Neocortical Pyramidal Neurons. *Cereb Cortex*, *32*(5), 1055-1076. https://doi.org/10.1093/cercor/bhab266

Nguyen, R., Venkatesan, S., Binko, M., Bang, J. Y., Cajanding, J. D., Briggs, C., Sargin, D., Imayoshi, I., Lambe, E. K., & Kim, J. C. (2020). Cholecystokinin-Expressing Interneurons of the

Medial Prefrontal Cortex Mediate Working Memory Retrieval. *J Neurosci*, *40*(11), 2314-2331. https://doi.org/10.1523/JNEUROSCI.1919-19.2020

Nimchinsky, E. A., Sabatini, B. L., & Svoboda, K. (2002). Structure and function of dendritic spines. *Annu Rev Physiol*, *64*, 313-353. https://doi.org/10.1146/annurev.physiol.64.081501.160008

Nissen, W., Szabo, A., Somogyi, J., Somogyi, P., & Lamsa, K. P. (2010). Cell type-specific long-term plasticity at glutamatergic synapses onto hippocampal interneurons expressing either parvalbumin or CB1 cannabinoid receptor. *J Neurosci*, *30*(4), 1337-1347. https://doi.org/10.1523/JNEUROSCI.3481-09.2010

Nusser, Z. (2009). Variability in the subcellular distribution of ion channels increases neuronal diversity. *Trends Neurosci*, *32*(5), 267-274. https://doi.org/10.1016/j.tins.2009.01.003

Nusser, Z. (2012). Differential subcellular distribution of ion channels and the diversity of neuronal function. *Curr Opin Neurobiol*, *22*(3), 366-371. https://doi.org/10.1016/j.conb.2011.10.006

Oh, S. W., Harris, J. A., Ng, L., Winslow, B., Cain, N., Mihalas, S., Wang, Q., Lau, C., Kuan, L., Henry, A. M., Mortrud, M. T., Ouellette, B., Nguyen, T. N., Sorensen, S. A., Slaughterbeck, C. R., Wakeman, W., Li, Y., Feng, D., Ho, A., Nicholas, E., Hirokawa, K. E., Bohn, P., Joines, K. M., Peng, H., Hawrylycz, M. J., Phillips, J. W., Hohmann, J. G., Wohnoutka, P., Gerfen, C. R., Koch, C., Bernard, A., Dang, C., Jones, A. R., & Zeng, H. (2014). A mesoscale connectome of the mouse brain. *Nature*, *508*(7495), 207-214. https://doi.org/10.1038/nature13186

Ongur, D., & Price, J. L. (2000). The organization of networks within the orbital and medial prefrontal cortex of rats, monkeys and humans. *Cereb Cortex*, *10*(3), 206-219. https://doi.org/10.1093/cercor/10.3.206

Ortiz, C., Navarro, J. F., Jurek, A., Martin, A., Lundeberg, J., & Meletis, K. (2020). Molecular atlas of the adult mouse brain. *Sci Adv*, *6*(26), eabb3446. https://doi.org/10.1126/sciadv.abb3446

Otsuka, T., & Kawaguchi, Y. (2008). Firing-pattern-dependent specificity of cortical excitatory feed-forward subnetworks. *J Neurosci*, *28*(44), 11186-11195. https://doi.org/10.1523/JNEUROSCI.1921-08.2008

Packer, A. M., & Yuste, R. (2011). Dense, unspecific connectivity of neocortical parvalbumin-positive interneurons: a canonical microcircuit for inhibition? *J Neurosci*, *31*(37), 13260-13271. https://doi.org/10.1523/JNEUROSCI.3131-11.2011

Palmer, L., Murayama, M., & Larkum, M. (2012). Inhibitory Regulation of Dendritic Activity in vivo. *Front Neural Circuits*, *6*, 26. https://doi.org/10.3389/fncir.2012.00026

Papp, E., Leinekugel, X., Henze, D. A., Lee, J., & Buzsaki, G. (2001). The apical shaft of CA1 pyramidal cells is under GABAergic interneuronal control. *Neuroscience*, *102*(4), 715-721. https://doi.org/10.1016/s0306-4522(00)00584-4

Papp, O. I., Karlocai, M. R., Toth, I. E., Freund, T. F., & Hajos, N. (2013). Different input and output properties characterize parvalbumin-positive basket and Axo-axonic cells in the hippocampal CA3 subfield. *Hippocampus*, *23*(10), 903-918. https://doi.org/10.1002/hipo.22147

Peters, J., Kalivas, P. W., & Quirk, G. J. (2009). Extinction circuits for fear and addiction overlap in prefrontal cortex. *Learn Mem*, *16*(5), 279-288. https://doi.org/10.1101/lm.1041309

Petersen, C. C. (2007). The functional organization of the barrel cortex. *Neuron*, *56*(2), 339-355. https://doi.org/10.1016/j.neuron.2007.09.017

Petilla Interneuron Nomenclature, G., Ascoli, G. A., Alonso-Nanclares, L., Anderson, S. A., Barrionuevo, G., Benavides-Piccione, R., Burkhalter, A., Buzsaki, G., Cauli, B., Defelipe, J., Fairen, A., Feldmeyer, D., Fishell, G., Fregnac, Y., Freund, T. F., Gardner, D., Gardner, E. P., Goldberg, J. H., Helmstaedter, M., Hestrin, S., Karube, F., Kisvarday, Z. F., Lambolez,

B., Lewis, D. A., Marin, O., Markram, H., Munoz, A., Packer, A., Petersen, C. C., Rockland, K. S., Rossier, J., Rudy, B., Somogyi, P., Staiger, J. F., Tamas, G., Thomson, A. M., Toledo-Rodriguez, M., Wang, Y., West, D. C., & Yuste, R. (2008). Petilla terminology: nomenclature of features of GABAergic interneurons of the cerebral cortex. *Nat Rev Neurosci*, *9*(7), 557-568. https://doi.org/10.1038/nrn2402

Pfeffer, C. K., Xue, M., He, M., Huang, Z. J., & Scanziani, M. (2013). Inhibition of inhibition in visual cortex: the logic of connections between molecularly distinct interneurons. *Nat Neurosci*, *16*(8), 1068-1076. https://doi.org/10.1038/nn.3446

Pi, H. J., Hangya, B., Kvitsiani, D., Sanders, J. I., Huang, Z. J., & Kepecs, A. (2013). Cortical interneurons that specialize in disinhibitory control. *Nature*, *503*(7477), 521-524. https://doi.org/10.1038/nature12676

Pierri, J. N., Chaudry, A. S., Woo, T. U., & Lewis, D. A. (1999). Alterations in chandelier neuron axon terminals in the prefrontal cortex of schizophrenic subjects. *Am J Psychiatry*, *156*(11), 1709-1719. https://doi.org/10.1176/ajp.156.11.1709

Pierri, J. N., Volk, C. L., Auh, S., Sampson, A., & Lewis, D. A. (2001). Decreased somal size of deep layer 3 pyramidal neurons in the prefrontal cortex of subjects with schizophrenia. *Arch Gen Psychiatry*, *58*(5), 466-473. https://doi.org/10.1001/archpsyc.58.5.466

Pinto, L., & Dan, Y. (2015). Cell-Type-Specific Activity in Prefrontal Cortex during Goal-Directed Behavior. *Neuron*, *87*(2), 437-450. https://doi.org/10.1016/j.neuron.2015.06.021

Pitler, T. A., & Alger, B. E. (1992). Postsynaptic spike firing reduces synaptic GABAA responses in hippocampal pyramidal cells. *J Neurosci*, *12*(10), 4122-4132. https://doi.org/10.1523/JNEUROSCI.12-10-04122.1992

Pouille, F., & Scanziani, M. (2004). Routing of spike series by dynamic circuits in the hippocampus. *Nature*, *429*(6993), 717-723. https://doi.org/10.1038/nature02615

Printz, Y., Patil, P., Mahn, M., Benjamin, A., Litvin, A., Levy, R., Bringmann, M., & Yizhar, O. (2023). Determinants of functional synaptic connectivity among amygdala-projecting prefrontal cortical neurons in male mice. *Nat Commun*, *14*(1), 1667. https://doi.org/10.1038/s41467-023-37318-x

Quinn, J. J., Ma, Q. D., Tinsley, M. R., Koch, C., & Fanselow, M. S. (2008). Inverse temporal contributions of the dorsal hippocampus and medial prefrontal cortex to the expression of long-term fear memories. *Learn Mem*, *15*(5), 368-372. https://doi.org/10.1101/lm.813608

Radhiyanti, P. T., Konno, A., Matsuzaki, Y., & Hirai, H. (2021). Comparative study of neuron-specific promoters in mouse brain transduced by intravenously administered AAV-PHP.eB. *Neurosci Lett*, *756*, 135956. https://doi.org/10.1016/j.neulet.2021.135956

Rajkowska, G., Selemon, L. D., & Goldman-Rakic, P. S. (1998). Neuronal and glial somal size in the prefrontal cortex: a postmortem morphometric study of schizophrenia and Huntington disease. *Arch Gen Psychiatry*, *55*(3), 215-224. https://doi.org/10.1001/archpsyc.55.3.215

Reiner, B., Crist, R., Stein, L., Weller, A., Doyle, G., Arauco-Shapiro, G., Turecki, G., Ferraro, T., Hayes, M., & Berrettini, W. (2021). Single-Nuclei Transcriptomics of Schizophrenia Prefrontal Cortex Primarily Implicates Neuronal Subtypes. *European Neuropsychopharmacology*, *51*, E182-E183. https://doi.org/10.1016/j.euroneuro.2021.08.157

Rose, J. E., & Woolsey, C. N. (1948). The orbitofrontal cortex and its connections with the mediodorsal nucleus in rabbit, sheep and cat. *Res Publ Assoc Res Nerv Ment Dis*, *27 (1 vol.)*, 210-232. https://www.ncbi.nlm.nih.gov/pubmed/18106857

Ross, C. A., Margolis, R. L., Reading, S. A., Pletnikov, M., & Coyle, J. T. (2006). Neurobiology of schizophrenia. *Neuron*, *52*(1), 139-153. https://doi.org/10.1016/j.neuron.2006.09.015

Rovira-Esteban, L., Gunduz-Cinar, O., Bukalo, O., Limoges, A., Brockway, E., Muller, K., Fenno, L., Kim, Y. S., Ramakrishnan, C., Andrasi, T., Deisseroth, K., Holmes, A., & Hajos, N. (2019). Excitation of Diverse Classes of Cholecystokinin Interneurons in the Basal Amygdala Facilitates Fear Extinction. *eNeuro*, *6*(6). https://doi.org/10.1523/ENEURO.0220-19.2019

Rovira-Esteban, L., Peterfi, Z., Vikor, A., Mate, Z., Szabo, G., & Hajos, N. (2017). Morphological and physiological properties of CCK/CB1R-expressing interneurons in the basal amygdala. *Brain Struct Funct*, *222*(8), 3543-3565. https://doi.org/10.1007/s00429-017-1417-z

Rudy, B., & McBain, C. J. (2001). Kv3 channels: voltage-gated K+ channels designed for high-frequency repetitive firing. *Trends Neurosci*, *24*(9), 517-526. https://doi.org/10.1016/s0166-2236(00)01892-0

Salat, D. H., Kaye, J. A., & Janowsky, J. S. (2001). Selective preservation and degeneration within the prefrontal cortex in aging and Alzheimer disease. *Arch Neurol*, *58*(9), 1403-1408. https://doi.org/10.1001/archneur.58.9.1403

Sanacora, G., Treccani, G., & Popoli, M. (2012). Towards a glutamate hypothesis of depression: an emerging frontier of neuropsychopharmacology for mood disorders. *Neuropharmacology*, *62*(1), 63-77. https://doi.org/10.1016/j.neuropharm.2011.07.036

Scheyltjens, I., Laramee, M. E., Van den Haute, C., Gijsbers, R., Debyser, Z., Baekelandt, V., Vreysen, S., & Arckens, L. (2015). Evaluation of the expression pattern of rAAV2/1, 2/5, 2/7, 2/8, and 2/9 serotypes with different promoters in the mouse visual cortex. *J Comp Neurol*, *523*(14), 2019-2042. https://doi.org/10.1002/cne.23819

Schlingloff, D., Kali, S., Freund, T. F., Hajos, N., & Gulyas, A. I. (2014). Mechanisms of sharp wave initiation and ripple generation. *J Neurosci*, *34*(34), 11385-11398. https://doi.org/10.1523/JNEUROSCI.0867-14.2014

Schneider-Mizell, C. M., Bodor, A. L., Collman, F., Brittain, D., Bleckert, A., Dorkenwald, S., Turner, N. L., Macrina, T., Lee, K., Lu, R., Wu, J., Zhuang, J., Nandi, A., Hu, B., Buchanan, J., Takeno, M. M., Torres, R., Mahalingam, G., Bumbarger, D. J., Li, Y., Chartrand, T., Kemnitz, N., Silversmith, W. M., Ih, D., Zung, J., Zlateski, A., Tartavull, I., Popovych, S., Wong, W., Castro, M., Jordan, C. S., Froudarakis, E., Becker, L., Suckow, S., Reimer, J., Tolias, A. S., Anastassiou, C. A., Seung, H. S., Reid, R. C., & Costa, N. M. D. (2021). Structure and function of axo-axonic inhibition. *Elife*, *10*. https://doi.org/10.7554/eLife.73783

Schulz, J. M., Knoflach, F., Hernandez, M. C., & Bischofberger, J. (2018). Dendrite-targeting interneurons control synaptic NMDA-receptor activation via nonlinear alpha5-GABA(A) receptors. *Nat Commun*, *9*(1), 3576. https://doi.org/10.1038/s41467-018-06004-8

Senzai, Y., Fernandez-Ruiz, A., & Buzsaki, G. (2019). Layer-Specific Physiological Features and Interlaminar Interactions in the Primary Visual Cortex of the Mouse. *Neuron*, *101*(3), 500-513 e505. https://doi.org/10.1016/j.neuron.2018.12.009

Sewards, T. V., & Sewards, M. A. (2002). The medial pain system: neural representations of the motivational aspect of pain. *Brain Res Bull*, *59*(3), 163-180. https://doi.org/10.1016/s0361-9230(02)00864-x

Siapas, A. G., & Wilson, M. A. (1998). Coordinated interactions between hippocampal ripples and cortical spindles during slow-wave sleep. *Neuron*, *21*(5), 1123-1128. https://doi.org/10.1016/s0896-6273(00)80629-7

Sierra-Mercado, D., Padilla-Coreano, N., & Quirk, G. J. (2011). Dissociable roles of prelimbic and infralimbic cortices, ventral hippocampus, and basolateral amygdala in the expression and extinction of conditioned fear. *Neuropsychopharmacology*, *36*(2), 529-538. https://doi.org/10.1038/npp.2010.184

Sik, A., Hajos, N., Gulacsi, A., Mody, I., & Freund, T. F. (1998). The absence of a major Ca2+ signaling pathway in GABAergic neurons of the hippocampus. *Proc Natl Acad Sci U S A*, *95*(6), 3245-3250. https://doi.org/10.1073/pnas.95.6.3245

Sik, A., Tamamaki, N., & Freund, T. F. (1993). Complete axon arborization of a single CA3 pyramidal cell in the rat hippocampus, and its relationship with postsynaptic parvalbumin-containing interneurons. *Eur J Neurosci*, *5*(12), 1719-1728. https://doi.org/10.1111/j.1460-9568.1993.tb00239.x

Sik, A., Ylinen, A., Penttonen, M., & Buzsaki, G. (1994). Inhibitory CA1-CA3-hilar region feedback in the hippocampus. *Science*, *265*(5179), 1722-1724. https://doi.org/10.1126/science.8085161

Sirota, A., Csicsvari, J., Buhl, D., & Buzsaki, G. (2003). Communication between neocortex and hippocampus during sleep in rodents. *Proc Natl Acad Sci U S A*, *100*(4), 2065-2069. https://doi.org/10.1073/pnas.0437938100

Sohal, V. S., Zhang, F., Yizhar, O., & Deisseroth, K. (2009). Parvalbumin neurons and gamma rhythms enhance cortical circuit performance. *Nature*, *459*(7247), 698-702. https://doi.org/10.1038/nature07991

Somogyi, P. (1977). A specific 'axo-axonal' interneuron in the visual cortex of the rat. *Brain Res*, *136*(2), 345-350. https://doi.org/10.1016/0006-8993(77)90808-3

Somogyi, P., Freund, T. F., & Cowey, A. (1982). The axo-axonic interneuron in the cerebral cortex of the rat, cat and monkey. *Neuroscience*, *7*(11), 2577-2607. https://doi.org/10.1016/0306-4522(82)90086-0

Somogyi, P., Tamas, G., Lujan, R., & Buhl, E. H. (1998). Salient features of synaptic organisation in the cerebral cortex. *Brain Res Brain Res Rev*, *26*(2-3), 113-135. https://doi.org/10.1016/s0165-0173(97)00061-1

Song, A. J., & Palmiter, R. D. (2018). Detecting and Avoiding Problems When Using the Cre-lox System. *Trends Genet*, *34*(5), 333-340. https://doi.org/10.1016/j.tig.2017.12.008

Spellman, T., Rigotti, M., Ahmari, S. E., Fusi, S., Gogos, J. A., & Gordon, J. A. (2015). Hippocampal-prefrontal input supports spatial encoding in working memory. *Nature*, *522*(7556), 309-314. https://doi.org/10.1038/nature14445

Spruston, N. (2008). Pyramidal neurons: dendritic structure and synaptic integration. *Nat Rev Neurosci*, *9*(3), 206-221. https://doi.org/10.1038/nrn2286

Staiger, J. F., Flagmeyer, I., Schubert, D., Zilles, K., Kotter, R., & Luhmann, H. J. (2004). Functional diversity of layer IV spiny neurons in rat somatosensory cortex: quantitative morphology of electrophysiologically characterized and biocytin labeled cells. *Cereb Cortex*, *14*(6), 690-701. https://doi.org/10.1093/cercor/bhh029

Stefanova, N. A., Ershov, N. I., Maksimova, K. Y., Muraleva, N. A., Tyumentsev, M. A., & Kolosova, N. G. (2019). The Rat Prefrontal-Cortex Transcriptome: Effects of Aging and Sporadic Alzheimer's Disease-Like Pathology. *J Gerontol A Biol Sci Med Sci*, *74*(1), 33-43. https://doi.org/10.1093/gerona/gly198

Stuart, G. J., & Sakmann, B. (1994). Active propagation of somatic action potentials into neocortical pyramidal cell dendrites. *Nature*, *367*(6458), 69-72. https://doi.org/10.1038/367069a0

Swanson, O. K., & Maffei, A. (2019). From Hiring to Firing: Activation of Inhibitory Neurons and Their Recruitment in Behavior. *Front Mol Neurosci*, *12*, 168. https://doi.org/10.3389/fnmol.2019.00168

Szabadics, J., Varga, C., Molnar, G., Olah, S., Barzo, P., & Tamas, G. (2006). Excitatory effect of GABAergic axo-axonic cells in cortical microcircuits. *Science*, *311*(5758), 233-235. https://doi.org/10.1126/science.1121325

Szabo, G. G., Holderith, N., Gulyas, A. I., Freund, T. F., & Hajos, N. (2010). Distinct synaptic properties of perisomatic inhibitory cell types and their different modulation by

cholinergic receptor activation in the CA3 region of the mouse hippocampus. *Eur J Neurosci*, *31*(12), 2234-2246. https://doi.org/10.1111/j.1460-9568.2010.07292.x

Szabo, G. G., Papp, O. I., Mate, Z., Szabo, G., & Hajos, N. (2014). Anatomically heterogeneous populations of CB1 cannabinoid receptor-expressing interneurons in the CA3 region of the hippocampus show homogeneous input-output characteristics. *Hippocampus*, *24*(12), 1506-1523. https://doi.org/10.1002/hipo.22330

Szentagothai, J., & Arbib, M. A. (1974). Conceptual models of neural organization. *Neurosci Res Program Bull*, *12*(3), 305-510. https://www.ncbi.nlm.nih.gov/pubmed/4437759

Takacs, V. T., Klausberger, T., Somogyi, P., Freund, T. F., & Gulyas, A. I. (2012). Extrinsic and local glutamatergic inputs of the rat hippocampal CA1 area differentially innervate pyramidal cells and interneurons. *Hippocampus*, *22*(6), 1379-1391. https://doi.org/10.1002/hipo.20974

Takacs, V. T., Szonyi, A., Freund, T. F., Nyiri, G., & Gulyas, A. I. (2015). Quantitative ultrastructural analysis of basket and axo-axonic cell terminals in the mouse hippocampus. *Brain Struct Funct*, *220*(2), 919-940. https://doi.org/10.1007/s00429-013-0692-6

Tamas, G., Buhl, E. H., Lorincz, A., & Somogyi, P. (2000). Proximally targeted GABAergic synapses and gap junctions synchronize cortical interneurons. *Nat Neurosci*, *3*(4), 366-371. https://doi.org/10.1038/73936

Tamas, G., Buhl, E. H., & Somogyi, P. (1997). Fast IPSPs elicited via multiple synaptic release sites by different types of GABAergic neurone in the cat visual cortex. *J Physiol*, *500 (Pt 3)*(Pt 3), 715-738. https://doi.org/10.1113/jphysiol.1997.sp022054

Tamas, G., Lorincz, A., Simon, A., & Szabadics, J. (2003). Identified sources and targets of slow inhibition in the neocortex. *Science*, *299*(5614), 1902-1905. https://doi.org/10.1126/science.1082053

Taniguchi, H., He, M., Wu, P., Kim, S., Paik, R., Sugino, K., Kvitsiani, D., Fu, Y., Lu, J., Lin, Y., Miyoshi, G., Shima, Y., Fishell, G., Nelson, S. B., & Huang, Z. J. (2011). A resource of Cre driver lines for genetic targeting of GABAergic neurons in cerebral cortex. *Neuron*, *71*(6), 995-1013. https://doi.org/10.1016/j.neuron.2011.07.026

Taniguchi, H., Lu, J., & Huang, Z. J. (2013). The spatial and temporal origin of chandelier cells in mouse neocortex. *Science*, *339*(6115), 70-74. https://doi.org/10.1126/science.1227622

Tasic, B., Yao, Z., Graybuck, L. T., Smith, K. A., Nguyen, T. N., Bertagnolli, D., Goldy, J., Garren, E., Economo, M. N., Viswanathan, S., Penn, O., Bakken, T., Menon, V., Miller, J., Fong, O., Hirokawa, K. E., Lathia, K., Rimorin, C., Tieu, M., Larsen, R., Casper, T., Barkan, E., Kroll, M., Parry, S., Shapovalova, N. V., Hirschstein, D., Pendergraft, J., Sullivan, H. A., Kim, T. K., Szafer, A., Dee, N., Groblewski, P., Wickersham, I., Cetin, A., Harris, J. A., Levi, B. P., Sunkin, S. M., Madisen, L., Daigle, T. L., Looger, L., Bernard, A., Phillips, J., Lein, E., Hawrylycz, M., Svoboda, K., Jones, A. R., Koch, C., & Zeng, H. (2018). Shared and distinct transcriptomic cell types across neocortical areas. *Nature*, *563*(7729), 72-78. https://doi.org/10.1038/s41586-018-0654-5

Tettamanti, M., & Weniger, D. (2006). Broca's area: a supramodal hierarchical processor? *Cortex*, *42*(4), 491-494. https://doi.org/10.1016/s0010-9452(08)70384-8

Toledo-Rodriguez, M., Goodman, P., Illic, M., Wu, C., & Markram, H. (2005). Neuropeptide and calcium-binding protein gene expression profiles predict neuronal anatomical type in the juvenile rat. *J Physiol*, *567*(Pt 2), 401-413. https://doi.org/10.1113/jphysiol.2005.089250

Tomioka, R., Okamoto, K., Furuta, T., Fujiyama, F., Iwasato, T., Yanagawa, Y., Obata, K., Kaneko, T., & Tamamaki, N. (2005). Demonstration of long-range GABAergic connections distributed throughout the mouse neocortex. *Eur J Neurosci*, *21*(6), 1587-1600. https://doi.org/10.1111/j.1460-9568.2005.03989.x

Toth, K., & Freund, T. F. (1992). Calbindin D28k-containing nonpyramidal cells in the rat hippocampus: their immunoreactivity for GABA and projection to the medial septum. *Neuroscience*, *49*(4), 793-805. https://doi.org/10.1016/0306-4522(92)90357-8

Tremblay, R., Lee, S., & Rudy, B. (2016). GABAergic Interneurons in the Neocortex: From Cellular Properties to Circuits. *Neuron*, *91*(2), 260-292. https://doi.org/10.1016/j.neuron.2016.06.033

Tronel, S., & Sara, S. J. (2003). Blockade of NMDA receptors in prelimbic cortex induces an enduring amnesia for odor-reward associative learning. *J Neurosci*, *23*(13), 5472-5476. https://doi.org/10.1523/JNEUROSCI.23-13-05472.2003

Tukker, J. J., Lasztoczi, B., Katona, L., Roberts, J. D., Pissadaki, E. K., Dalezios, Y., Marton, L., Zhang, L., Klausberger, T., & Somogyi, P. (2013). Distinct dendritic arborization and in vivo firing patterns of parvalbumin-expressing basket cells in the hippocampal area CA3. *J Neurosci*, *33*(16), 6809-6825. https://doi.org/10.1523/JNEUROSCI.5052-12.2013

Uylings, H. B., Groenewegen, H. J., & Kolb, B. (2003). Do rats have a prefrontal cortex? *Behav Brain Res*, *146*(1-2), 3-17. https://doi.org/10.1016/j.bbr.2003.09.028

Van De Werd, H. J., Rajkowska, G., Evers, P., & Uylings, H. B. (2010). Cytoarchitectonic and chemoarchitectonic characterization of the prefrontal cortical areas in the mouse. *Brain Struct Funct*, *214*(4), 339-353. https://doi.org/10.1007/s00429-010-0247-z

Van De Werd, H. J., & Uylings, H. B. (2008). The rat orbital and agranular insular prefrontal cortical areas: a cytoarchitectonic and chemoarchitectonic study. *Brain Struct Funct*, *212*(5), 387-401. https://doi.org/10.1007/s00429-007-0164-y

Van De Werd, H. J., & Uylings, H. B. (2014). Comparison of (stereotactic) parcellations in mouse prefrontal cortex. *Brain Struct Funct*, *219*(2), 433-459. https://doi.org/10.1007/s00429-013-0630-7

Varga, C., Lee, S. Y., & Soltesz, I. (2010). Target-selective GABAergic control of entorhinal cortex output. *Nat Neurosci*, *13*(7), 822-824. https://doi.org/10.1038/nn.2570

Varga, C., Oijala, M., Lish, J., Szabo, G. G., Bezaire, M., Marchionni, I., Golshani, P., & Soltesz, I. (2014). Functional fission of parvalbumin interneuron classes during fast network events. *Elife*, *3*. https://doi.org/10.7554/eLife.04006

Vereczki, V. K., Veres, J. M., Muller, K., Nagy, G. A., Racz, B., Barsy, B., & Hajos, N. (2016). Synaptic Organization of Perisomatic GABAergic Inputs onto the Principal Cells of the Mouse Basolateral Amygdala. *Front Neuroanat*, *10*, 20. https://doi.org/10.3389/fnana.2016.00020

Veres, J. M., Nagy, G. A., & Hajos, N. (2017). Perisomatic GABAergic synapses of basket cells effectively control principal neuron activity in amygdala networks. *Elife*, *6*. https://doi.org/10.7554/eLife.20721

Veres, J. M., Nagy, G. A., Vereczki, V. K., Andrasi, T., & Hajos, N. (2014). Strategically positioned inhibitory synapses of axo-axonic cells potently control principal neuron spiking in the basolateral amygdala. *J Neurosci*, *34*(49), 16194-16206. https://doi.org/10.1523/JNEUROSCI.2232-14.2014

Vervaeke, K., Lorincz, A., Gleeson, P., Farinella, M., Nusser, Z., & Silver, R. A. (2010). Rapid desynchronization of an electrically coupled interneuron network with sparse excitatory synaptic input. *Neuron*, *67*(3), 435-451. https://doi.org/10.1016/j.neuron.2010.06.028

Viney, T. J., Lasztoczi, B., Katona, L., Crump, M. G., Tukker, J. J., Klausberger, T., & Somogyi, P. (2013). Network state-dependent inhibition of identified hippocampal CA3 axo-axonic cells in vivo. *Nat Neurosci*, *16*(12), 1802-1811. https://doi.org/10.1038/nn.3550

Volk, D. W., & Lewis, D. A. (2002). Impaired prefrontal inhibition in schizophrenia: relevance for cognitive dysfunction. *Physiol Behav*, *77*(4-5), 501-505. https://doi.org/10.1016/s0031-9384(02)00936-8

Wang, X., Allen, W. E., Wright, M. A., Sylwestrak, E. L., Samusik, N., Vesuna, S., Evans, K., Liu, C., Ramakrishnan, C., Liu, J., Nolan, G. P., Bava, F. A., & Deisseroth, K. (2018). Three-dimensional intact-tissue sequencing of single-cell transcriptional states. *Science*, *361*(6400). https://doi.org/10.1126/science.aat5691

Watakabe, A., Ohtsuka, M., Kinoshita, M., Takaji, M., Isa, K., Mizukami, H., Ozawa, K., Isa, T., & Yamamori, T. (2015). Comparative analyses of adeno-associated viral vector serotypes 1, 2, 5, 8 and 9 in marmoset, mouse and macaque cerebral cortex. *Neurosci Res*, *93*, 144-157. https://doi.org/10.1016/j.neures.2014.09.002

Wilson, R. I., Kunos, G., & Nicoll, R. A. (2001). Presynaptic specificity of endocannabinoid signaling in the hippocampus. *Neuron*, *31*(3), 453-462. https://doi.org/10.1016/s0896-6273(01)00372-5

Wilson, R. I., & Nicoll, R. A. (2001). Endogenous cannabinoids mediate retrograde signalling at hippocampal synapses. *Nature*, *410*(6828), 588-592. https://doi.org/10.1038/35069076

Wise, S. P., & Murray, E. A. (2000). Arbitrary associations between antecedents and actions. *Trends Neurosci*, *23*(6), 271-276. https://doi.org/10.1016/s0166-2236(00)01570-8

Yang, S. S., Mack, N. R., Shu, Y., & Gao, W. J. (2021). Prefrontal GABAergic Interneurons Gate Long-Range Afferents to Regulate Prefrontal Cortex-Associated Complex Behaviors. *Front Neural Circuits*, *15*, 716408. https://doi.org/10.3389/fncir.2021.716408

Yuste, R. (2011). Dendritic spines and distributed circuits. *Neuron*, *71*(5), 772-781. https://doi.org/10.1016/j.neuron.2011.07.024

Zemankovics, R., Veres, J. M., Oren, I., & Hajos, N. (2013). Feedforward inhibition underlies the propagation of cholinergically induced gamma oscillations from hippocampal CA3 to CA1. *J Neurosci*, *33*(30), 12337-12351. https://doi.org/10.1523/JNEUROSCI.3680-12.2013

Zingg, B., Chou, X. L., Zhang, Z. G., Mesik, L., Liang, F., Tao, H. W., & Zhang, L. I. (2017). AAV-Mediated Anterograde Transsynaptic Tagging: Mapping Corticocollicular Input-Defined Neural Pathways for Defense Behaviors. *Neuron*, *93*(1), 33-47. https://doi.org/10.1016/j.neuron.2016.11.045

10. Bibliography of the candidate's publications

Publications related to this thesis

Nagy-Pal P., Veres J. M., Fekete Zs., Karlocai M. R., Weisz F., Barabas B., Reeb Zs., Hajos N.
Structural organisation of perisomatic inhibition in the mouse medial prefrontal cortex.
JOURNAL OF NEUROSCIENCE 2023 Paper: DOI: 10.1523/JNEUROSCI.0432-23.2023 (2023)

Veres J.M., Andrasi T., Nagy-Pal P., Hajos N.
CaMKIIα Promoter-Controlled Circuit Manipulations Target Both Pyramidal Cells and Inhibitory Interneurons in Cortical Networks
ENEURO 10 : 4 Paper: 0070-23.2023 , 11 p. (2023)

Other publication

Rhomberg Thomas, Rovira-Esteban Laura, Vikor Attila, Paradiso Enrica, Kremser Christian, Nagy-Pal Petra, Papp Orsolya I, Tasan Ramon, Erdelyi Ferenc, Szabo Gabor, Ferraguti Francesco, Hajos Norbert
Vasoactive Intestinal Polypeptide-Immunoreactive Interneurons within Circuits of the Mouse Basolateral Amygdala
JOURNAL OF NEUROSCIENCE 38 : 31 pp. 6983-7003. , 21 p. (2018)

11. Acknowledgements

I would like to express my sincere gratitude to the many people that have played a pivotal role in the completion of my PhD thesis. This journey has been challenging and I am deeply appreciative of the support and assistance I have been received along the way.

First and foremost, I am indebted to my supervisor, Norbert Hájos, for his unwavering guidance, expertise and patience. His mentorship has been instrumental in shaping my research and fostering my growth as a scientist. I would like to thank Judit, my mentor, for her invaluable insights, constructive feedback and valuable contribution to my work. Her collective expertise has enriched this thesis significantly. I would like to acknowledge the patience and help of Erzsi, who taught me to the details of distinct anatomical methods. I am grateful to every old and recent members of the Hájos's lab, who made every minute spent in the lab delightful with their dedicated works and advices. The exchange of ideas and knowledge within this community has been a constant source of inspiration. I would especially like to thank Zsófi, Zsuzsi, Bence and Peti for their invested works, energy and contribution to my thesis.

I am truly grateful to Andi and Attila, who helped to make my thesis even better with their magnificent perceptions and suggestions.

Lastly, I would like to thank my family for their unwavering encouragement, understanding and patience during the last years.